Photoconversion of DNA-binding dyes
and its application in super-resolution microscopy

Dominika Żurek-Biesiada

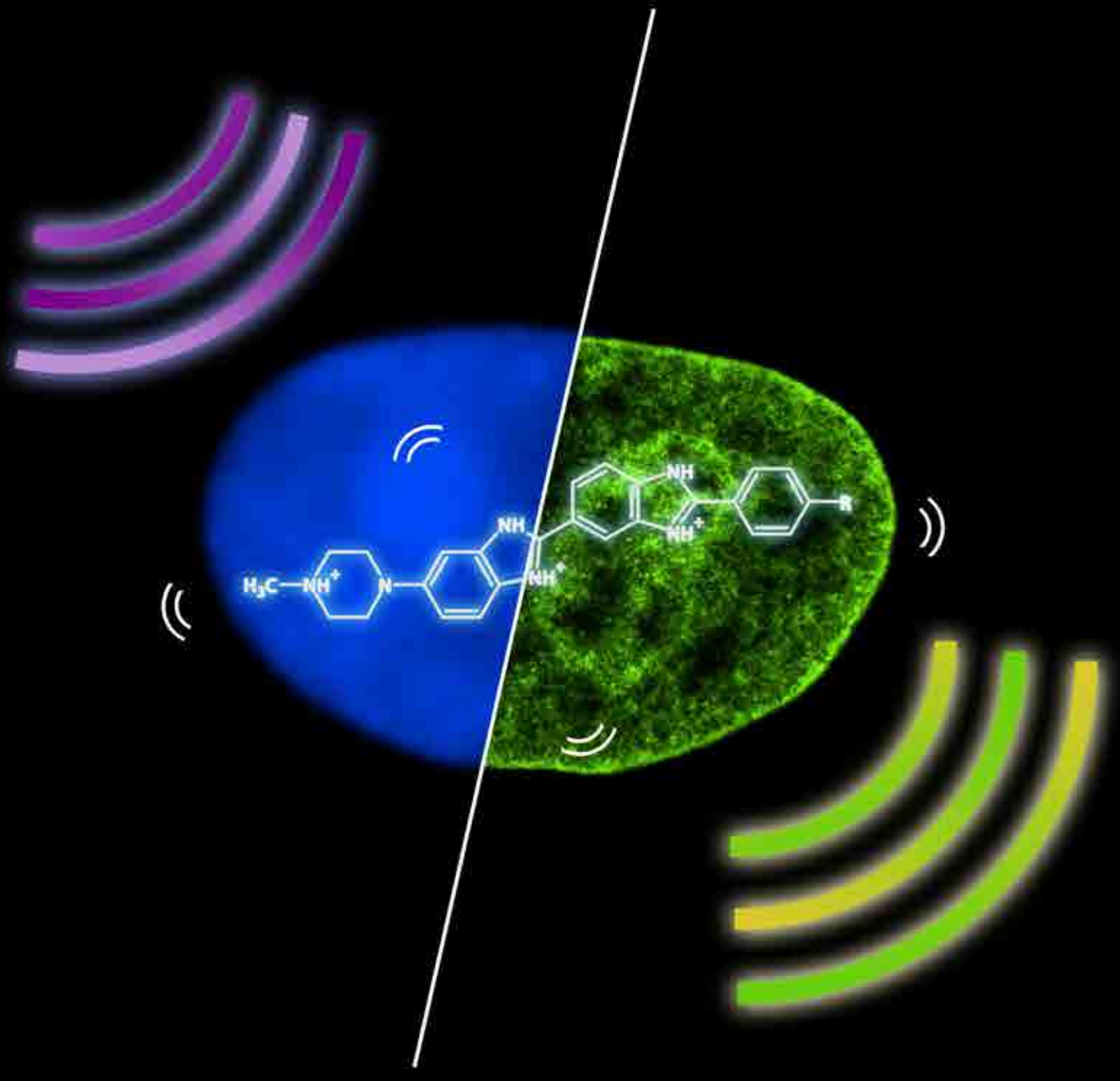

JAGIELLONIAN UNIVERSITY
IN KRAKÓW

Faculty of Biochemistry, Biophysics and Biotechnology
Laboratory of Cell Biophysics

DOMINIKA ŻUREK-BIESIADA

PHOTOCONVERSION OF DNA-BINDING DYES AND ITS APPLICATION IN SUPER-RESOLUTION MICROSCOPY

PhD Thesis

Thesis Supervisor
prof. dr hab. Jerzy W. Dobrucki

Kraków 2015

Cover image: a schematic representation of improvement of image resolution achieved by exploiting photoconversion of UV-excited Hoechst 33258 into a green-emitting form. Left: widefield image of a slice of a cell nucleus. Right: super-resolution image of a slice of a cell nucleus. The chemical structure represents Hoechst dyes.

Project co-financed by the European Union under the European Social Fund
DOCTUS - Małopolska Scholarship Fund for PhD Students

I would like to express my deepest gratitude to my Supervisor, ***Professor Jerzy W. Dobrucki****. Thank you for your support, sharing your knowledge, all the advices and nice collaboration through all these years.*

I am very grateful to ***Professor Christoph Cremer*** *for the possibility of working in his SMLM laboratory and a very nice collaboration.*

I would also like to express my thanks to ***Dr Piotr Waligórski*** *for the help with mass spectrometry experiments and all the time spent together.*

I would also like to thank ***Dr Sylwia Kędracka-Krok*** *and* ***Dr Małgorzata Jemioła-Rzemińska*** *for their help with mass spectrometry and spectrofluorimetry experiments.*

I am immensely grateful to ***Dr Agnieszka Waligórska, Dr Mirosław Zarębski, Mgr Magdalena Kordon, Dr Dominika Trembecka-Lucas, Mgr Krzysztof Berniak****, and all my Co-Workers from the Division of Cell Biophysics. Without you this lab would not exist!*

Special thanks to my BFF ***Mgr Joanna Latasiewicz*** *for all the support, understanding and a wonderful friendship* ♡

I am also grateful to ***Mgr Aleksander Szczurek*** *for our very nice collaboration, all the talks and joint projects. Working with you was a pleasure!*

Very special thanks to my ***Family*** *and* ***Friends****. Your support and encouragement means everything to me. Thank you for being there for me!*

To my Best Friend and Husband,
Alek

Contents

List of Figures

List of Tables

List of Abbreviations

Abbreviation	Meaning
3D-SIM	Three Dimensional Structured Illumination Microscopy
A and T / A-T	adenine and thymine
A405	Alexa Fluor 405/ Alexa Fluor® 405
advancedSPDM	reconstruction algorithm described in PAPER3
AMC	7-amino-4-methylcoumarin
APD	avalanche photodiode
BALM	Binding-Activated Localisation Microscopy
bp	base pair
CLSM	Confocal Laser Scanning Microscopy
CW-STED	Continuous Wave Stimulated Emission Depletion
Cy3, Cy5, Cy5.5, Cy7	cyanine dyes
DA	5-dimethyloaminonaphthalene-1sulfonyl aziridine (dansyl aziridine)
DNA	deoxyribonucleic acid
DPH	1,6-diphenyl-1,3,5-hexatriene
dsDNA	double stranded deoxyribonucleic acid
DPH	1,6-Diphenyl-1,3,5-hexatriene
EM	Electron Microscopy
Em.	emission
EosFP	Eos Fluorescent Protein
Et	N-iodoacetyl-n'-(5-sulfo-1-naphthyl)ethylenediamine
Ex.	excitation
fastSPDM	reconstruction algorithm described in [219]
FISH	Fluorescence In Situ Hybrydyzation
fPALM	fluorescence PhotoActivated Localisation Microscopy
FPs	fluorescent proteins
GFP	Green Fluorescent Protein
gSTED	gated Stimulated Emission Depletion
H33258	Hoechst 33258
H33342	Hoechst 33342
IrisFP	Iris Fluorescent Protein
MS	mass spectrometry
NA	numerical aperture
PA-GFP	PhotoActivable Green Fluorescent Protein
PAFPs	PhotoActivable Fluorescent Proteins

Continued on next page

Abbreviation	Meaning
PALM	PhotoActivated Localisation Microscopy
PAmCherry	PhotoActivable mCherry
PBS	Phosphate Buffered Saline
PMT	photomultiplier
PS-CFP	PhotoSwitchable Cyan Fluorescent Protein
PSF	Point Spread Function
PSmOrange	PhotoSwitchable mOrange
RAM	Random Access Memory
RNA	ribonucleic acid
rsTagRFP	rsTag Red Fluorescent Protein
SIM	Structured Illumination Microscopy
SMLM	Single Molecule Localisation Microscopy
SPDM	Spectral Precision Distance Microscopy
STED	Stimulated Emission Depletion
tdEosFP	tdEos Fluorescent Protein
TIRFM	Total Internal Reflection Fluorescence Microscopy
UV	ultraviolet
VdcV	Vybrant® DyeCycle™ Violet
wtGFP	wild type GFP
Zn-Se QD	Zn-Se Quantum Dot

Summary

DAPI, Hoechst 33258/33342 and Vybrant® DyeCycle™ Violet are DNA-binding fluorescent dyes that have their excitation and emission maxima at 350/461, 355/465, 340/454 and 369/437 nm, respectively. When illuminated with UV or 405 nm light, these dyes convert to forms which are easily excited with blue light and have their emission maxima around 540 nm of the visible light spectrum. The original forms of these dyes and their respective photoproducts (in forms bound to DNA), after approximately 60 minutes, reach equilibrium, and remain stable for several hours. The process of their photoconversion is independent of the presence of DNA, and the amount of the generated photoproducts is proportional to the dose of light used during the illumination of the specimen. Hoechst 33258 and Vybrant® DyeCycle™ Violet (in solution and in forms bound to DNA), when treated with hydrogen peroxide, convert to forms, which have the same spectral properties as their UV-generated photoproducts. The forms generated in a hydrogen peroxide environment are excited with blue light and emit fluorescence in the green range of the visible spectrum, with their emission maximum around 540 nm. Fluorescence emission of Hoechst 33258 and VdcV is strongly dependent on pH. Low pH environment, similarly to UV-illumination and oxidising conditions, allows generating green-emitting products of Hoechst 33258 and VdcV. Mass spectrometry analysis of Hoechst 33258 and DAPI showed that the chemical change that leads to the changed fluorescence properties is protonation. In the case of DAPI two protonated forms of the dye were observed, with mass-to-charge ratios at 278.1 and 139.5, for the mono- and the di-cation, respectively. In the case of Hoechst 33258 three protonated forms of the dye were observed in the mass spectrometry spectra, with mass-to-charge ratios at 425.2, 213.1, and 142.4, for the mono-, di-, and tri-cation, respectively. The combined mass spectrometry and fluorescence data suggest that a 4+ cation of Hoechst 33258 also exists. The protonated forms of Hoechst 33258 bind differently to nucleic acids. While forms 1+, 2+ and 3+ exhibit affinity to DNA, the putative form 4+ binds to RNA. Along with subsequent protonation steps, the fluorescence properties of the protonated forms of Hoechst 33258 change as well. The 1+ form of Hoechst 33258 is most likely the blue-emitting form, while the 3+ and 4+ forms of Hoechst 33258 emit green fluorescence. Understanding the photophysics of the process of photoconversion of the investigated dyes facilitated their exploitation in super-resolution microscopy. The green-emitting products of DAPI, Hoechst 33258/33342 and VdcV, in a controlled environment, and under specific illumination, exhibit blinking behaviour. This enables spatial isolation of single molecule fluorescent bursts, and consequently, acquisition of high-resolution images of the DNA structures. For Hoechst 33258/33342 it was possible to register up to approximately 3 x 10^5 single molecules in an individual measurement, which allowed for reconstruction of a good quality super-resolution image of DNA density in a cell nucleus. Vybrant® DyeCycle™ Violet yields even better re-

sults and with this dye up to 10^6 precisely localised individual single molecule fluorescent bursts were detected. Additionally, VdcV does not require illumination with two different wavelengths (contrary to Hoechst 33258/33342 and DAPI). Elimination of UV or 405 nm illumination is preferable, since it simplifies data acquisition and the instrumentation required to detect fluorescence bursts. Moreover, in the case of VdcV the intensity of the 491 nm laser light, which was used to visualise single molecules, was lower than in experiments involving Hoechst 33258/33342 and DAPI. Concluding, understanding of the photophysical behaviour of the investigated dyes facilitated employment of the process of their photoconversion in super-resolution microscopy, and allowed to obtain high quality super-resolution images of the DNA structures.

Streszczenie

DAPI, Hoechst 33258/33342 oraz Vybrant® DyeCycle™ Violet to barwniki fluorescencyjne wykazujące powinowactwo do DNA. Maksima widm wzbudzenia/emisji tych barwników mają odpowiednio wartości: 350/461, 355/465, 340/454 oraz 369/437 nm. Naświetlanie tych barwników światłem o długości fali 405 nm lub promieniowaniem UV wywołuje ich konwersję do form, które wzbudzane są światłem niebieskim i emitują fluorescencję w zakresie długości fal światła zielonego. Maksimum widma emisji tak powstałych form ma wartość 540 nm. Podstawowe formy barwników oraz ich fotoprodukty (w formie związanej z DNA), po około 60 minutach, wchodzą w równowagę ilościową i w takim stanie pozostają stabilne przez kilka godzin. Proces fotokonwersji nie zależy od obecności DNA. Ilość wygenerowanego fotoproduktu jest proporcjonalna do dawki światła wykorzystanego do jego wytworzenia. Barwniki Hoechst 33258 oraz Vybrant® DyeCycle™ Violet (w roztworze lub w formie związanej z DNA) poddane działaniu nadtlenku wodoru konwertują się do form, które wykazują identyczne właściwości spektralne jak formy, które powstały po naświetleniu ich UV/405 nm. Formy te również wzbudzane są światłem niebieskim i emitują fluorescencję w zakresie długości fal światła zielonego. Maksimum widma emisji tych form ma wartość 540 nm. Emisja fluorescencji barwników Hoechst 33258 oraz VdcV jest silnie zależna od pH. Niskie pH, podobnie jak wpływ promieniowania UV oraz warunków utleniających, pozwala na wytworzenie form tych barwników, które emitują fluorescencję w zakresie długości fal światła zielonego. Badania barwników Hoechst 33258 oraz DAPI za pomocą metod spektrometrii masowej wykazały, że zmiana chemiczna, która towarzyszy zmieniającym się ich właściwościom fluorescencyjnym to protonacja. W przypadku barwnika DAPI zarejestrowano dwie formy uprotonowane o stosunkach mas do ładunków: 278,1 oraz 139,5, dla odpowiednio: formy jednokrotnie i dwukrotnie uprotonowanej. W przypadku barwnika Hoechst 33258 zarejestrowano trzy formy uprotonowane, tj. o stosunkach mas do ładunków: 425,2, 213,1 oraz 142,4, dla odpowiednio: formy jednokrotnie, dwukrotnie i trzykrotnie uprotonowanej. Wnioski płynące z analizy danych pochodzących ze spektrometrii masowej oraz mikroskopii fluorescencyjnej sugerują, że istnieje również forma barwnika Hoechst 33258, która jest czterokrotnie uprotonowana. Uprotonowane formy barwnika Hoechst 33258 w różny sposób wiążą się z kwasami nukleinowymi. Podczas gdy formy 1+, 2+ oraz 3+ wykazują powinowactwo do DNA, domniemana forma 4+ wykazuje powinowactwo do RNA. Dodatkowo, razem ze wzrostem stopnia uprotonowania tego barwnika zmieniają się także jego właściwości fluorescencyjne. Jednokrotnie uprotonowana forma barwnika Hoechst 33258 to forma emitująca prawdopodobnie fluorescencję w zakresie długości fal światła niebieskiego, podczas gdy formy trzy- i cztero-krotnie uprotonowane, to formy emitujące fluorescencję w zakresie długości fal światła zielonego. Dokładne zrozumienie fotofizyki procesu fotokonwersji ułatwiło jego wykorzystanie we fluorescen-

cyjnej mikroskopii wysokorozdzielczej. Badane barwniki do DNA, w kontrolowanym środowisku i pod kontrolowanym oświetleniem, wykazują zjawisko migotania (ang. *blinking*). Pozwala to na rozdzielenie w przestrzeni sygnałów fluorescencyjnych pojedynczych molekuł, a co za tym idzie na otrzymanie wysokorozdzielczych obrazów struktur DNA, które zostały wybarwione barwnikami DAPI, Hoechst 33258/33342 lub VdcV. Wysokorozdzielcze obrazy struktur DNA wybarwionych barwnikami Hoechst 33258/33342 zawierały aż do 3 x 10^5 sygnałów fluorescencyjnych pojedynczych molekuł. Barwnik Vybrant® DyeCycle™ Violet daje jeszcze lepsze rezultaty. Zdjęcia struktur DNA wybarwionych barwnikiem VdcV zawierały aż 10^6 sygnałów fluorescencyjnych pojedynczych molekuł. W przeciwieństwie do barwników Hoechst 33258/33342 oraz DAPI, barwnik VdcV nie wymaga użycia dwóch laserów o różnych długościach fal. Eliminacja jednego z laserów (tj. linii 405 nm) znacząco ułatwia proces rejestrowania danych i upraszcza układ optyczny. Podsumowując, dzięki zrozumieniu właściwości fotofizycznych badanych barwników, możliwym stało się wykorzystanie procesu fotokonwersji barwników DAPI, Hoechst 33258/33342 oraz Vybrant® DyeCycle™ Violet w mikroskopii wysokorozdzielczej. Pozwoliło to na uzyskanie obrazów struktur DNA o wysokiej rozdzielczości.

The aim of this doctoral thesis was to investigate the process of photoconversion of the DNA binding dyes, DAPI, Hoechst 33258/33342, and Vybrant® DyeCycle™ Violet, and to apply it in super-resolution fluorescence microscopy.

Background And Description Of The Conducted Research

CHAPTER 1. MICROSCOPY

1.1 Resolution of Images in Optical Microscopy

One of the most important parameters describing the quality of a microscopic image is its **resolution**. If the concept of resolution is considered purely theoretically it could be defined as *the shortest distance between two points in the specimen that are still visualised as separate entities*. In optical microscopy resolution in the lateral (horizontal) plane (1.1) is approximately two times better than the resolution in the axial plane (1.2), and both of them can be presented by the following equations (based on the theory described by E. Abbe in the second half of the 19^{th} century [1]):

$$Resolution(xy) = \frac{\lambda}{2(\eta * sin(\alpha))} \tag{1.1}$$

$$Resolution(z) = \frac{2\lambda}{(\eta * sin(\alpha))^2} \tag{1.2}$$

where η is the refractive index of the imaging medium, λ is the wavelength of light employed, and $\boldsymbol{n * sin(\alpha)}$ is the numerical aperture (NA) of the objective lens. However, in practice, the concept of resolution is much more complex. First of all, Abbe's microscopic definition of resolution does not refer to separation of single molecules, but to separation of the entire objects/structures (which are seen through a standard optical microscope, using transmitted light). It says that *if two objects (structures) are located at a distance smaller than the diffraction limit, then their visual separation is not possible*. A stained specimen usually contains many molecules, which, when illuminated, fluoresce simultaneously. Fluorescence signals of those molecules overlap and their visual separation becomes impossible. Second of all, the achievable resolution of an image is not only the result of the physical limitation of the light itself. Some other important factors that contribute significantly to the loss of resolution are: improper alignment of the microscope, using of incompatible immersion oils, inhomogeneity of the sample, application of coverslips having thickness outside of the optimum range, noise signal produced by the equipment, or aberrations of the optical system. Theoretically, using standard oil objective lenses that have the highest possible numerical aperture and wavelengths, which are applied to live cell imaging (i.e. wavelengths longer than 400 nm), the highest obtainable (by a typical confocal microscope) resolution is 180 nanometres in lateral (xy) and 500 nanometres in axial (z) plane [2]. However, in practice, due to aforementioned resolution-limiting factors, it is very hard to achieve the theoretical 180- and 500-nanometre limit.

In order to properly define the concept of resolution one more factor needs to be taken into consideration, i.e. the thickness of the sample. Even if the focus is set on the plane of interest, lasers applied to excite the molecules in focus will excite also other fluorescent molecules that are located below and above the investigated plane. These molecules will also emit fluorescence that will reach the detector. If the signal that comes from the investigated focal plane is not strong enough in comparison to the signal coming from the surrounding planes, then the contrast of the obtained image will be decreased. This is because in the final image blurred fluorescence signal of the molecules located outside of the focal plane will appear as well. This unwanted signal generates a *background* to the signal of interest. Thus, one should always consider the concept of microscopic resolution with reference to the thickness of the sample, and thereby with reference to **contrast** (where contrast is defined as *the difference in light intensity between the image of a fluorescent structure and its adjacent background*).

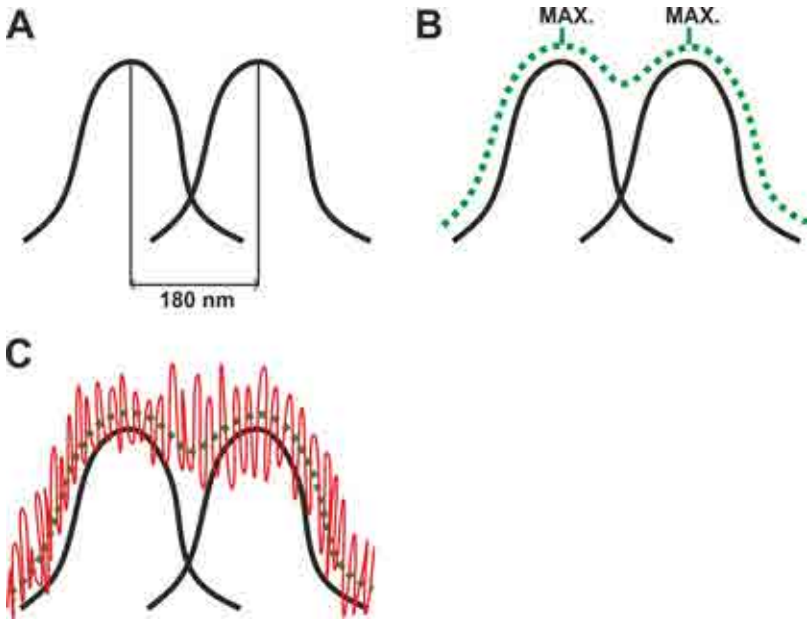

Figure 1.1 Fluorescence profiles of two biological structures located at the distance of 180 nm from each other, and the disruption of this signal by noise. A - Schematic fluorescence profiles of two biological structures located at the distance of 180 nm from each other. **B** - Schematic accumulated fluorescence signal generated after overlapping of the fluorescence profiles of the two molecules. **C** - Schematic noise signal that precludes visual separation of the two objects.

To illustrate this problem better the following example is presented. Figure 1.1A shows two fluorescence profiles representing objects that are located at the discussed theoretical distance of 180 nanometres. According to Abbe's diffraction limit it should be possible to resolve these objects as two separate entities. The fluorescence profiles of these two molecules overlap, and the fluorescence signal that could be registered by the microscope is presented in Figure 1.1B (*green line*). Using a perfect optical system (that is not impaired by any of the resolution-limiting factors discussed in the previous paragraph), the local maxima of the two functions representing the objects could be calculated and the presented structures could be resolved (Figure 1.1B). However, in reality the obtained signal is usually disrupted by the noise signal (Figure 1.1C, *red line*). Noise can be gen-

erated by the detector or by the overlapping signals coming from the excited fluorescent molecules located in the planes outside of the focus. Because the amount of the noise signal is large then, in reality, visual separation of these two objects is not possible.

In fluorescence microscopy signals are usually weak. If signals are weak then a low signal-to-noise ratio becomes a serious resolution-limiting factor. The actual resolution becomes much worse than the one described by E. Abbe. Elimination of the unwanted noise signals improves the resolution. It won't allow reaching a resolution beyond Abbe's limit, but at least it will allow reaching the theoretical 180-nanometre limit. Therefore, many modifications to standard fluorescence methods have been introduced in order to improve the resolution of the images. Some of the modifications are described below.

1.2 Improving Image Resolution

Over the years various modifications to standard fluorescence microscopy have been introduced in order to improve the quality of the images. One of the methods allowing increasing the image resolution is **Confocal Laser Scanning Microscopy (CLSM)** [3–5], where an additional pinhole (the size of which can be adjusted) is placed right before the detector (i.e. a photomultiplier (PMT) or an avalanche photo diode (APD)). This allows cutting off all of the light that is out of focus. A sample is illuminated with a focused light beam, and a specialised mechanical system scans the beam over the sample and collects fluorescence from a given region of the specimen [6]. Later, the image is reconstructed. By applying an additional confocal pinhole the thickness of the imaging section of the specimen is significantly decreased (down to ∼500 nm). Since the sample section is much thinner, many of the signals of the excited molecules that are out of the focus plane are cut off, and a significant improvement of the contrast (and thus resolution) of the acquired images is achieved.

In another example, for both techniques, **4Pi** [7–9] and **I^{5}M microscopy** [10], a set of two high aperture lenses placed opposing to each other is employed. With wavelengths interfering constructively these methods produce a narrower spot along the z axis, and hence an improved resolution up to ∼100 nm in the axial direction. The axial resolution is improved significantly, however, the resolution in the lateral direction remains unaltered.

In another approach a technique called **Multiphoton Absorption Microscopy** [11] employs a simultaneous absorption of two (in the case of two-photon microscopy) or three (in the case of three-photon microscopy) photons by the fluorophore. Two-photon microscopy uses red shifted excitation light, which minimises scattering in the tissue and enables great suppression of the *background*.

Another technique, **Total Internal Reflection Fluorescence Microscopy (TIRFM)** [12, 13], employs the phenomenon of generating an evanescent wave to illuminate and excite the fluorophores located close to the surface of glass, within a standard biological preparation. This technique exploits the phenomenon descibed by Snell's law. Light, after passing through an objective, reaches the glass medium (i.e. the cover slip) and later

the aqueous sample. If the incident light is directed at the angle θ, which is greater than the *critical angle* (θc), then it undergoes the phenomenon of *total internal reflection*. This critical angle is described by Snell's law: $\boldsymbol{\theta c = \arcsin(n_2/n_1)}$, where $\mathbf{n}_2$ is the refractive index of the aqueous medium and $\mathbf{n}_1$ is the refractive index of the glass medium (i.e. the coverslip), and $\mathbf{n}_2 < \mathbf{n}_1$. When θ is greater than θc, light, instead of being refracted onto the sample, undergoes total internal reflection (and never reaches the sample). At the same time some of the energy of the incident light is being propagated into the sample in a form of a very thin electromagnetic field called *evanescent field/wave*. This electromagnetic field/wave penetrates into the sample usually at depth smaller than 200 nm and has an identical frequency to that of the incident light (thus, it can excite fluorophores in the sample). With the increasing distance from the surface, the evanescent wave (or field) undergoes an exponential decay. Consequently, TIRFM can be used specifically for imaging very thin sections (usually < 200 nm) that are located very close to the coverslip. Since the imaged section of the sample is very thin, the *background* signal (coming from the molecules that are localised above and below the focal plane) is significantly lower than the signal of the molecules of interest (i.e. those localised in the focal plane). As a result, the output images have higher contrast.

The last example of improvement of the quality of images is **deconvolution** [14–16]. Deconvolution is an operation of reversing the process of convolution of n functions. This mathematical operation uses a PSF (*Point Spread Function*) and calculates the most probable object, which could have produced the microscopic image. Using this calculation all of the signals that produced blurry images (as they were not in focus) can be set back into focus, and then re-blurring of the single point images can be achieved. A very desirable *side effect* of this mathematical image processing is a significantly improved contrast of the processed images.

Although a series of resolution-limiting factors may affect and decrease the output resolution of an image, the major problem of fluorescence imaging is low signal-to-noise ratio. In widefield microscopy the imaged section of a specimen is thick and contains a lot of information not only from the focal plane (which is the plane of interest), but also from other planes above and below this plane (in a form of blurred signals). The *background* level of the structures of interest will never have low values, and the resolution of such obtained images will always be worse than the one described by Abbe's formula. In reality, any microscopic method that allows registering fluorescence signals from a thinner optical slice will hereby provide better resolution. That is why CLSM provides better resolution than standard widefield microscopy. That is also why TIRFM provides better resolution. And finally, that is why the concept of resolution should always be considered with reference to the concept of contrast.

1.3 Electron Microscopy (EM)

An alternative method to light microscopy that allows visualising specimens with resolution even down to $\sim$1 nm has been introduced in 1935 by M. Knoll and is called **Electron Microscopy (EM)** [17]. This method, instead of photons (as it is in the case of

light microscopy), uses accelerated electrons in order to collect images. However, electron microscopy is a relatively expensive, technically demanding and a very time-consuming method. Chemical fixation of the sample generates artefacts in the micrographs, moreover, electron microscopy precludes the possibility of imaging living organisms.

1.4 Optical Super-Resolution Microscopy

In the past two decades an optical microscopy technique called **super-resolution microscopy** has been introduced. The term super-resolution may be applied to any optical microscopy technique that allows increasing the resolution beyond the theoretical Abbe's limit. Conventional microscopy techniques are strongly limited by the imposed 180-nanometre resolution limit, while super-resolution techniques circumvent this restriction (*for details see below*). Even though super-resolution microscopy applies similar laser illuminations and similar objectives as those used in traditional microscopy, yet it manages to obtain much better resolution than any conventional microscopic method. The obtained (super-) resolution is indeed better than the one described by Abbe's formula, but not because the laws of physics have changed, or the formula isn't valid anymore. It is better because the microscope operates in a different way from a conventional microscope (as has been described *below*).

At this moment there are three main approaches to optical super-resolution microscopy, i.e. **Structured Illumination Microscopy (SIM)**, **Stimulation Emission Depletion (STED)** Microscopy, and **Single Molecule Localisation Microscopy (SMLM)**. All of these techniques are described below.

1.4.1 Structured Illumination Microscopy (SIM)

In **Structured Illumination Microscopy (SIM)** [18] the sample is illuminated with a patterned light to render high-resolution information that is normally unresolvable by conventional microscopy. This leads to an increase of the image resolution. In this technique a grid pattern of high spatial frequency (that has a known structure) is superimposed on the unknown pattern of the biological specimen. The grid is rotated generating Moiré fringes. Moiré fringes appear by mixing of the frequencies. One of the frequencies is the high spatial frequency of the applied illumination and the other is the frequency of the sample. Moiré fringes contain high-resolution information that cannot be resolved by a conventional microscope. During the measurement several images are taken at different positions and orientations, and later are computationally restored into a super-resolution image. Compared to widefield microscopy, this technique allows a two-fold improvement of the lateral xy resolution [18]. SIM is a very desirable and attractive technique due to the fact that almost all of the currently existing fluorescent dyes/probes are eligible for this method. Not only no special dyes/probes are required for SIM, but also all of the conventional multicolour combinations of labelling are possible in this method. Since one may use all conventional fluorescent dyes/probes, SIM gives a much broader choice of the fluorescent dyes/probes than any other current super-resolution imaging technique. However, the stability of the sample during image acquisition is an important issue. Images are taken one by one, and a typical acquisition takes time, so the image should remain still

during the entire experiment. 3D-SIM employs three illumination beams directed onto the sample. The light from the three illumination beams interferes and creates a spatially structured illumination pattern that is later used in the enhancement of the resolution of the images. With the doubled resolution in all three dimensions [19] SIM provides an option, which until today has not yet been commercially offered by STED microscopy.

1.4.2 Stimulated Emission Depletion (STED)

Stimulation Emission Depletion (STED) was first introduced by Stefan W. Hell in 1994 [20]. The main feature of this technique is that it applies two illumination beams to simultaneously excite the fluorescence and reduce the area where the fluorescence emission is observed (i.e. to an area much smaller than in the case of confocal microscopy). This allows the researcher to successfully separate fluorescence signals of interest from the signals of the surrounding molecules. As the area of the registered fluorescence is significantly decreased the signals are being separated not only from their *background* (i.e. blurry images of molecules from the planes above and below the focal plane), but also from signals of molecules that are adjacent to the registered ones (in the same focal plane). This way, the contrast, and hereby resolution, of the images are substantially increased. To achieve this, two laser beams are used during the experiment. The first laser is used to excite the fluorescence of the fluorophores. The second laser (the STED beam) is used to transfer back the excited fluorophores to their ground states by means of stimulated depletion. The STED beam is red shifted and has a specific cross-section shape resembling an American doughnut, with the high light intensity in a form of a ring that surrounds a small empty spot. The shape of the STED laser beam is formed by passing it through a phase plate. This way, all fluorophores that are off the centre of the PSF are illuminated with the STED beam and their emission is depleted. Fluorophores that are in the centre of the beam emit fluorescence since the intensity of the STED beam in this region falls to zero. Thus, signals of the fluorophores that are localised in the centre of the illumination beam are very efficiently separated from the fluorescence signals of the surrounding molecules.

Nonetheless, STED is not a simple method since it requires employment of specific fluorophores that reach an excited state, which can be depleted by a wavelength longer than their excitation. Moreover, those fluorophores should emit very bright fluorescence. Also, light intensity of the STED beam needs to be high enough to sufficiently deplete the excited states of the fluorophores. The higher the intensity of the STED beam, the smaller the region of the fluorescence that is not depleted, thus, the better the resolution [21]. One has to also remember that the used dye should not be excited with the STED beam, and the absorption of the wavelength of the STED beam (by the fluorophore) should not take place (since photobleaching is an undesirable outcome). Therefore, availability of fluorescent dyes/probes eligible for STED microscopy is limited. Despite the obstacles, this technique has been developed over the years, and so far successfully applied to biological specimens [22–24]. For example, two colour STED has already been introduced [25]. STED has also already been applied to live cell imaging [26–31]. Multicolour STED imaging still poses a lot of problems due to the fact that fluorescence spectra of fluorophores overlap. So far resolution up to 20 nm in the lateral plane [25, 32] and 45

nm in all three dimensions [33] has been achieved in STED microscopy. Even though this technique has become very popular and found its application in many branches of research, the equipment setup is still quite complicated. A limited choice of fluorophores constitutes the major limitation to this method.

In conventional STED microscopy a pulsed laser is used. Illumination with this laser is applied in synchronised cycles, i.e. immediately after exciting the fluorophore. At the same time, this STED illumination is applied for a fixed period of time, which is usually much shorter than the time of fluorescence emission of the fluorophore. Therefore, not all of the fluorescence emitted by the investigated fluorophores may be depleted. To avoid this problem a continuous wave STED (CW-STED) illumination may be introduced [34]. However, CW-STED illumination is usually applied at much lower intensities (than the intensity of STED beam in pulse-STED), and hence, it produces a less pronounced on-off contrast of the doughnut shaped beam. This, of course, means poorer resolution of the final image [34]. Since a successful depletion is not only a matter of the intensity of the STED beam that is responsible for the resolution, but also of the number of photons that a fluorescent molecule has been exposed to, a modification to standard STED microscopy has been introduced and is called **gated STED (gSTED)** [35–37]. Gated STED microscopy uses two types of illumination. For excitation of the fluorophores a pulsed laser is employed, and for depletion of the excited states of fluorophores a CW-STED beam with time-gated detection of the fluorescence is used [35]. Detection of the fluorescence takes place after a certain time delay (T_g) to make sure that the excited fluorophores had been exposed to STED illumination for a sufficient amount of time, to successfully deplete their excited states. At the same time, gated detection of the fluorescence allows increasing the on-off contrast of the fluorescence signals of the fluorophores, and, as a result, allows increasing the resolution of the acquired images. What is more, it allows applying a STED beam of lower (than in the case of conventional STED microscopy) power.

1.4.3 Single Molecule Localisation Microscopy (SMLM)

The third known group of methods of super-resolution optical microscopy relies on **Single Molecule Localisation Microscopy (SMLM)**. In this method positions of single fluorescent molecules are identified and registered in order to obtain high quality images. A fluorescently stained specimen consists of many molecules that can emit fluorescence. If the exact position of each of those molecules could be determined, a super-resolution image of the specimen could be reconstructed. Investigation of single molecules has been already pursued for many years [38–41], and nowadays has become extremely popular among various microscopic techniques. Localisation of a single molecule can be calculated using the following equation: $\textbf{localisation} = \mathbf{s}/\sqrt{N}$, where **s** is the standard deviation of the PSF and **N** is the number of the detected photons. The uncertainty in determining the single molecule position (so called *localisation precision*) can be presented by the following formula: $\textbf{localisation precision} = \Delta/\sqrt{N}$, where Δ is the width of the PSF and **N** is the number of the detected photons [42]. A stained biological sample contains many fluorescent molecules that are spaced closely together, and when excited, they all fluoresce simultaneously. Therefore, in a diffraction-limited area (which

contains thousands of simultaneously fluorescing molecules), it becomes impossible to visually separate single molecules. Due to overlapping of the fluorescence signals of the single molecules, the area becomes blurred. SMLM overcomes this problem by separating fluorescence signals in time (see Figure 1.2). By using photoswitchable, photoconvertible, or photoactivable dyes/probes (*for definition see below*) one can activate the fluorescence of only a few molecules at a time, leaving all of the remaining molecules in an inactive (non-fluorescent) state. Thus, one excitation cycle allows registering fluorescence signals of only a small fraction of fluorophores (the positions of which can be later determined). In this method, switching fluorophores *on* is done stochastically (contrary to STED microscopy), therefore, during one image acquisition this cycle is repeated over and over again until a sufficient number of single molecules is collected to fully reconstruct a super-resolution image. There are various SMLM techniques, which have different equipment setups or use various imaging conditions. Some examples include: **Spectral Precision Distance Microscopy (SPDM)** [43–45], **STochastic Optical Reconstruction Microscopy (STORM)** [46], **PhotoActivated Localisation Microscopy (PALM)** [47], or **fluorescence PhotoActivated Localisation Microscopy (fPALM)** [48]. However, regardless of the name and the differences between them, *all of these techniques are based on the same phenomenon – detecting the positions of single molecules.* A schematic drawing presenting the basis of single molecule localisation microscopy has been shown in Figure 1.2.

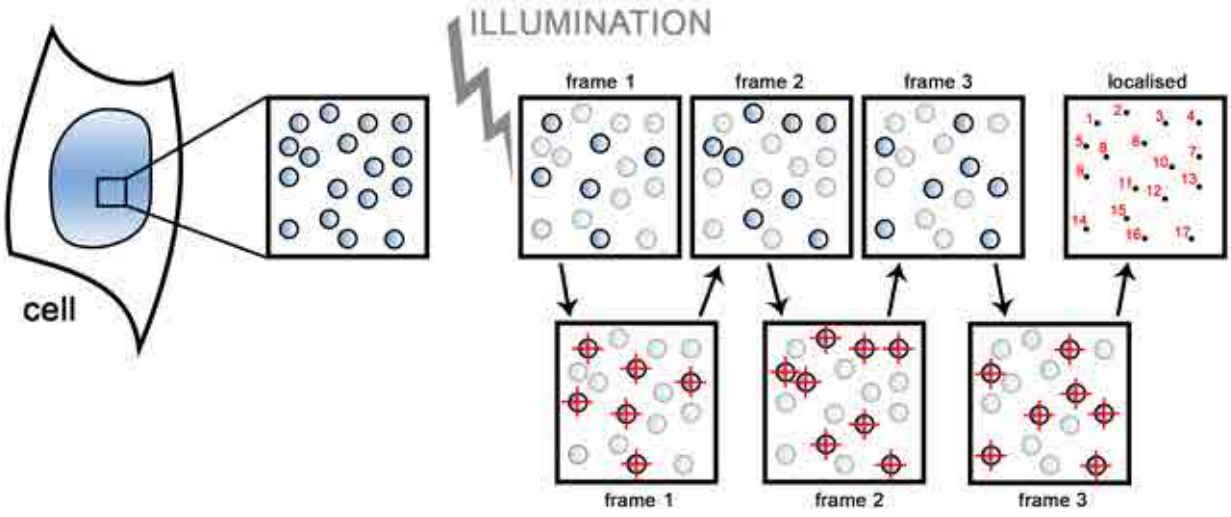

Figure 1.2 A scheme of a single molecule localisation microscopy experiment. The investigated biological specimen is stained with a chosen fluorescent dye. There are many single molecules of the dye piled together and fluorescing simultaneously. By employing specific environment and illumination only a few fluorescent molecules become fluorescent at a time. Images of stochastically appearing fluorescing single molecules are registered until a sufficient number of single molecules is collected in order to reconstruct a super-resolution image of an investigated specimen. Positions of single molecules are localised with high precision, and later a super-resolution image is reconstructed.

A part of the research presented in this doctoral dissertation was conducted in the laboratory of professor Christoph Cremer in Mainz, using the technique called **Spectral Precision Distance Microscopy (SPDM)** [43–45, 49]. SPDM is a single molecule

localisation microscopy technique based on reversible bleaching of fluorescent molecules. There are already many known fluorophores that, after being bleached, recover their original fluorescence properties in time. If such fluorophores are placed in a special oxidative-reducing environment, bleaching of their fluorescence and its recovery can be strictly controlled. First, the stained sample is illuminated with high power laser, to reversibly bleach the fluorophores. Later, a stochastic recovery of fluorescence is observed. Due to the strictly controlled imaging environment, this recovery of fluorescence takes place only for a few molecules at a time (for more details see Chapter 2, paragraph *Dark State Engineering*). Stochastically appearing fluorescing molecules are collected in a multi-frame image acquisition (each frame contains different molecules), analysed, and later reconstructed into a high-resolution image of the biological specimen. Three fundamental states of fluorophores appear in SPDM, i.e. the reversibly bleached state, the active state, and the irreversibly bleached state of the fluorophore. The ratio between the three states is strictly controlled by the environment of the fluorophore, as well as by the illumination of the sample with light of appropriate wavelength. One of the major advantages of SPDM is that the reversibly bleached state of a fluorophore can be obtained for many conventional fluorophores. At the same time, the method itself does not require any specific equipment, i.e. additional wavelengths etc. This simplifies the imaging equipment setup and staining procedures.

All of the described super-resolution techniques present particular advantages and disadvantages. None of the currently existing techniques enables quick, non-invasive, and effective visualisation of living specimens with significantly enhanced resolution in all three dimensions. One improvement is always at the expense of another. For example, SIM does allow imaging with an enhanced resolution in all three directions, but STED and SMLM reach much better resolution in the *xy* plane. Image acquisition using STED microscopy is significantly shorter than in the case of SMLM or SIM microscopy, therefore, STED is much more suitable for live cell imaging. However, laser powers applied in STED microscopy are very high, and thus, very often harmful to living specimens. Some SMLM techniques enable application of conventional fluorescent dyes, which do not have to possess any special properties, but since the acquisition of the images is quite long and the environment in which *blinking* behaviour is favoured is deprived of oxygen, visualisation of living specimens is much more difficult. Thus, there is a need for a constant development of the already existing methods, as well as, of the currently used (and new) fluorophores. However, one important fact should be emphasised, as even though super-resolution methods are not perfect yet (as they have been introduced just recently), all of them allow obtaining images with resolution much better than the resolution provided by any conventional microscopic technique. This step is so important, that in **October 2014 a Nobel Prize in Chemistry was awarded to Eric Betzig, Stefan W. Hell and William E. Moerner** '*for the development of super-resolved fluorescence microscopy*' [50]. Stefan W. Hell is the creator of the first STED microscope, while Eric Betzig and William E. Moerner have been awarded for their significant contribution to development of single molecule localisation microscopy. Nobel Prize is the most prestigious prize that can be awarded to a scientist, which only emphasises the fact that super-resolution microscopy are groundbreaking, important developments. A few years earlier a **Nobel Prize in Chemistry 2008 has been awarded jointly to Osamu**

Shimomura, Martin Chalfie and Roger Y. Tsien '*for the discovery and development of the green fluorescent protein, GFP*' [51]. This is another example of appreciation of how important this field of science is. Without fluorescent molecules today there would be no super-resolution optical microscopy. There would be no fluorescence microscopy. The described techniques of super-resolution microscopy are still very young and face years and years of development and improvements, but even at such young stage of their application, they have already taken microscopic imaging to a whole new level.

As the investigated dyes, DAPI, Hoechst 33258/33342 and Vybrant® DyeCycle™ Violet, have proven to be excellent candidates for SMLM imaging of the DNA structure (PAPER 1-3, [52]), the rest of this thesis will be focused on Single Molecule Localisation Microscopy.

1.5 Fluorescent Dyes/Probes for Single Molecule Localisation Microscopy

Specialised fluorescent dyes/probes applied in single molecule localisation microscopy have played an important role in development of this method. In conventional fluorescence microscopy dyes/probes are excited and their fluorescence is detected. The applied excitation induces not only their fluorescence emission but also their photobleaching. Photobleaching leads to loss of the fluorescence signal, and for years this process was thought to be irreversible. Therefore, new fluorophores have been continuously developed, in order to create dyes/probes that would be very bright and resistant to the process of photobleaching. However, over time it appeared that for some fluorophores, the process of photobleaching is in fact reversible, and the loss of the fluorescence by the fluorophore (previously ascribed to its photobleaching) may be compensated by the appearance of emission of its fluorescence at another wavelength, as the molecule itself would undergo some photo-induced reaction. The phenomenon of changing spectral properties of fluorophores was not new to science. Many examples of fluorescence changes associated with the environment of the sample had been already known (e.g. pH sensitive dyes [53], or e.g. Ca^{2+} indicators [54]). In many cases, though, the changing fluorescence properties were thought to be more of a *problem* than an asset. For years there was no apparent connection between the described spectral changes and a chance for obtaining better resolution of microscopic images. Only through better understanding of the structures and emission properties of the fluorescent dyes/probes this *problem* became in reality a *solution*. The light induced change of spectral properties turned out to be extremely useful in single molecule localisation microscopy, where the process of turning *on* and *off* of the fluorescence of various dyes/probes (using various wavelengths) is constantly applied. First single molecule localisation microscopy experiments were carried out using fluorescent proteins (e.g. Kaede [55], DendFP [56], EosFP, Dendra [57], PSmOrange [58]). Only later it was discovered that low molecular weight fluorescent dyes are suitable for this type of microscopy as well [59, 60]. This opened new possibilities.

Single molecule localisation microscopy requires employment of specialised fluorescent dyes/probes. A regular fluorescent dye/probe, when excited, emits fluorescence at specific wavelength, while the dyes/probes used in single molecule imaging present two modes of fluorescing. They can either be switched *on* and *off* between the *bright* (fluorescing) and *dark* (non-fluorescing) state, or they can change their spectral characteristics by changing their fluorescence emission. These dyes/probes can be divided into three major groups: photoactivable, photoconvertible and photoswitchable. **Photoactivable** dyes/probes can be activated from a *dark* state to *bright* fluorescence emission upon illumination with UV or violet light. **Photoconvertible** dyes/probes can be optically transformed from one fluorescence bandwidth to another. **Photoswitchable** dyes/probes have emission characteristics that can be alternatively turned *on* or *off* with specific illumination. Therefore, it is possible to create such conditions in which only a few molecules become fluorescent at a time, and their emission can be detected. This way, even molecules that are spatially located closer than the width of the PSF can be visually separated, circumventing the practical Abbe's diffraction limit. The only limitation to this method is the precision of determining the localisation of a single molecule. Until today, it has been shown that single molecules of the fluorescent dyes can be localised with precision reaching even 1.5 nm [61].

Fluorescent dyes/probes used for super-resolution microscopy should meet a number of conditions. A perfect fluorophore should be bright when activated. It should also provide an excellent contrast over the *background*. Spectral profiles for the active and inactive states should be well separated, and the fluorophore should be thermally stable. The fluorophore cannot randomly switch between the fluorescent and non-fluorescent states, except in a strictly controlled environment. The light controlled activation energy of the fluorophore should be higher than its spontaneous inter-conversion energies. Over the years many chemical compounds emerged as candidates for labelling cellular components in SMLM [62, 63]. They can be divided into several groups like: **Fluorescent Proteins (FPs)** (e.g. PA-GFP [64], mCherry [65], PS-CFP [66], Kaede [55], Dronpa2 [57], Phamret [67], EosFP [68, 69], mEos2 [70], mKikGR [71], Dendra [57], IrisFP [72], mOrange, mKate, and HcRed1 [73]), **low molecular weight dyes** (e.g. Carbocyanine dyes [74], Rhodamine B [75], Caged Q-Rhodamine [76], ATTO532 [32], Alexa Fluor 647 [77], Cy5, Cy5.5, Cy7 [77], DAPI, Hoechst 33258/33342, and Vybrant® DyeCycle™ Violet [PAPER 1-3, [52]]), **quantum dots** (e.g. Zn-Se QD [78]), or **hybrid systems** [79,80] with a genetically modified peptide attached to a synthetic membrane-permeant component. Every group of the aforementioned fluorescent compounds has its advantages and disadvantages. Synthetic fluorophores and quatum dots are brighter in comparison with fluorescent proteins, therefore, they provide better contrast for imaging [63]. PAFPs, on the other hand, provide a broader choice of the fluorophores. Nevertheless, fluorescent dyes are more versatile for labelling cellular components and are smaller in size, which usually means they can penetrate better into the sample. Some methods of labelling can be direct, with the fluorophore directly attached to the labelled component, and some labelling procedures require special techniques like immunostaining, which may hamper visualisation of living specimens.

Table 1.1 Spectral properties of some photoconvertible organic dyes and fluorescent proteins.

Fluorophore	Act. wave-length (nm)	Pre-Act. Abs. Max. (nm)	Pre-Act. Em. Max. (nm)	Post-Act. Abs. Max.	Post-Act. Em. Max.	Reference
Fluorescent proteins:						
EosFP	405	506	516	571	581	[68]
PAmCherry	405	-	-	564	595	[65]
KFP1	405	-	-	590	600	[81]
Dendra2	405	490	507	553	573	[82]
Kaede	405	508	518	572	582	[55]
Dronpa	405	-	-	503	518	[83]
Dronpa2, Dronpa3	405	-	-	486	513	[84]
rsFastLime	405	-	-	496	518	[85]
KikGr	405	507	517	583	593	[86]
PA-GFP	405	400	515	504	517	[64]
PA-CFP2	405	400	468	490	511	[66]
Organic dyes:						
Photochromic rodhamine B	375	-	-	565	580	[75]
Caged Q rhodamine	405	-	-	545	575	[Invitrogen]
Caged fluorescein	405	-	-	497	516	[Invitrogen]
DAPI	405	350	461	460	540	PAPER 1-3, [52]
Hoechst 33258	405	350	461	460	540	PAPER 1-3, [52]
Hoechst 33342	405	340	454	460	540	PAPER 1-3, [52]
Vybrant® DyeCycle™ Violet	405	369	437	460	540	PAPER 1-3, [52]

1.6 Hoechst, DAPI and VdcV as Candidates for SMLM Imaging of DNA

Controlled manipulation between the *on* and *off* states of the applied fluorophores is fundamental to single molecule localisation microscopy. With the high doses of light used in SMLM modern fluorophores should be photoresistant, i.e. when photoconverted, or in their *on/off* states, they should not undergo any additional chemical photoreaction, which would lead to the loss of their observed fluorescence. The current choice of fluorescent dyes/probes eligible for single molecule localisation microscopy is rather broad, and the research based on these fluorophores is constantly developing. Nevertheless, so far, the majority of the conducted research has been focused on cell structures that are easily accessible to the dyes/probes, like microtubules or actin filaments (e.g. by applying low molecular weight dyes (like e.g. Alexa Fluor 488) conjugated to antibodies [87]). One very

important field that seeks further investigation is research on DNA structure. DNA, due to its extremely dense packing in a cell nucleus, forms complicated structures. There are not many fluorescent dyes/probes eligible for super-resolution imaging of DNA. Even if the indirect forms of labelling are considered (e.g. fusions with proteins, immunolabelling) and the direct forms of labelling (e.g. using small DNA binding dyes), the choice of eligible fluorophores is still very limited. Additionally, it is not preferable to employ methods that require indirect sample labelling. For example, labelled histones, even though distributed regularly along the nucleic acids, sometimes fail to represent the exact distribution of DNA. Labelled histones do not reach each spot where the nucleic acids are located. Also the dyes/probes that are attached to histones sometimes can detach. This leads to a loss of a fluorescent signal. Therefore, the perfect fluorophore for imaging DNA should not only meet the expectations of the perfect SMLM probe, but preferably should be a directly binding molecule. Additionally, the denser the staining of DNA, the higher the spatial resolution can be achieved. Hence, small sized dyes are preferable. SMLM techniques have been available for nine years now, and so far several dyes have been presented as candidates for super-resolution imaging of DNA (e.g. YOYO, SYTO [88]). However, some of these dyes cause significant technical problems. For example, YOYO-1, even though has proven to be useful in super-resolution visualisation of chromatin [88]] initiates photo cleavage of DNA [89]. Another issue that is worth mentioning is the binding mode of the DNA dyes. YOYO-1 is an intercalator, which means that it binds to nucleic acids more strongly than any minor groove binding dye, and thus, it may perturb the structure of chromatin. Imaging of living cells stained with intercalating dyes that change the structure of DNA is strongly undesired. A more detailed description of the current research on super-resolution imaging of DNA can be found below in the paragraph entitled *Current Super-Resolution Imaging of DNA*.

Taking into account the currently existing need for small sized, directly binding DNA dyes, **excellent candidates for super-resolution imaging of DNA**, i.e. **DAPI, Hoechst 33258/33342**, and **Vybrant® DyeCycle™ Violet** [PAPER 1-3, [52]] are presented here. Even though DAPI and Hoechst dyes have been known for many years now, their exploitation in super-resolution microscopy has not been described so far, as their *blinking* behaviour has not been reported. The key to their successful exploitation in super-resolution microscopy is the process of their photoconversion, and generation of the green-emitting photoproducts [PAPER 1-2]. DAPI and Hoechst dyes bind to DNA by means of minor groove binding, which is an undeniable advantage, as the dyes themselves do not significantly perturb the chromatin structure. Additionally, all of the proposed dyes enable direct and dense labelling of DNA. They are of low molecular weight and they penetrate into the chromatin structures much more easily than antibodies or big fluorescent proteins. Photoconversion of DAPI, Hoechst dyes or VdcV so far has not been described, but the problem of the unusual fluorescence behaviour of Hoechst dyes and DAPI has been discussed for over 15 years on the confocal mailing list. Scientists have repeatedly raised this issue and tried to solve the enigma of an unexpected green/red fluorescence emitted in some experiments by DAPI or Hoechst dyes. No solution to this problem had been presented until 2010, when our Laboratory came up with an idea that the aforementioned enigmatic process of photoconversion of DAPI and Hoechst dyes may, in the future, prove useful for super-resolution imaging of DNA. In the light of so many

fluorescent photoconvertible dyes/probes applied in super-resolution microscopy, DAPI and Hoechst dyes looked as very promising candidates for imaging DNA with high resolution. While the research described in this dissertation was under way, at the beginning of 2012, an article was published describing photoconversion of DAPI [90]. This article only partly explained the phenomena of photoconversion of the dye in question. The authors did not elucidate the occurring process, nor did they describe the fluorescence properties of the photoproduct. The authors acknowledge only the phenomenon of photoconversion of DAPI. What is more, Piterburg et al. 2012 [90] even state that, despite the attempts, the authors have not observed photoconversion of Hoechst 33342. Shortly after publishing this article another paper was published [91]. In this paper the problem of using DAPI in combination with other green-emitting dyes is highlighted. Authors emphasise the fact that the signal of the photoconverted DAPI may overlap with the green fluorescence signal of other used dyes/probes, generating a false positive result of the experiment.

In the light of the existing lack of fluorophores eligible for visualisation of DNA, DAPI, Hoechst dyes and VdcV *came to the rescue*. Even though these dyes have been known for years now, they have not been applied in super-resolution microscopy yet. Even if the blue-emitting form of Hoechst dyes was forced to blink, the results were unsatisfactory, as the efficiency of the *blinking* process of the original blue-emitting form of Hoechst 33258/33342 was very low (almost negligible) [Żurek-Biesiada et al., unpublished]. However, we had an idea of applying the process of the photoconversion of the investigated dyes to obtain high-resolution images of the DNA structures. But first, the photophysics of this process had to be understood. Research using super-resolution microscopy has been focused for years now on structures of cellular components other than DNA. The structure of DNA is complicated and densely packed. It is not an easy structure to visualise. It is much easier to image biological components that are easily accessible to the already known fluorescent dyes/proteins. With DNA it is different. DNA is densely packed and the choice of dyes/probes eligible for visualisation of chromatin is limited. By explaining the process of photoconversion of DAPI, Hoechst dyes and VdcV, excellent candidates for DNA imaging have been provided. Research over the photoconversion process of the investigated DNA-binding dyes took several years, as the process itself is quite complicated [PAPER 1-2]. This dissertation demonstrates that only by proper understanding of the photophysical properties of the investigated dyes, DAPI, Hoechst and VdcV, these dyes became useful in SMLM. They bring new possibilities and new options to super-resolution imaging of DNA. The direct DNA binding mode, the small size of the dyes, a prospect of using them in live cell imaging – those are all undeniable assets. Big potential in these dyes lie in multicolour imaging, as we were already able to obtain dual-colour images of the DNA structures [52]. Another promising aspect of application of the investigated dyes lies in live cell imaging of DNA. Hoechst 33342 and VdcV pass easily through an intact biological membrane. The research described in this dissertation is just the beginning and only opens the multiple possibilities of obtaining better and better images of various DNA structures.

1.7 Investigated Dyes

Hoechst dyes belong to the family of *bis-benzimides*. They have strong affinity to DNA [92–97]. After binding to chromatin Hoechst 33258 may present a monomeric as well as a dimeric form [92]. There are four known commercial forms of Hoechst, which differ in one functional group: Hoechst 33258, Hoechst 33342, Hoechst 34580, and Nuclear Yellow (Hoechst S769121) [Invitrogen]. The chemical structure of Hoechst dyes is shown in Figure 1.3:

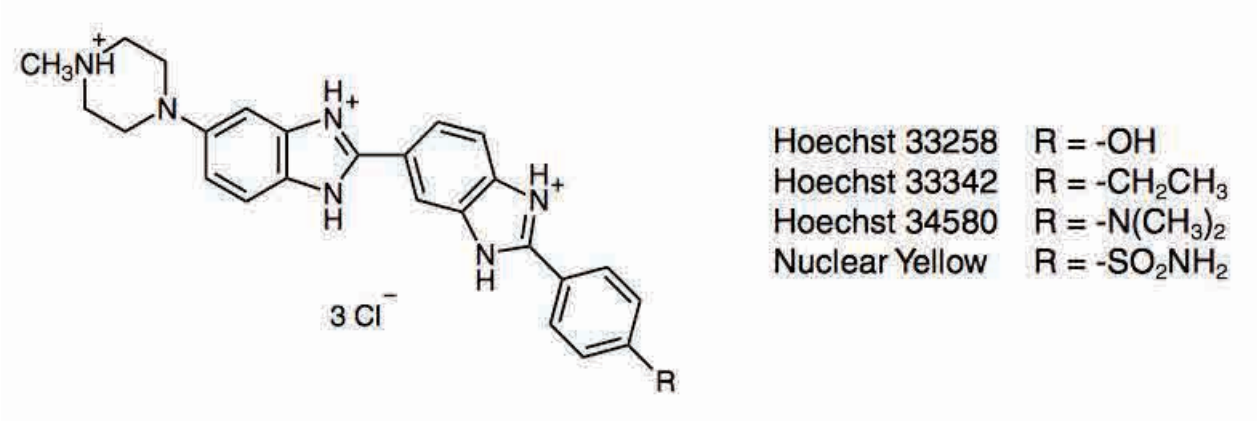

Figure 1.3 Chemical structure of Hoechst dyes. Source: [98]

Hoechst dyes are excited with UV and emit fluorescence in the blue range of the visible spectrum [99, 100]. Big Stokes shift permits application of these dyes in multicolour fluorescence microscopy. Maxima of the excitation and emission spectra for Hoechst dyes are presented in Table 1.2.

Table 1.2 Excitation and emission maxima of different forms of Hoechst.

Form of Hoechst	Excitation Maximum (nm)	Excitation Minimum (nm)
Hoechst 333258	350	461
Hoechst 33342	355	465
Hoechst 34580	392	440
Nuclear Yellow	335	495

The most commonly used forms of Hoechst dyes are the 33258 and 33342. Hoechst 33342 passes more easily through intact cell membrane, therefore, it is more often used for staining live cells. Hoechst 33258 is more often used for staining fixed samples. Hoechst dyes are soluble in water and relatively non-toxic, which permits visualisation of live samples for even up to two days.

Hoechst dyes are minor groove binders [101–104] that have strong affinity to A-T bases of the nucleic acids [102, 105–108]. After binding to DNA the fluorescence quantum yield

of these dyes increases significantly [94, 109–111], due to attaining a planary structure. Hoechst dyes also tend to form aggregates, especially at high concentrations (e.g. $>$ 10 mM [112] or 40 mM [111]).

Hoechst dyes are often used as fluorescence probes for measuring DNA quantity in a sample [113–117]. They inhibit topoisomerase I [118, 119] and topoisomerase II [120]. Hoechst dyes have antitumor [121] and antimicrobial [122] properties, and many discussions about their radioprotective role have been initiated [123–127]. Hoechst dyes are commonly used in testing against mycoplasma in cells *in vivo* [128].

DAPI (4',6-diamidino-2-phenylindole)

DAPI is a fluorescent dye used for visualisation of chromatin [129–131]. Even though its chemical structure varies from the structure of Hoechst dyes, it shares similar fluorescence properties. Maximum of excitation of this dye, in a form bound to DNA, can be observed at 340 nm, while maximum of fluorescence emission at 454 nm [132]. The chemical structure of DAPI is presented in Figure 1.4, below:

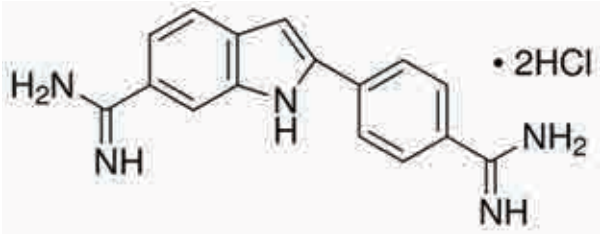

Figure 1.4 Chemical structure of DAPI. Source: [133]

DAPI can bind to RNA, nevertheless, this bond is much weaker than binding of DAPI to DNA [134]. DAPI, similarly to Hoechst dyes, is also a minor groove binder, and has strong affinity to A-T bases [135, 136]. In case of binding to RNA, DAPI intercalates and shows affinity to A and U [130, 135]. Just as in the case of Hoechst dyes, the efficacy of DAPI fluorescence increases significantly after binding to DNA [136].

DAPI can pass through intact cell membranes, and thus, can be used for staining live cells [137]. Nevertheless, in a fixed specimen it passes through cell membranes much more easily (than in the case of live intact cells), and therefore, is used mainly for staining fixed samples. DAPI can be used for detecting mycoplasma [138] or viruses [139] in a cell culture.

Vybrant® DyeCycle™ Violet

VdcV is a fluorescent dye with strong affinity to DNA. Fluorescence properties of this fluorophore are very similar to the aforementioned dyes, i.e. Hoechst dyes and DAPI. Maximum of the excitation spectrum of VdcV (bound to DNA) can be observed at 369 nm, and maximum of the emission spectrum at 437 nm. VdcV easily passes through intact cell membranes, and hence is used as a fluorescent dye for visualisation of DNA

in vivo [LifeTechnologies]. The chemical structure of VdcV remains unknown, as our request for disclosing the structure has been refused by the manufacturer (LifeTechnologies).

VdcV can be also used as a probe for assessing the quantity of DNA in the sample, since the emitted fluorescence signal is proportional to the DNA mass. This dye has low toxicity and, contrary to other DNA dyes, requires very low concentration to properly stain DNA *in vivo*. [LifeTechnologies].

1.8 Current Super-Resolution Imaging of DNA

Several approaches to super-resolution visualisation of the DNA structures have been introduced, but most of those approaches have major disadvantages. Intercalating dyes used for visualisation of DNA (i.e. YOYO-1, SYTO family [88]) can bind also to RNA [140], or their *blinking* behaviour might depend on the G-C content of the nucleic acids [141] (in order to objectively evaluate the applicability of Hoechst dyes in SMLM, I would like to point out that in a highly acidic environment Hoechst 33258 binds to RNA as well [PAPER 2], however, this only happens in a specific environment, and thus, can be controlled). YOYO causes photocleavage of DNA [89]. Various methods have been introduced to visualise DNA, including techniques of labelling of histones [142, 143], Fluorescence In Situ Hybridization (FISH) in combination with SMLM to visualise specific regions of DNA that contain repeated sequences [144], SIM performed on fixed cells [145], or STED performed on isolated DNA [146]. Also approaches of indirect DNA labelling, i.e. labelling of the associated proteins, have been introduced [142, 143, 147–149]. Unfortunately, none of these methods enable high-density labelling of DNA and reconstruction of images with high localisation precision (of single molecules) at the same time. The dyes presented in this dissertation enable both. By using DAPI, Hoechst 33258/33342 and VdcV it is possible to obtain high-density DNA staining along with high localisation precision of the registered single molecules.

In order to obtain high-density labelling of the DNA a click chemistry reaction for DNA labelling [150] in combination with carbocyanine fluorophores has been introduced [151]. The authors present images that contain up to 10^6 DNA-bound fluorophores. Here, I would like to point out that by using Vybrant® DyeCycle™ Violet it was also possible to detect 10^6 DNA-bound fluorophores [52], as well as more (even up to 5 x 10^6 fluorophores) [Żurek-Biesiada et al., unpublished].

Non-covalent binding of a dye to DNA constitutes an advantage. Non-covalent binding of the dye employs a much easier protocol, and has a smaller effect of sample perturbation. Using YOYO-1, which is a cyanine dye, one may obtain spatial resolution of 40 nm [141]. Another dye, which is less toxic than YOYO-1 is called SYTO-13 and can also be used in SMLM of the DNA imaging [141]. YO-PRO-1 has also proven useful in SMLM imaging of DNA [152]. PicoGreen has been shown to blink in dSTORM [153], and the main advantage of using PicoGreen is the fact that it specifically binds to dsDNA (and does not bind to RNA, like YOYO or SYTO).

Binding-Activated Localisation Microscopy (BALM) [154] employs the fact that a significant increase in quantum yield (800 times) of the fluorescence of YOYO-1 takes place upon binding to DNA [155]. Authors stained lambda phage DNA with an intercalating dye YOYO-1, and observed its *blinking* behaviour upon binding to DNA. The frequency of the binding behaviour was controlled via concentration of the dye. The authors reached the resolution of 14 nm and a high localisation density of YOYO-1. This method has been applied for a dye binding with a different mechanism – a minor groove binder PicoGreen, reaching spatial resolution down to 27 nm.

Another example of DNA imaging is a combination of the fluorescence activation by binding to DNA and single molecule imaging with photobleaching [156]. Here, two methods are used. One of them employs visualisation of single molecules based on the rate of their photobleaching (by subtracting the preceding image from the current one, which contains all molecules plus the fluorescence of the molecules that underwent bleaching in the current image). In the second method only bound molecules become fluorescent and bright, allowing localising them with high accuracy and obtaining resolution down to 25 nm [157]. Three fluorescent DNA dyes were used in this work: YOYO-1, POPO-3 and SYTO-16.

High-density DNA labelling is also possible using the Cy3-Cy5 pair and its photoswitching mechanism [158–160]. This pair can be activated at 532 nm, and deactivated at 633 nm. Cytosine base analogues can be incorporated into DNA [161], and when placed in close contact with a thiol compound, they can be used as a photoswitch. Not only the density of the fluorescent staining by Cy3-Cy5 is very high, but also the aforementioned process of photoswitching is reversible. The reversibility of this process allows controlling the photoswitching of Cy3-Cy5. What is more, these dyes are very bright, and therefore, provide bright images upon binding to DNA.

In the context of the existing research on super-resolution imaging of DNA, Hoechst dyes, DAPI and Vybrant® DyeCycle™ Violet are excellent candidates for high-density direct labelling of chromatin, and thus, for obtaining high-resolution images of the DNA structures (PAPER 3, [52]). DAPI and Hoechst dyes bind to DNA by means of minor groove binding, and do not significantly perturb the structure of chromatin. Moreover, the presented dyes are cell permeable, which facilitates their introduction into the cell nucleus and should simplify their application in super-resolution imaging of living specimens. This dissertation demonstrates that the key to their successful application in single molecule localisation microscopy imaging of DNA lies in understanding of the process of their photoconversion [PAPER 1-2]. Not only do the dyes enable unperturbed and direct labelling of the DNA structures, but they also enable DNA labelling with high density [52]. This phenomenon constitutes an excellent supplement for super-resolution imaging of DNA, as the newly introduced super-resolution methods are commonly applied, but still struggle with a significant deficiency in the suitable fluorescent dyes/probes.

CHAPTER 2. PHOTOPHYSICS

2.1 Electromagnetic Radiation

Electromagnetic radiation is built of waves of electric and magnetic fields travelling in space. Electromagnetic field oscillates, and this periodic change can be described by sinus and cosinus functions. Vectors of both components (of the electric and the magnetic field) change simultaneously perpendicular to each other, and perpendicular to the direction of the propagation of the electromagnetic field (x). The electromagnetic spectrum consists of various wavelengths of radiation (having various energies). The visible form of radiation is called **light**, which along with **UV** constitutes only a small part of the entire electromagnetic spectrum (see Figure 2.1). **Light** is a form of electromagnetic radiation that presents dual nature. It exhibits properties of not only particles, but also waves. This phenomenon is called *wave-particle duality of light*. It means that for some phenomena the properties of light can be described better using the *wave theory*, and for other they can be described better using the *particle theory*. From the point of view of the wave theory, light can be described by its **wavelength (λ)**, **number of oscillations of the field that take place during one second *(υ)***, and **number of oscillations of the field that will happen when light travels one centimetre ($\upsilon*$)**. From the point of view of the particle theory, light is a collection of **portions of energy**, i.e. **quants of energy**, which travel in the direction of propagation of the electromagnetic field. The single quantum of energy is called a **photon** and has the energy of Planck's quantum $\mathbf{hc}/\lambda$, where **h** is the Planck's constant, **c** represents the speed of light (c = 2.99 x 10^8 m/s), and λ is the wavelength of radiation. Planck's quantum theory unifies the particle and wave nature of light. It says that the energy carried by light is inversely proportional to its wavelength, what can be presented as follows: $\mathbf{E}\lambda = \mathbf{hc}$, where **E** is the photon energy, λ is photon's wavelength, **h** is Planck's constant, and **c** is the speed of light.

Ultraviolet (UV) radiation ranges in wavelength from 10 to 400 nm. It demonstrates very high biological activity [162]. Three bands of UV radiation are distinguished (UV-A: 315 - 400 nm, UV-B: 280 - 315 nm, and UV-C < 280nm) [163]. Ultraviolet can be harmful to living organisms as it is absorbed specifically by DNA and RNA, and can compromise genome integrity [164–169]. At the same time, many of the commercially applied fluorophores are excited with UV or 405 nm illumination. Some examples include: Alexa Fluor 350; Cascade Blue, Marina Blue, Pacific Blue, DAPI, Hoechst 33258/33342, 7-amino-4-methylcoumarin (AMC), Calcein Blue, Dansyl derivatives, Fluoro Gold, Pyrene, or True Blue. UV illumination is also the most commonly used wavelength to cause photoconversion of the PAFPs, some examples include: PA-GFP, Kaede, PS-CFP-2, tdEosFP, Den-

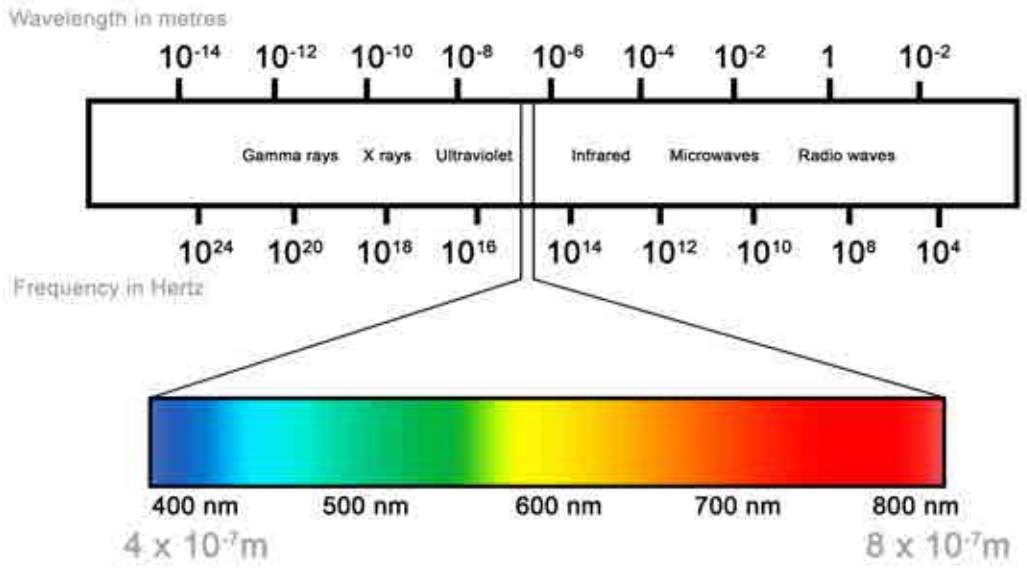

Figure 2.1 The electromagnetic spectrum.

dra2, Dronpa, PamRFP-1, KikGR, or PAmCherry [170]. Most of the listed dyes/probes are excited with UV and emit fluorescence in the blue region of the visible spectrum. Thus, they can be applied in combination with other, green-, yellow-, or red-emitting dyes/probes (i.e. in multicolour labelling of the sample).

2.2 Photochemical Reactions

Photochemistry is the basis of all of the photo-biological reactions. Before excitation the electronic configuration of a molecule (**M**) is described as a ground state. Upon excitation, when the molecule (**M**) absorbs a quantum of light, electrons of the molecule are raised to a higher energy state, and the molecule reaches an excited (activated) state ($\mathbf{M}^*$). This phenomenon can be described as follows:

$$\mathbf{M} + \mathbf{light} \rightarrow \mathbf{M}^*$$

Molecules in their excited states often present different spectral or chemical properties (than in their non-excited states), since the distribution of electrons change, and so do the forces between the nuclei. Excited molecules aim to release this extra dose of energy. How they release it depends strongly on the type and form of the molecule (i.e. in form of e.g. light, or e.g. heat). **The First Law of Photochemistry (the Grotthus-Draper law)** says that for a photochemical reaction to occur light has to be absorbed by the molecule. **The Second Law of Photochemistry (the Stark-Einstein Law)** says that in a chemical system one molecule absorbs only one photon of light. However, this rule applies to regularly applied low power lasers. If a high power laser is used, two- or even three-photon absorptions may occur.

There are several types of photochemical reactions, some examples include: **linear additions to unsaturated molecules** (e.g. the photochemical crosslinking of the DNA

with proteins), **cycloadditions of unsaturated molecules** (e.g. dimerisation of the thymine bases in DNA), **photofragmentation** (e.g. riboflavin can be fragmented to form lumiflavin), **photooxidation** (e.g. cholesterol can be photooxidised by addition of the peroxy group), **photohydratation** (e.g. after UV-illumination uracil can add a molecule of water), ***cis-trans* isomerisation** (e.g. conversion of *trans*-retinal to *cis*-retinal, ethane $H_2C{=}CH_2$), or **photorearrangement** (e.g. conversion of the 7-dehydrocholesterol into vitamin D_3).

Photoconversion is a chemical reaction that can be assigned to the category of photo-rearrangement reactions. The word *photoconversion* consists of two words, *photo*, suggesting the involvement of light, and *conversion*, suggesting rearrangement. For the purpose of this thesis *photoconversion* (in the context of fluorescence microscopy) has been defined as the **chemical transformation of the fluorophore, which is caused by exposing the fluorophore to irradiation of specific wavelength, intensity, and duration, and leads to a change of the spectral properties of the illuminated dye**.

Protonation, on the other hand, is **the chemical reaction in which a proton (H^+) is added to an atom, molecule, or an ion**. Living organisms keep a very strict control over the intracellular pH dynamics in order to protect their components from any influence of acidic or alkaline factors. Even a slight change in pH may change the ionisation state of all of the weak bases or acids in the cell. Protons are very prone to attaching themselves to surrounding molecules (e.g. as a result of exposure to UV). Protonation that is accompanying spectral changes of fluorophores is not an unusual phenomenon in microscopy [171–174]. Additionally, it is often accompanied by *cis-trans* isomerisation of a fluorescent molecule [175, 176], which in the end leads to a change in spectral properties of the fluorophore.

2.3 Known Mechanisms of Photoconversion of PAFPs

Photochromism is a common phenomenon in fluorescence microscopy. The changing spectral properties of various dyes were already investigated almost two decades ago [177]. Since nowadays photoswitchable fluorescent dyes/probes have become so useful in super-resolution microscopy, many scientists try to understand the mechanisms underlying changes in their fluorescence emission. Based on their photochemical properties, PAFPs can be divided into three categories.

The first category consists of PAFPs that undergo irreversible photoconversion. For PA-GFP [64], PS-CFP and its variant PS-CFP-2 [66], PAmRFP-1 [178], and PAmCherry [65], the mechanism underlying the change in spectral properties is deprotonation of the chromophore. The excitation spectrum of the wild type Green Fluorescent Protein (wtGFP) contains two peaks, at 396 nm and 476 nm. These peaks correspond to the neutral (protonated) and anionic (deprotonated) form of the GFP chromophore, respectively [179–181]. Illumination with UV can change the ratio of the protonated and deprotonated forms in favour of the anionic form [182]. Upon UV illumination, decar-

boxylation of Glu222 takes place, which leads to rearrangement of the hydrogen-bonding network and a subsequent deprotonation of the GFP molecule [183, 184]. The PA-GFP is a form of GFP, in which threonine has been replaced with histidine at position 203. The probe exists mostly in its neutral form [64]. UV irradiation causes an irreversible conversion of the PA-GFP chromophore from neutral to its anionic form. The inactive form of PA-GFP has its excitation/emission maxima at 400/515 nm. Illumination of this inactive form with UV causes its irreversible photoconversion to an anionic form, which is easily excited at 504 nm, and emits fluorescence at 517 nm. The photoconversion results also in a 100-fold increase in the green fluorescence intensity of the anionic form [64]. PS-CFP and PS-CFP-2, in their ground states, have their excitation/emission maxima peaks at 400/470 nm. When PS-CFP-2 is illuminated with UV, it converts to a form that is easily excited with 490 nm and emits fluorescence at 511 nm. Also, a significant (400-fold) increase in the green fluorescence emission takes place. Another probe, PAmCherry, in its ground state, is non-fluorescent. Upon UV illumination deprotonation of the chromophore takes place and the protein becomes fluorescent. When fluorescent, it is easily excited at 564 nm and emits fluorescence at 595 nm. An increase in the red fluorescence intensity in the case of PAmCherry is 4000-fold.

The second category of PAFPs contains proteins such as: Kaede [55], EosFP and its variants [68], KikGR [86], Dendra [57], and Dendra2 [82]. For these proteins the mechanism of photoconversion is different. The green-emitting properties of Kaede are the result of the presence of a tripeptide His62-Tyr63-Gly64 in its chromophore. Once the protein is illuminated with UV, a cleavage appears between the amide nitrogen and the α carbon (C_α) of the His62 residue of the chromophore. Subsequently, a double bond is formed between the two carbon atoms of the His64 residue (C_α and C_β), which results in a red-shifted emission of Kaede [185]. The process is irreversible.

The third category consists of proteins, such as: KFP-1 [81, 186] and Dronpa family [187] (rsFastLime [85], Dronpa-2 and Dronpa-3 [84]). In the case of these fluorescent probes photoconversion can be either irreversible or reversible, from a *dark* (non-fluorescent) to a *bright* (fluorescent) state. The suggested mechanism underlying the spectral changes is *cis-trans* isomerisation accompanied by deprotonation. Unless illuminated with green or yellow light, KFP-1 remains non-fluorescent. Upon illumination with green light it converts to a form that is easily excited at 580 nm and emits fluorescence at 600 nm. When illumination is stopped, the chromophore slowly relaxes back to its non-fluorescent, ground state [188]. The process of KFP-1 photoconversion can be easily reversed by illumination of the fluorescent form with blue light. *Cis-trans* isomerisation has been proposed to explain the photoconversion of KFP-1 [186,189,190]. *Cis-trans* isomerisation has been also suggested to be the photoconversion mechanism for asFP595 [191], IrisFP [72], Padron [192]; Faro, 2011 [193], and rsTagRFP [171]. The mechanism underlying the spectral changes of Dronpa [57, 187] is still under debate. One possibility for explaining the photoswitching behaviour of Dronpa is *cis-trans* isomerisation of this protein [194]. In this scheme the protein converts from a fluorescent (green-emitting) form to a non-fluorescent form upon illumination with blue light. Blue light converts Dronpa to its neutral (non-fluorescent) form. This process is reversible, and the non-fluorescent form can be re-activated using 400 nm light. The second possibility to explain the photocover-

sion of Dronpa excludes *cis-trans* isomerisation. A protonation/deprotonation scheme has been proposed [83, 195–197], in which protonation and deprotonation (which are induced by light) of the chromophore lead to changes in flexibility of the surrounding structure of the chromophore. The changing structure of the protein is manifested in changing spectral properties. However, this process does not necessarily require *cis-trans* isomerisation of the molecule.

2.4 Dark State Engineering

Many PAFPs undergo the phenomenon of photoconversion enabling controllable switching between their fluorescence emissions. Another approach to visualise single molecules is based on stochastic recovery of the fluorescence of a fluorophore (i.e. it is applied in SPDM). The idea underlying this approach is to transfer the majority of the fluorescing molecules into their *dark* (non-fluorescent) state, and allow slow recovery of the fluorescence by only a few random molecules at a time. This approach is called **dark state engineering** [60, 198]. By controlling the electron transfer reactions one may control reaching the *dark* state of the molecule [199]. Basically, a molecule oscillates between three states: the *ground state (G)*, the *bright state (B)*, and the *dark state (D)* [60]. It is possible to induce a *dark state* for almost every fluorophore [198], which eliminates the need to apply special photoconvertible or photoactivable dyes, and provides a very broad choice for the fluorophores. Also fluorescent proteins can be driven into the *dark* states [177]. The key to a successful application of dark state engineering in super-resolution microscopy is to achieve conditions in which molecules exhibit short and very bright *bright* states, and long and dark *dark* states, to successfully separate the bright molecules from the others - the inactive ones. In recent studies it has been shown that by using a special embedding media (polyvinyl alcohol, glucose oxidase, catalase) one may induce *dark* states of conventional fluorochromes [200]. It has been also proven that for some fluorophores glucose oxidase oxygen scavenging system promotes *blinking* [200]. Other papers showed that inducing *dark* states of the fluorophores was also possible in standard aqueous or glycerol media (for Alexa 488, Alexa 568, tetramethyl rhodamine iso-thiocyanate and fluorescein) [60]. Reversible photobleaching of these dyes was also observed in the air, in dry samples [60]. Many attempts to explain the mechanism underlying dark state engineering have been made, and models proposing a triplet state [200], electron transfer between the dye and the buffer [62, 88, 152, 198, 199], or the reversible addition of thiol radicals [201, 202] have been presented.

PAPER 1:

UV-Activated Conversion of Hoechst 33258, DAPI, and Vybrant DyeCycle Fluorescent Dyes into Blue-Excited, Green-Emitting Protonated Forms

Cytometry PART A

UV-Activated Conversion of Hoechst 33258, DAPI, and Vybrant DyeCycle Fluorescent Dyes into Blue-Excited, Green-Emitting Protonated Forms

Dominika Żurek-Biesiada,[1] Sylwia Kędracka-Krok,[2] Jurek W. Dobrucki[1]*

[1]Division of Cell Biophysics, Faculty of Biochemistry, Biophysics, and Biotechnology, Jagiellonian University, Kraków, Poland

[2]Department of Physical Biochemistry, Faculty of Biochemistry, Biophysics and Biotechnology, Jagiellonian University, Kraków, Poland

Received 29 October 2012; Revision Received 11 December 2012; Accepted 5 January 2013

Grant sponsor: Polish National Committee for Science; Grant number: UMO-2011/01/B/NZ3/00609; Grant sponsor: EU structural funds; Grant number: POIG.02.01.00-12-064/08.

*Correspondence to: Jurek W. Dobrucki; Division of Cell Biophysics, Faculty of Biochemistry, Biophysics, and Biotechnology, Jagiellonian University, Gronostajowa 7, 30-387 Kraków, Poland

Email: jerzy.dobrucki@uj.edu.pl

Published online 15 February 2013 in Wiley Online Library (wileyonlinelibrary.com)

DOI: 10.1002/cyto.a.22260

Abstract

Hoechst 33258, DAPI and Vybrant DyeCycle are commonly known DNA fluorescent dyes that are excited by UV and emit in the blue region of the spectrum of visible light. Conveniently, they leave the reminder of the spectrum for microscopy detection of other cellular targets labeled with probes emitting in green, yellow or red. However, an exposure of these dyes to UV induces their photoconversion and results in production of the forms of these dyes that are excited by blue light and show fluoresce maxima in green and a detectable fluorescence in yellow and orange regions of the spectrum. Photoconversion of Hoechst 33258 and DAPI is reversible and independent of the dye concentration or the presence of DNA. Spectrofluorimetry and mass spectrometry analyses indicate that exposure to UV induces protonation of Hoechst 33258 and DAPI.

Key terms

Hoechst 33258; DAPI; Vybrant DyeCycle; UV-excited DNA dyes; photoconversion; protonation

Introduction

Hoechst 33258, DAPI, and Vybrant DyeCycle Violet are common fluorescent dyes used for staining DNA and visualization of chromatin in cell nuclei by fluorescence and confocal microscopy. DNA-bound Hoechst 33258, DAPI, and DyeCycle Violet have their excitation maxima in the UV region of the spectrum and their emission maxima in the 430–470 nm region (exc./em. 355/465; 364/454, 369/437 nm, respectively). These spectral properties make Hoechst 33258, DAPI, and Vybrant DyeCycle Violet convenient nuclear dyes as the remaining range of the visible spectrum can be used for detecting other subcellular targets, using dyes emitting in green, yellow, up to infrared. We demonstrate, however, that the UV-excited dyes are not entirely stable when excited with the UV emitted by mercury arc lamps or 405 nm wavelength light emitted by a laser. Exposure to ultraviolet light of a biological specimen stained with Hoechst 33258, DAPI or Vybrant DyeCycle™ Violet during a typical fluorescence or confocal microscopy observation leads to conversion of these dyes into forms that can be excited by blue light and emit green fluorescence (em. max. approx. 520 nm, with detectable signal intensities in the yellow to orange region of the spectrum). Using mass spectrometry we demonstrate that UV induces protonation of Hoechst 33258 and DAPI. Photoconversion of UV-excited dyes bound to DNA in biological samples may pose problems for image analysis in multicolor fluorescence microscopy. Even relatively small doses of UV result in creating a false positive—a green fluorescence signal derived from the DNA-bound dye, which is expected to fluoresce in the blue region. Following photoconversion, the unexpected emission arising from Hoechst or DAPI may be mistakenly interpreted as a green fluorescent signal expected to arise from another fluorescent probe used in the same

ISAC International Society for Advancement of Cytometry

experiment. Problems arising from light-induced changes of the spectral properties of DAPI and Hoechst have been reported by the subscribers of the confocal microscopy list server and in recent published work (1).

Materials and Methods

Cells

MSU 1.1 human fibroblasts (2) were grown in Dulbecco's Modified Eagles Medium (Sigma-Aldrich, Poland) supplemented with 10% fetal bovine serum, penicillin (50 units/ml), and streptomycin (50 μg/ml), in tissue culture Petri dishes (Techno Plastic Products AG, Switzerland) at 37°C, in a humidified atmosphere of 95% air and 5% CO_2. Cells were grown on 20 mm-diameter coverslips (Menzel-Gläser, Germany).

Cells were fixed with 4% formaldehyde (Electron Microscopy Science) using standard formaldehyde fixation protocol and later stored in 1% formaldehyde solution for 1–2 weeks before the experiment.

Cell Staining

Cells were stained with DAPI (4′,6-diamidino-2-phenylindole) (3,4) (Sigma-Aldrich, Poland) at 1 μM, Hoechst 33258 (5–7) (Sigma-Aldrich, Poland) at 2 μg/ml, or Vybrant DyeCycle™ Violet (Invitrogen) at 1 μM. Cells were rinsed three times with PBS, permeabilized with 70% ethanol (30 s) and incubated in a dye solution for 30 minutes at room temperature (RT).

Acquisition of Fluorescence Images

Images were recorded using Leica TCS SP5 confocal microscope (Leica Microsystems, Germany), equipped with a 63 × 1.4 NA oil immersion lens. The 512 × 512 pixel images (field of view 82 × 82 μm or 145 × 145 μm) were recorded. PMT gain was set at 860 V; confocal iris was set at 1 Airy disk. When studying the process of UV-excited dye photoconversion, coverslips with the attached fixed cells were mounted in custom made steel holders, placed in a microscope stage and imaged at RT or 37°C in PBS (fixed cells). For excitation Ar ion gas (458, 476, 488, 496, 514 nm, 100 mW output) and 405 nm diode (3 mW output) lasers were used. For imaging DAPI and Hoechst photoproducts, the intensity of all Ar laser lines was adjusted to 1.25 mW or 0.95 mW. Fluorescent dyes were photoconverted using UV light emitted by a Leica EL6000 mercury metal halide lamp passed through a 360/40 nm emission filter (11 mW, measured with a FieldMaxII Laser Power Meter [Coherent, Santa Clara, CA]). Over 40 experiments were performed to demonstrate the process of DAPI photoconversion and over 60 for Hoechst 33258.

Studies of Hoechst 33528 and DAPI Immobilized in a Polymer Block

To immobilize the dye, a polyvinyl polymer [described in (8)] doped with DAPI at the concentration of 10 μM, or Hoechst 33258 at the concentration of 20 μg/ml, was made.

Data Analysis

Images were analyzed and processed using LAS AF Lite (Leica Microsystems, Germany) and MacBiophotonics ImageJ (http://rsbweb.nih.gov/ij/) software. The displayed images were not manipulated beyond adjusting the γ-function, as noted in figure legends.

Mass Spectrometry

For mass spectrometry (MS) measurements the solutions of DAPI at 70 μg/ml and Hoechst 33258 at 100 μg/ml were used. Protonation products were detected in the solutions of the dyes following addition of H_2O_2 (4% final concentration). Exposure to the UV was performed on a microscope stage of the confocal system, by illuminating the samples with the light emitted from a Leica EL6000 mercury metal halide lamp equipped with a 360/40 nm filter. Measurements were performed with the MicrOTOF-QII mass spectrometer (Bruker, Germany) in a positive ionization mode, using an Appollo Source ESI sprayer. Before measurements the device was calibrated with TuneMix solution. The MS spectra were analyzed using Data Analysis 4.0 software (Bruker, Germany).

Spectrofluorimetry

DAPI or Hoechst 33258 (10 μM) were dissolved in distilled water or in a 30% hydrogen peroxide solution (Sigma-Aldrich, Poland). Samples were placed in quartz cuvettes and analyzed using Horiba Jobin Yvon Fluoromax-P spectrofluorimeter.

Results

UV-Induced Changes of Spectral Characteristics of Hoechst 33258 and DAPI

We first examined spectral properties of the Hoechst 33258 and DAPI samples used in this work. The free dyes in solutions as well as the dyes bound to DNA were investigated by spectrofluorimetry and spectrally resolved confocal microscopy (Figs. 1A–1F). Their spectral characteristics were in agreement with the published data (3,7).

When cells stained with Hoechst 33258 were examined using a fluorescence confocal microscope, the expected blue emission excited by 405 nm light was readily seen in nuclei (Fig. 2D) and only a negligible signal of the green fluorescence of Hoechst 33258 was detected (exc./em. 458/480–600 nm) (Fig. 2E). A 60 second exposure of the specimen to the UV emitted by a standard mercury halide lamp resulted in a decrease of the blue fluorescence that would typically be ascribed to photobleaching (see below). Following an exposure to UV, we also detected a concomitant appearance of green fluorescence that was readily excited by blue light in the nuclei of the imaged cells (Fig. 2F). This green emission was only marginally excited by the 405 nm light. The adjacent cells, which had not been exposed to UV previously, exhibited only a negligible green emission. Thus, the green fluorescence was clearly induced by an illumination with the UV or 405 nm light. A similar appearance of the green emitting forms of the dyes was observed when DAPI or Vybrant DyeCycle™ Violet

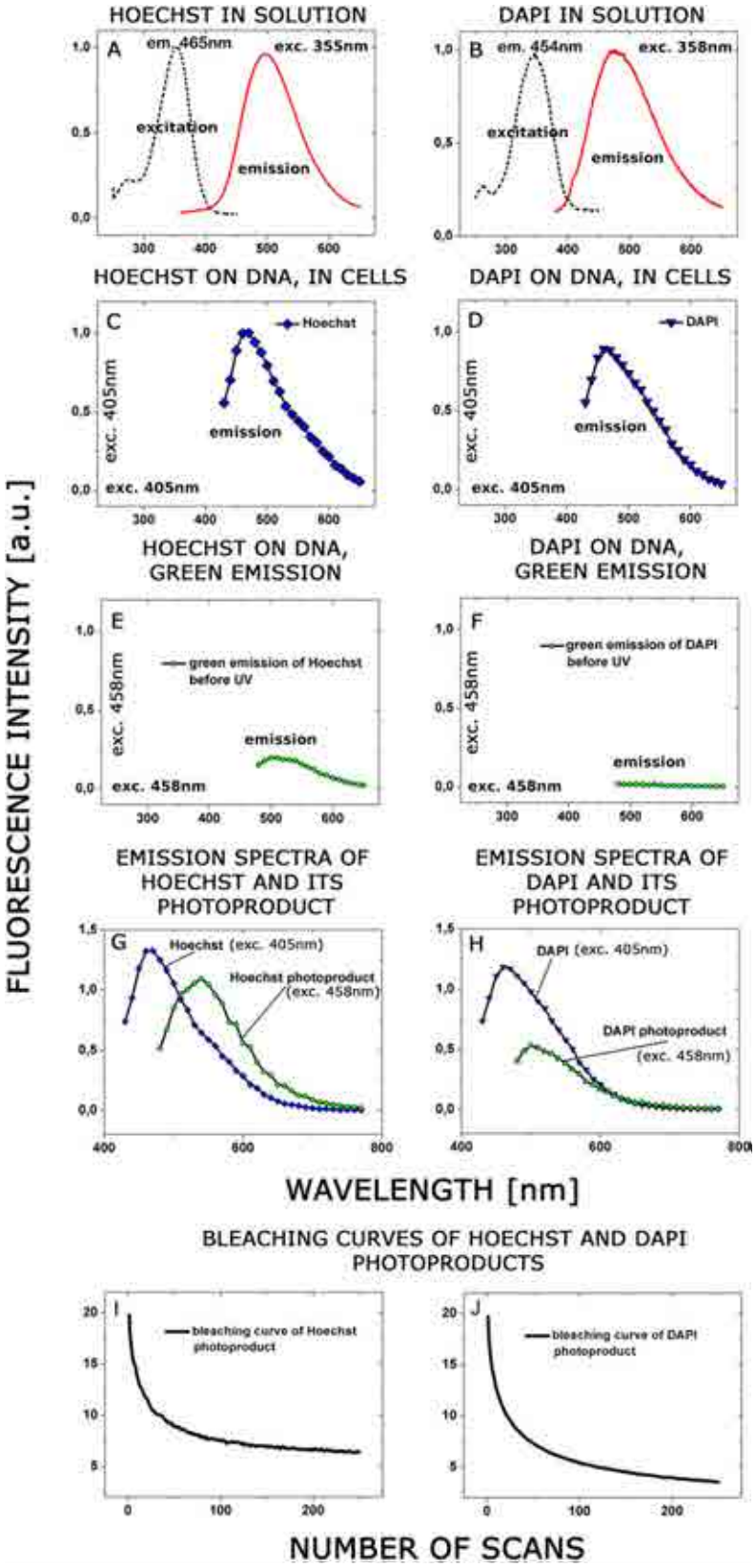

Figure 1. Spectral properties of Hoechst 33258 and DAPI and their respective photoproducts, studied by spectrofluorimetry (**A**,**B**) and confocal microscopy (**C**-**J**). **A**,**B**: excitation and emission spectra of Hoechst (**A**) and DAPI (**B**) in solution measured in a spectrofluorimeter. **C**,**D**: emission of the blue fluorescence by Hoechst 33258 and DAPI (exc. 405 nm) in fixed cells, measured in a confocal microscope. **E**,**F**: emission of the green fluorescence by Hoechst 33258 and DAPI (exc. 458 nm) prior to UV illumination, i.e., before generation of the photoproduct. **G**,**H**: emission spectra of Hoechst and DAPI original dyes and their respective photoproducts, measured in a microscope. **I**,**J**: photobleaching of the photoproducts of Hoechst 33258 and DAPI in nuclei of fixed cells, exposed to 458 nm light. Cells were scanned with the laser beam in a manner identical with standard imaging, as described in Materials and Methods. [Color figure can be viewed in the online issue, which is available at wileyonlinelibrary.com.]

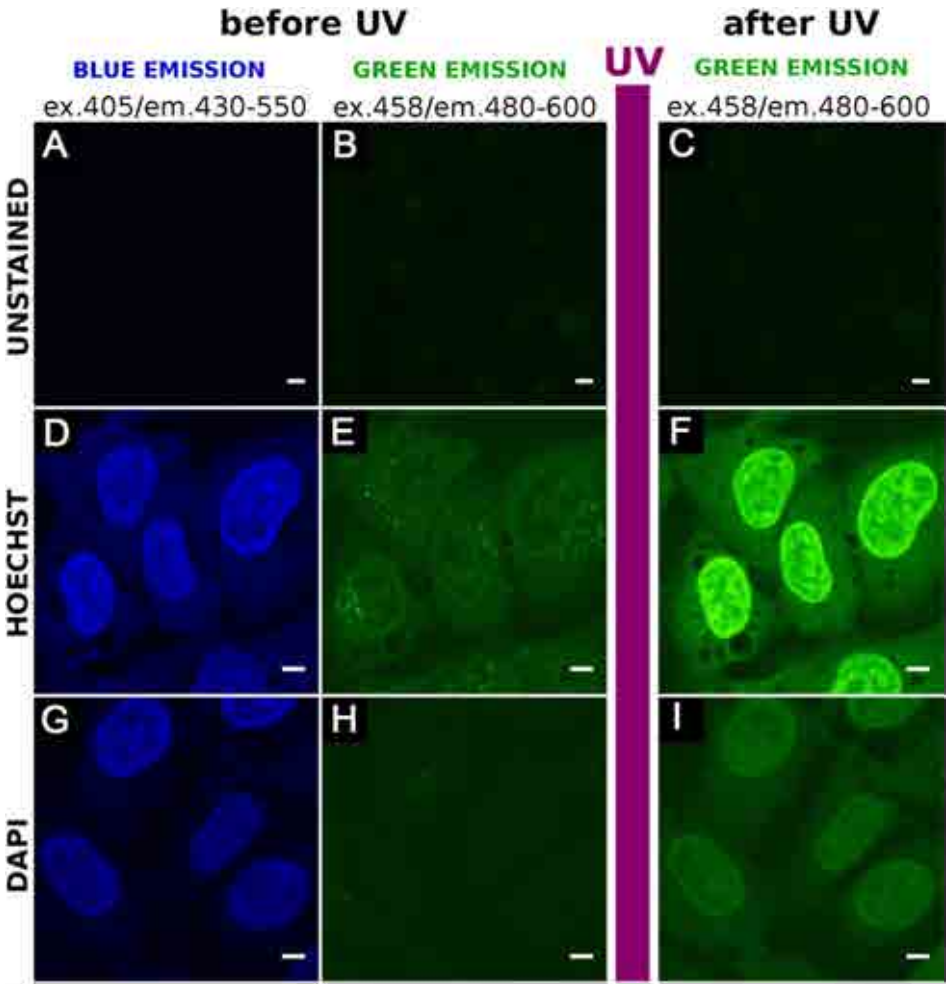

Figure 2. UV-induced photoconversion of Hoechst 33258 (**D-F**) and DAPI (**G-I**) in fixed cells. **A,B**: images of unstained cells before the exposure to UV light exhibit no blue (**A**) and very weak green (**B**) autofluorescence; **C**: image of unstained cells after exposure to UV shows only very weak green autofluorescence; **D,G**: images of the blue fluorescence of cells stained with Hoechst 33258 and DAPI; DNA-bound dyes are excited by 405 nm; **E,H**: images of the green emission (excited by blue light) of the stained cells before the onset of UV illumination, the green fluorescence is very weak; **F,I**: images of the green emission of the photoproducts of Hoechst 33258 and DAPI excited by blue light, following a 1 minute exposure to UV-illumination (marked symbolically by the vertical line). The γ-function of the images was set to 0.3. [Color figure can be viewed in the online issue, which is available at wileyonlinelibrary.com.]

were exposed to UV (Figs. 2G–2I, and data not shown, respectively). The induction of the green fluorescence suggests that new forms of both dyes (photoproducts) were generated. In an attempt to estimate the shape of the excitation spectrum of the putative photoproducts, we exposed the cells stained with Hoechst 33258 or DAPI to UV, generated the green-emitting forms and recorded the fluorescence emissions using several available excitation wavelengths (and equal intensities of the exciting light). Figure 3 demonstrates that the fluorescence of the photoproducts of Hoechst 33258 and DAPI have the highest intensities when excited by the blue light. Figures 3C and 3K demonstrate that, before an illumination of the sample with the UV, the intensity of the green fluorescence excited by 458 nm light was very weak. Clearly, while the 405 laser line was capable of generating photoproducts of Hoechst 33258 and DAPI, it did not excite the green fluorescence of the photoproducts. This indicates that the excitation maxima of Hoechst and DAPI shifted on photoconversion to longer wavelengths, into the region of 450–490 nm. We also measured the emission spectra of Hoechst 33258 and DAPI photoproducts in a confocal microscope (Figs. 1G and 1H). The emission maxima of both photoproducts generated by the UV are in the green region of the spectrum, with the tails of these curves reaching into the red region. Photostability of the photoconverted derivatives of Hoechst 33258 and DAPI was poor, as demonstrated by the photobleaching curves shown in Figures 1I and 1J.

Reversal of Photoconversion of Hoechst 33528 and DAPI

Fluorescence intensity of Hoechst 33258 and its photoproduct follow a conspicuous pattern of behavior following a short illumination with UV. Although the Hoechst blue signal

was bleached out readily by the UV, within 1 hour the blue fluorescence recovered to a level of ~50% of the initial value (Figs. 4A and 4B). At the same time the green signal of the Hoechst 33258 photoproduct, which was induced by the UV illumination, decreased to the level of ~50% of the initial value (Figs. 4A and 4B). These complementary changes of the intensity of fluorescence of Hoechst 33258 and the photoproduct may indicate that a subpopulation of molecules of the photoproduct reverted to the original form of the dye (i.e., the blue emitting form). Both forms, i.e., the original dye and the photoproduct, reached an equilibrium that lasted for at least 2 hours following the exposure to UV (Figs. 4A and 4B). A similar phenomenon was observed in the case of DAPI (Figs. 4C and 4D).

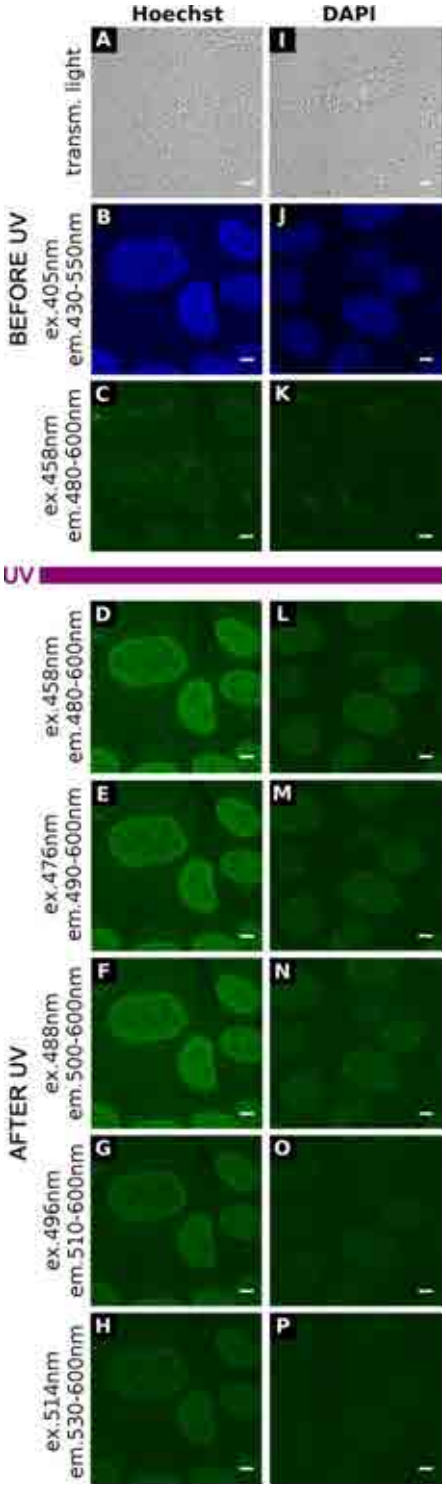

Photoconversion of Hoechst 33258 and DAPI as a Function of the UV Dose

The concentrations of the UV-induced photoproducts of Hoechst 33258 and DAPI were proportional to the dose of the delivered UV light. A continuous UV illumination of the Hoechst 33258- and DAPI-stained cells resulted in a continuous growth of the intensity of fluorescence of their photoproducts, as demonstrated in Figure 5 (until the whole pool of the dye was photoconverted). It is important to note that this experiment required an exposure of the stained cells not only to the UV (to generate the photoproduct) but to the 458 nm light (in order to record the fluorescence of the photoproducts); therefore, some photobleaching of the photoproducts must have occurred during image recording. Thus, the increasing intensities of fluorescence of the photoproducts, which are shown in Figure 5, represent a minor underestimate of the actual levels of the generated photoproducts.

Reversible Changes of Hoechst 33528 Emission Induced by Hydrogen Peroxide

Several reports indicated that an exposure to exciting light induces photooxidation of fluorescent dyes (9–13). In order to investigate whether an exposure of Hoechst 33258 to hydrogen peroxide will yield a molecule that exhibits fluorescence similar to the photoproducts, we measured the spectral characteristics of Hoechst 33258 in a specimen of fixed cells exposed to H_2O_2 (30% solution). A green fluorescence signal, similar to the UV-induced change, was detected by spectrally resolved confocal microscopy (Figs. 6A and 6B). In another experiment, we used spectrofluorimetry to measure fluorescence spectra of Hoechst 33258 and DAPI solutions in distilled water, after an exposure to 30% hydrogen peroxide. The intensity of the green fluorescence of the putative oxidized Hoechst 33258 increased gradually during exposure to hydrogen peroxide. Immediately after addition of H_2O_2 the fluorescence in-

Figure 3. Spectral characteristics of the green fluorescence of UV-induced photoproducts of Hoechst 33258 (**D**–**H**) and DAPI (**L**–**P**). Light intensity reaching the sample was adjusted to 0,95 mW for Ar-laser lines of 458, 476, 488, 496, and 514 nm. **A,I**: transmitted light images of fixed MSU 1.1 cells; **B,J**: the blue fluorescence of Hoechst 33258 and DAPI (excitation 405 nm); **C,K**: the green fluorescence (exc. 458 nm) of the stained cells, before UV-illumination (UV exposure is marked symbolically by the horizontal line); **D**–**H**, **L**–**P**: the green emissions of UV-generated photoproducts excited by 458 nm (em. 480—600 nm), 476 nm (em. 490—600 nm), 488 nm (em. 500—600 nm), 496 nm (em. 510—600 nm) and 514 nm (em. 530—600 nm). The γ-function of the images was set to 0.5. [Color figure can be viewed in the online issue, which is available at wileyonlinelibrary.com.]

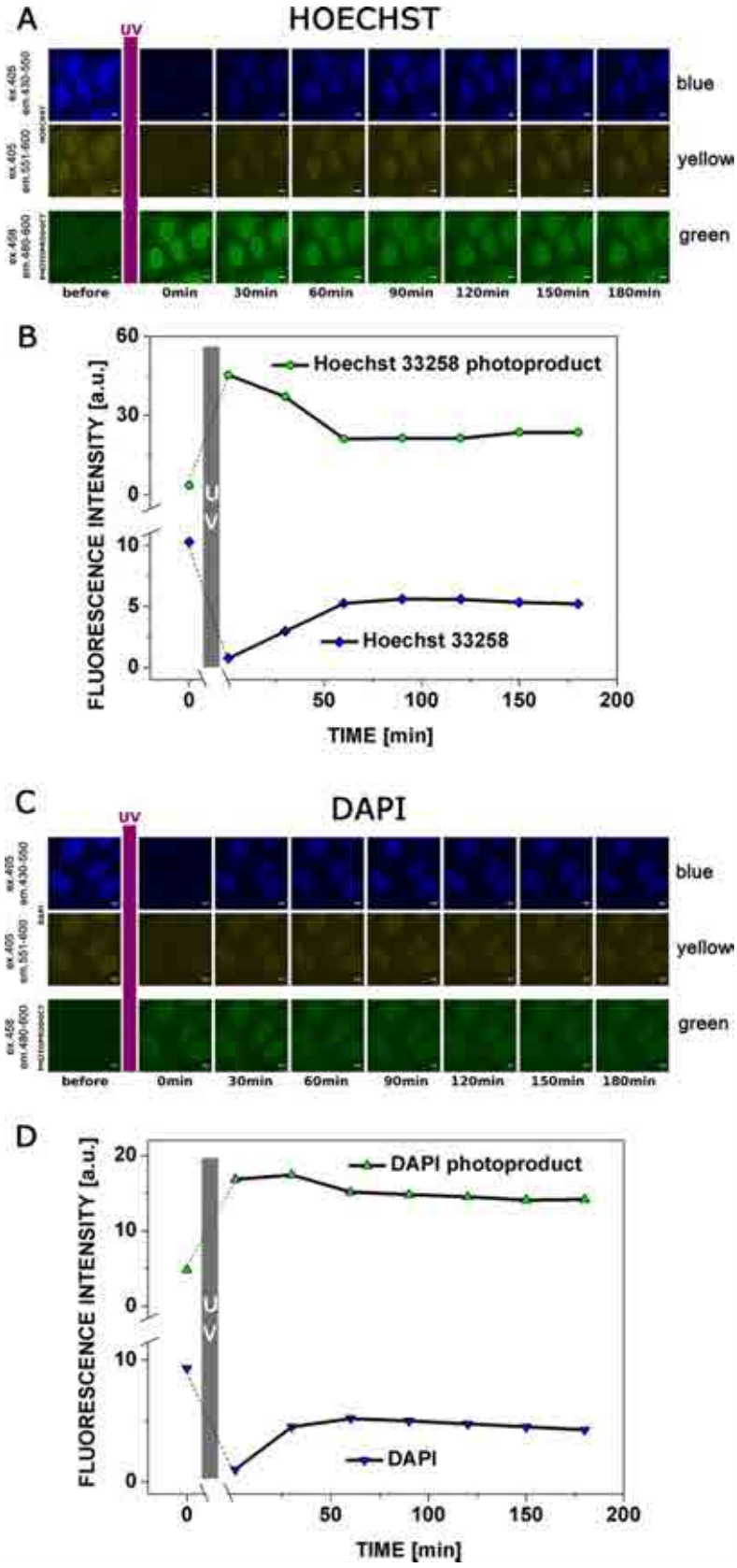

Figure 4. Reversibility of photoconversion of Hoechst 33258 and DAPI. **A,C**: a partial reversal of photoconversion of Hoechst 33258 (**A**) and DAPI (**C**). Left panels: images of stained cells before a 1 minute UV illumination (shown symbolically by the vertical line). Panels from left to right: images collected at 30 minutes intervals following the exposure to UV. Hoechst (**A**) and DAPI (**C**): excitation 405 nm; emission detected in the ranges 430—550 (top row) nm and 551—600 nm (middle row). Hoechst 33258 (**A**) and DAPI (**C**) photoproduct: excitation 458 nm; emission detected in the range 480—600 nm (bottom row). The γ-function of the images was set to 0.5. **B,D**: reversal of photoconversion of Hoechst 33258 (**B**) and DAPI (**D**) at different times after UV illumination (vertical bar). [Color figure can be viewed in the online issue, which is available at wileyonlinelibrary.com.]

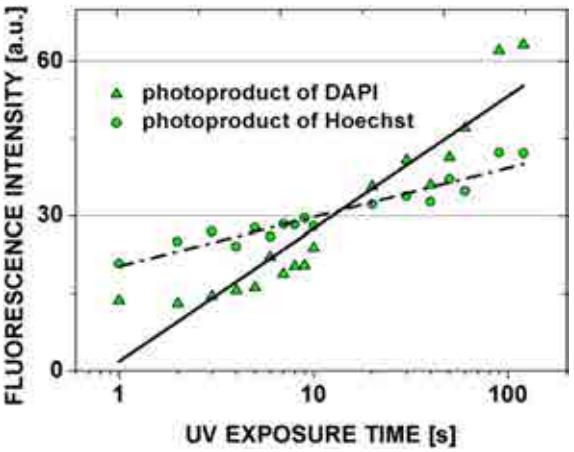

Figure 5. Generation of the photoproducts of Hoechst 33258 and DAPI, in fixed cells, during a continuous exposure to UV. Fixed cells were stained with Hoechst 33258 or DAPI. [Color figure can be viewed in the online issue, which is available at wileyonlinelibrary.com.]

tensity of the blue emission of the original dye increased as well. With time, the intensity of the blue emission decreased again, whereas the green fluorescence continued to increase (Figs. 6C and 6D). In the next experiment, we exposed Hoechst bound to DNA in fixed cells to hydrogen peroxide and subsequently replaced the hydrogen peroxide solution with physiological saline, i.e., a solution that was devoid of any reductants or oxidants (except for the dissolved oxygen). In this environment the fluorescence of the green emitting form decreased and became undetectable (Fig. 6G). Reintroduction of hydrogen peroxide brought about a return of the green fluorescence. Repeating this cycle of exposures to oxidizing and nonoxidizing conditions resulted in appearance and disappearance of the green fluorescence emission signal (Fig. 6G). A similar, but weak conversion of DAPI to the green-emitting form was induced by hydrogen peroxide, as shown in Figures 6E and 6F.

Photoconversion of DAPI and Hoechst 33258 in the Absence of DNA

The UV-induced photoconversion was first observed in Hoechst 33258 or DAPI bound to DNA in fixed cells. However, we also observed that the photoconversion of Hoechst 33258 and DAPI took place in a dye solution placed on a microscope slide and exposed to the exciting UV light (data not shown). In order to establish if photoconversion of Hoechst 33258 and DAPI is indeed independent of binding and the presence of DNA, and whether the water environment is required, we also studied the influence of UV excitation on Hoechst 33258 or DAPI immobilized in a polyvinyl polymer (8), i.e., outside of water or solution, and in the absence of cellular DNA. Under such conditions we also observed generation of a green-emitting form (Fig. 7). Apparently photoconversion of both dyes can occur outside of water solution and in the absence of DNA.

Photoconversion versus Dye Concentration and pH

We investigated whether the concentration of DNA-bound Hoechst 33258 or DAPI has any impact on the process of photoconversion. This experiment is complicated by changes in the cellular staining pattern that accompany the increasing concentrations of the dye. At high Hoechst 33258 or DAPI concentrations (3, 7, and 10 μM) fluorescence signal of Hoechst as well as DAPI bound to DNA diminished, probably due to self-quenching, whereas the signal from RNA became detectable. Nevertheless, the high dye concentrations did not inhibit the photoconversion process (Fig. 8A). The green-emitting forms of Hoechst 33258 and DAPI were detected in both concentrations of the dyes tested.

We have also investigated the influence of pH on photoconversion of Hoechst 33258 and DAPI. First, the acidity itself did have a pronounced impact on Hoechst 33258 fluorescence emission. Acidic environment (pH 2.0 or 5.1) caused a significant increase of the blue emission (ex. 405 nm, em. 430–550 nm) as well as the blue-excited green emission of this dye (ex. 458 nm, em. 480–600 nm). This observation can be explained by the increase of the quantum efficiency of Hoechst fluorescence in a low pH environment, which has been reported (14). Nevertheless, after the UV exposure of Hoechst-stained cells maintained in an acidic environment, no further increase of the green fluorescence was observed, suggesting that photoconversion did not occur, or that the photoproduct was highly unstable. Alkaline pH of 11.5 caused a reduction of the blue and green fluorescence signals of Hoechst 33258. In this environment, the UV-induced photoconversion was still detected (Fig. 8B).

Low pH did not influence the intensity of the blue or green emission of DAPI. Exposure to UV resulted in a clear photoconversion of DAPI. Alkaline pH of 11.5 caused a slight loss of fluorescence of DAPI, but it did not affect the process of its photoconversion (Fig. 8B). We conclude that photoconversion of DAPI can occur in alkaline and acidic environment, whereas Hoechst 33258 can be easily photoconverted only in alkaline environment.

Nature of the Photoconverted Derivatives of Hoechst and DAPI

In order to identify the chemical nature of the products of UV-induced photoconversion of Hoechst 33258 and DAPI, we subjected Hoechst or DAPI solutions to UV illumination (on a microscope slide) or to hydrogen peroxide (4% solution). Subsequently, the samples were analyzed by mass spectrometry.

The peaks originating from a single charge state of both dyes were prominent in the MS spectra of the dyes dissolved in water (Figs. 9A and 9B); this confirmed the presence of the original forms of the dyes in the samples. Very weak signals representing the double charged states of Hoechst and DAPI were also detected. Following exposure to UV or 4% hydrogen peroxide the ratio of the double protonated states of Hoechst and DAPI to the single protonated states of the dyes increased significantly (213.1/425.2 and 139.55/278.1 for Hoechst and DAPI, respectively) (Figs. 9A and 9B, Table 1). This increase

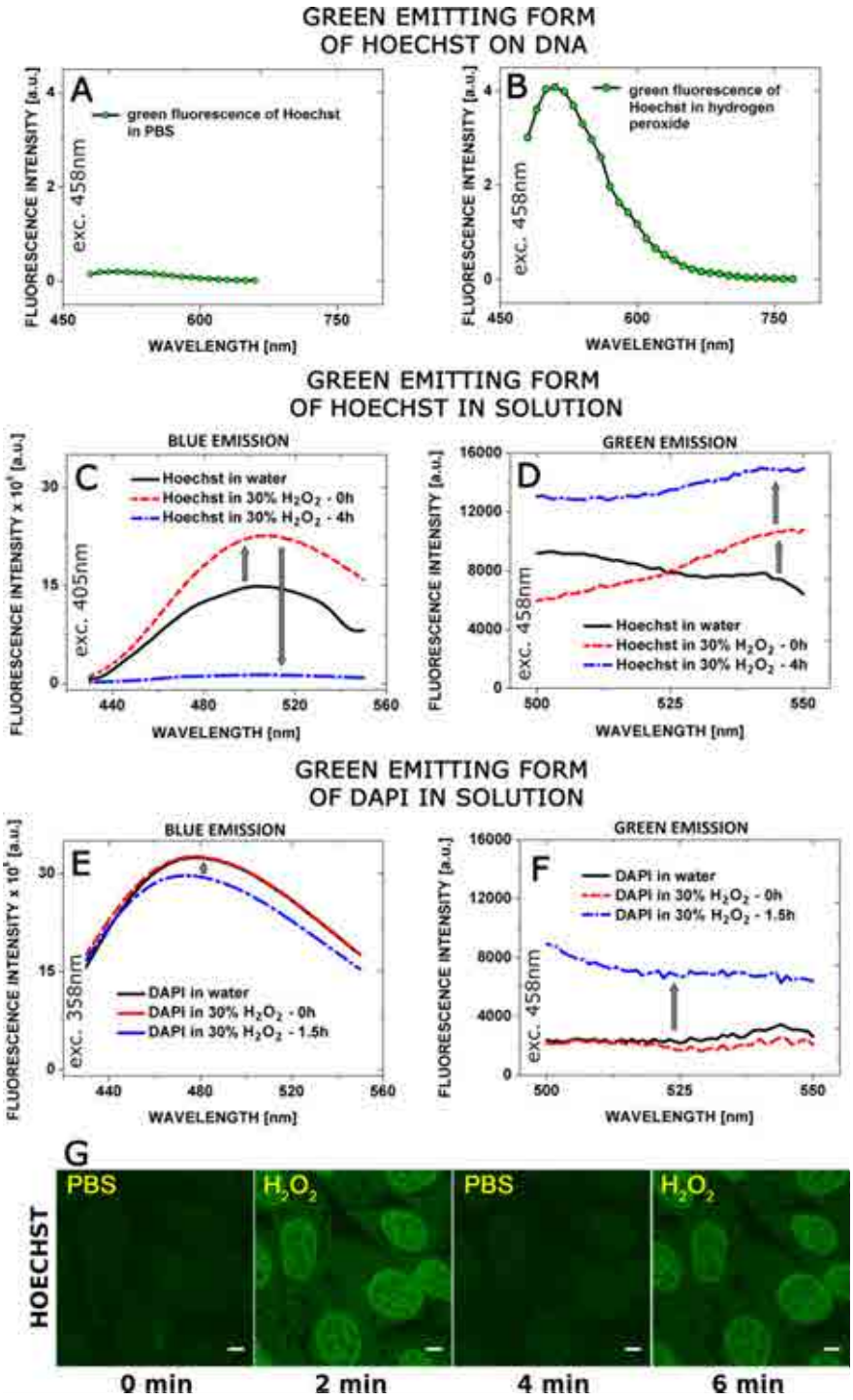

Figure 6. Spectral characteristics of the green-emitting forms of Hoechst 33258 and DAPI induced by hydrogen peroxide. **A,B**: emission spectrum of Hoechst 33258 (**A**) (exc. 405 nm) and its green emitting form generated by 30% H_2O_2 (**B**) (exc. 458 nm), measured in a confocal microscope. **C–F**: changes of the emission spectra of Hoechst 33258 (**C,D**) and DAPI (**E,F**) and their respective green emitting forms induced by hydrogen peroxide in solution, measured in a spectrofluorimeter. Addition of 30% H_2O_2 yielded an initial increase of the fluorescence intensity of Hoechst 33258, which was followed by a decrease (**C**) and an increased fluorescence intensity of the green emitting form of Hoechst; the growth continued for up to 4 hours (**D**). Addition of 30% H_2O_2 did not result in an immediate increase of fluorescence intensity of DAPI (as was observed with Hoechst), but the intensity of the blue fluorescence decreased within 1.5 hours (**E**). Adding H_2O_2 (30%) resulted in increased fluorescence intensity of the green-emitting form of DAPI after 1.5 hrs (**F**). **G**: induction and disappearance of the green fluorescence emission signal during the exposure of Hoechst 33258 (bound in fixed cells) to oxidizing (30% H_2O_2) and nonoxidizing conditions (PBS), measured in a confocal microscope. The γ-function of the images was set to 0.5. [Color figure can be viewed in the online issue, which is available at wileyonlinelibrary.com.]

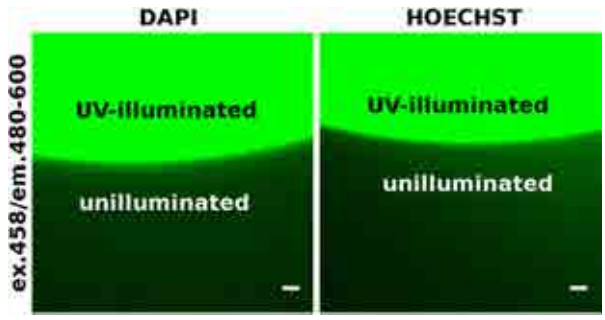

Figure 7. Photoconversion of Hoechst 33258 and DAPI immobilized in a polymer. Generation of a green emitting form in the part of the polymer block which was illuminated with the UV emitted by a mercury metal halide lamp (beam intensity 11 mW, 60 s exposure) is shown. [Color figure can be viewed in the online issue, which is available at wileyonlinelibrary.com.]

indicated that the exposure to UV as well as the incubation with hydrogen peroxide led to protonation of the molecules of both dyes. No other prominent peaks were detected in the MS of both dyes, suggesting that the main products of exposure to UV or hydrogen peroxide were the protonated forms of the dyes.

Discussion

Hoechst 33258 and DAPI bleach under the exciting light and their blue emission may seem lost permanently. We demonstrate that bleaching of these dyes has an interesting aspect—a change of spectral properties rather than just a loss of the blue emission. During exposure to UV both dyes (and Vybrant DyeCycle Violet, which we investigated in some experiments) undergo photoconversion into different but still fluorescent forms. The UV-induced chemical change is manifested by a shift of the excitation and the emission bands toward the longer wavelength. Generation of the photoproducts is proportional to the dose of the exciting light. It does not require the presence of DNA or water, and occurs at various dye concentrations, in acidic, neutral, and alkaline pH (except for the acidic environment in the case of Hoechst 33258). Spectrofluorimetry and mass spectrometry indicate that the chemical change induced by UV or hydrogen peroxide is protonation. This hypothesis appears to agree with the earlier description of changes of quantum efficiency of fluorescence on protonation of Hoechst 33258 (15). The preliminary mass spectrometry data require further refinement as it is not known if the photoproducts are stable during ionization procedure. As a consequence it is not known if the peaks in the mass spectra can be used for accurate quantitative assessment of concentrations of the photoproducts. The products of photoconversion are readily bleached by the exciting blue light. It remains to be established if this loss of fluorescence of the photoproducts constitutes further protonation or a different chemical reaction.

Following UV-induced photoconversion, further reactions between the dye and the photoproduct appear to take place. After photoconversion, both Hoechst 33258 and DAPI appear to reach some equilibrium with their respective photoproducts. It is possible that these reactions occur spontaneously in the dark, but we cannot rule out a possibility that small doses of UV and/or blue light are required for this process to occur (see the conditions of the experiment shown in Fig. 4).

It is conceivable that, following generation of the photoproducts, FRET between the original dye and the photoproduct occurs under the UV excitation. We observed an increase of the blue emission of Hoechst and DAPI during bleaching of the photoproduct. Such a phenomenon would be expected to occur in the case of acceptor photobleaching. Further studies are needed to establish if FRET occurs in this system.

Photoconversion of fluorescent proteins and reversible redox reactions of low molecular weight dyes attracted considerable attention recently because of potential applications of

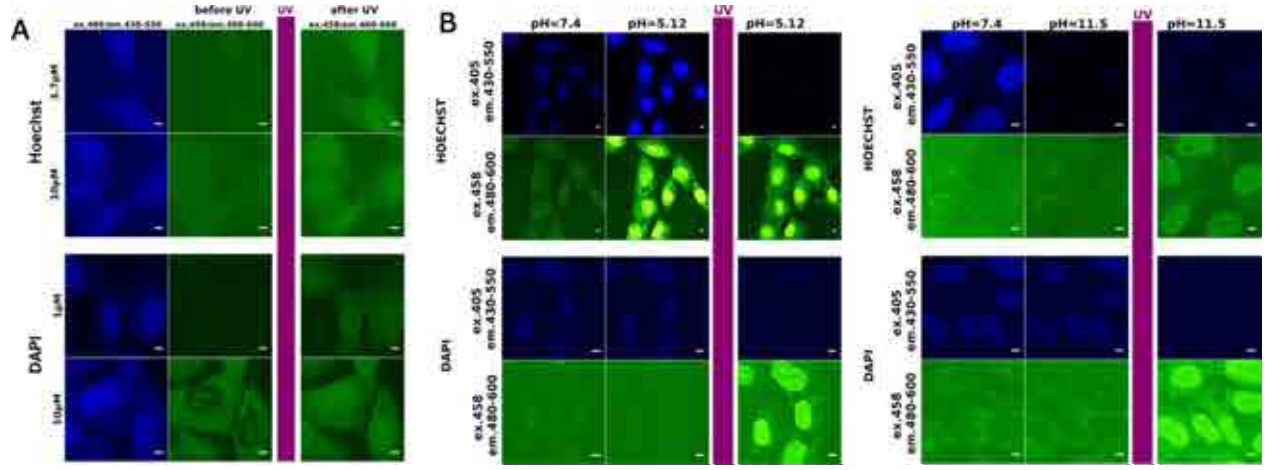

Figure 8. Photoconversion of Hoechst 33258 and DAPI vs. dye concentration (**A**) and acidity of the environment (**B**). **A**: changes in the cellular staining pattern can be observed when various concentrations of fluorescent dyes are used. Despite of the complications resulting from the changed staining patterns, an increased dye concentration did not inhibit the photoconversion process. The green-emitting forms can be detected. **B**: low pH causes a significant increase of the intensity of the blue emission as well as blue-excited green signal of Hoechst 33258. Photoconversion of DAPI can occur in alkaline and acidic environment, while Hoechst 33258 can be easily photoconverted only in an alkaline environment. [Color figure can be viewed in the online issue, which is available at wileyonlinelibrary.com.]

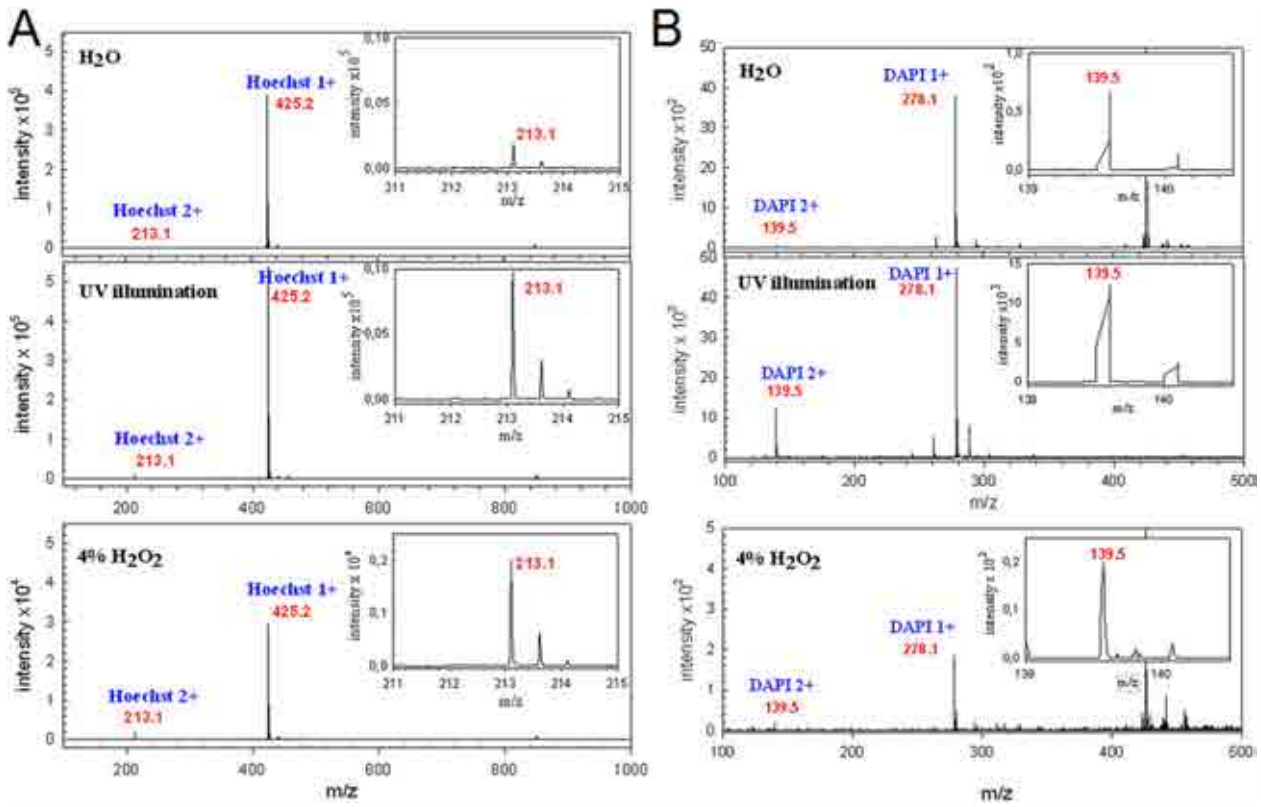

Figure 9. Mass spectrometry spectra of Hoechst 33258 (**A**) and DAPI (**B**) in solution, and the dyes exposed to UV or hydrogen peroxide (4%). The insets show the enlarged areas of the MS spectrum representing the double protonated state of Hoechst 33258 and DAPI. [Color figure can be viewed in the online issue, which is available at wileyonlinelibrary.com.]

these phenomena in superresolution microscopies (16–18). Because photoconversion of Hoechst 33258 and DAPI is apparently reversible, both dyes may become useful in superresolution microscopy approaches that rely on photoswitching of fluorescent probes. Another interesting aspect of photoconversion of Hoechst and DAPI is their potential use for detection of oxidative stress exerted on DNA. Preliminary experiments conducted in our laboratory demonstrated that such an application is feasible.

A less welcome aspect of the photoconversion of Hoechst 33258 and DAPI is the issue of generation of unexpected green fluorescence signals in microscopy specimens labeled with the UV-excited and some other green, yellow or red emitting dyes. Even a small dose of UV may cause an increase in the green fluorescence signal derived from the investigated DNA dyes. This emission can be mistaken for a green fluorescence emitted by a different, blue-excited probe like fluorescein, Alexa 488 or GFP.

Table 1. Mass spectrometry analysis of UV- or H_2O_2-generated products of Hoechst and DAPI.

A. Mass or mass-to-charge values of the original blue-emitting dyes and their H_2O_2-generated products of protonation			
IONS	MONOISOTOPIC MASS (Da)	MASS-TO-CHARGE ($1H^+$)	MASS-TO-CHARGE ($2H^+$)
Hoechst 33258	~424.20	~425.2	~213.1
DAPI	~277.13	~278.1	~139.5
B. Proportional contents of double-protonated forms			
$2H^+$ IONS	In H_2O	In 4% H_2O_2	AFTER UV ILLUMINATION
Hoechst 33258	~0.4%	~6.0%	~1.5%
DAPI	~1.75%	~13%	~27%

Acknowledgments

The authors would like to thank Mrs Małgorzata Jemioła-Rzemińska, M.Sc., for help with spectrofluorimetry measurements and Mr Artur Piróg, M.Sc., for assistance during mass spectrometry measurements. Travel fellowship awarded by ISAC and 'Doctus' scholarship awarded by Małopolska Centre of Entrepreneurship to DZ-B are gratefully acknowledged.

Literature Cited

1. Piterburg M, Panet H, Weiss A. Photoconversion of DAPI following UV or violet excitation can cause DAPI to fluoresce with blue or cyan excitation. J Microsc 2012;246:89–95.
2. Morgan TL, Yang DJ, Fry DG, Hurlin PJ, Kohler SK, Maher VM, McCormick JJ. Characteristics of an infinite life span diploid human fibroblast cell strain and a near-diploid strain arising from a clone of cells expressing a transfected v-myc oncogene. Exp Cell Res 1991;197:125–136.
3. Kapuscinski J. DAPI: A DNA-specific fluorescent probe. Biotech Histochem 1995;70:220–233.
4. De Castro LFP, Zacharias M. DAPI binding to the DNA minor groove: A continuum solvent analysis. J Mol Recognit 2002;15:209–220.
5. Latt SA, Stetten G. Spectral studies on 33258 Hoechst and related bisbenzimidazole dyes useful for fluorescent detection of deoxyribonucleic acid synthesis. J Histochem Cytochem 1976;24:24–33.
6. Stokke T, Steen HB. Fluorescence spectra of Hoechst 33258 bound to chromatin. Biochim Biophys Acta 1986;868:17–23.
7. Weisblum B, Haenssler E. Fluorometric properties of the bibenzimidazole derivative Hoechst 33258, a fluorescent probe specific for AT concentration in chromosomal DNA. Chromosoma 1974;46:255–260.
8. Kedziora KM, Prehn JHM, Dobrucki J, Bernas T. Method of calibration of a fluorescence microscope for quantitative studies. J Microsc 2011;244:101–111.
9. Andresen M, Stiel AC, Fölling J, Wenzel D, Schönle A, Egner A, Eggeling C, Hell SW, Jakobs S. Photoswitchable fluorescent proteins enable monochromatic multilabel imaging and dual color fluorescence nanoscopy. Nat Biotechnol 2008;26:1035–1040.
10. Henriques R, Griffiths C, Hesper Rego E, Mhlanga MM. PALM and STORM: Unlocking live-cell super-resolution. Biopolymers 2011;95:322–331.
11. Lippincott-Schwartz J, Altan-Bonnet N, Patterson GH. Photobleaching and photoactivation: Following protein dynamics in living cells. Nat Cell Biol 2003;S7–S14.
12. Lippincott-Schwartz J, Patterson GH. Fluorescent proteins for photoactivation experiments. Methods Cell Biol 2008;85:45–61.
13. Patterson GH. Photoactivation and imaging of photoactivatable fluorescent proteins. Curr Protoc Cell Biol 2008;21:21.6.
14. Barooah N, Mohanty J, Pal H, Sarkar SK, Mukherjee T, Bhasikuttan AC. pH and temperature dependent relaxation dynamics of Hoechst-33258: A time resolved fluorescence study. Photochem Photobiol Sci 2011;10:35–41.
15. Görner H. Direct and sensitized photoprocesses of bis-benzimidazole dyes and the effects of surfactants and DNA. Photochem Photobiol 2001;73:339–348.
16. Baddeley D, Jayasinghe ID, Cremer C, Cannell MB, Soeller C. Light-induced dark states of organic fluochromes enable 30 nm resolution imaging in standard media. Biophys J 2009;96:L22–L24.
17. Heilemann M. Fluorescence microscopy beyond the diffraction limit. J Biotechnol 2010;149:243–251.
18. Flors C. Photoswitching of monomeric and dimeric DNA-intercalating cyanine dyes for super-resolution microscopy applications. Photochem Photobiol Sci 2010;9:643–648.

PAPER 2:

UV-induced Spectral Shift and Protonation of DNA Fluorescent Dye Hoechst 33258

J Fluoresc
DOI 10.1007/s10895-014-1468-y

ORIGINAL PAPER

UV-induced Spectral Shift and Protonation of DNA Fluorescent Dye Hoechst 33258

Dominika Żurek-Biesiada · Piotr Waligórski · Jurek W. Dobrucki

Received: 2 June 2014 / Accepted: 29 September 2014

Abstract DNA-bound Hoechst 33258 is readily excited with UV light and emits blue fluorescence, however, upon exposure to UV, the dye undergoes photobleaching as well as photoconversion to a blue-excited green-emitting form. We demonstrate that the UV-generated green-emitting form of Hoechst 33258 exhibits spectral properties very similar to the form of the dye that can be obtained by subjecting it to an acidic environment (pH 0.5–3.0). We also demonstrate that exposure of Hoechst 33258 to UV light (or hydrogen peroxide) leads to generation of the protonated (1+, 2+, 3+ and possibly the 4+) forms of the dye. Photoconversion of Hoechst 33258 has recently been exploited in single molecule localisation microscopy, thus understanding photophysics of this process can facilitate further development of high resolution optical imaging.

Keywords Photoconversion · Hoechst · DNA · Super-resolution microscopy

Introduction

Hoechst 33258 is a common fluorescent dye used for staining and visualisation of DNA by fluorescence wide field and confocal microscopy. DNA-bound Hoechst 33258 is readily excited with UV and emits fluorescence in the blue region of the visible light spectrum (exc./em. maxima 355/465 nm). We have recently reported that, upon excitation with UV, Hoechst 33258 undergoes photoconversion [1]. Although a typical loss of fluorescence (photobleaching) was observed, apparently a fraction of the blue-emitting dye molecules did not lose their ability to fluoresce, but were converted to a blue-excited, green-emitting form. We have also demonstrated that the amount of the photoproduct is proportional to the dose of exciting light delivered, and that photoconversion does not require the presence of DNA or water [1]. Preliminary mass spectrometry data suggested that the observed spectral changes were associated with UV-induced protonation of Hoechst molecules [1].

Protonation of Hoechst occurring in solutions of low pH has been described in several reports [2–6]. The hypothetical protonated forms of Hoechst 33258, as described in [3], are redrawn in Fig. 1. To our knowledge, changes of spectral properties of Hoechst that accompany single, double and triple protonation have not been described in detail so far. It is known, however, that the quantum yield of the fluorescence of Hoechst increases 20-fold upon a shift of pH from neutral to 4.5, and falls 80-fold when pH decreases from 4.5 to 1.5 [5]. Based on the available photophysical data one may postulate that it is a protonated form of DNA-bound Hoechst that contributes predominantly to the blue emission typically observed in fluorescence microscopy images of cells maintained in neutral pH. In fact it is known that the blue signals of Hoechst in cell nuclei are more intense if the mounting medium has a low rather than neutral pH.

So far the green emission of photoconverted Hoechst 33258 molecules has been recognised as a nuisance in multicolor fluorescence microscopy, however our recent findings suggest that it can be exploited in super-resolution microscopy [7]. The key to a successful use of the phenomenon of photoconversion of this dye is an understanding of the photophysics of this process. Therefore, in this report we focus our attention on photophysical phenomena underlying

D. Żurek-Biesiada · J. W. Dobrucki (✉)
Division of Cell Biophysics, Faculty of Biochemistry, Biophysics and Biotechnology, Jagiellonian University, ul. Gronostajowa 7, 30-387 Kraków, Poland
e-mail: jerzy.dobrucki@uj.edu.pl

P. Waligórski
The Franciszek Górski Institute of Plant Physiology, Polish Academy of Sciences, ul. Niezapominajek 21, 30-239 Kraków, Poland

Published online: 14 October 2014

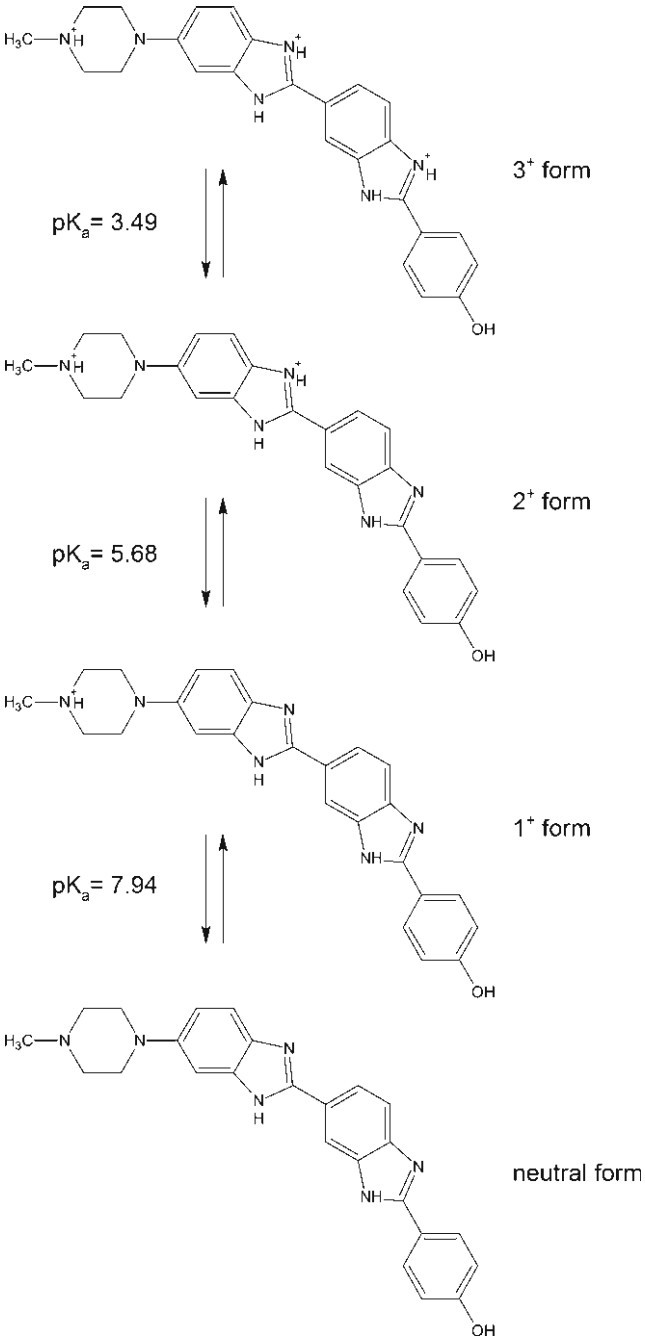

Fig. 1 The sequence of protonation of Hoechst 33258 and pKa values, based on Ladinig et al. 2005. Note that the structures proposed here do not include a number of other possible forms, for instance the neutral form, which contains one negative and one positive charge, as described in Aleman et al. 2005, or the 3+ form with protons on different nitrogen atoms

the spectral changes induced by UV excitation of Hoechst 33258. We demonstrate that the UV-generated green-emitting form (or forms) of Hoechst 33258 exhibit the same spectral properties as the forms of the dye that can be obtained by subjecting it to a highly acidic environment (pH 0.5–3.0). By using mass spectrometry and spectrofluorimetry we demonstrate that exposing Hoechst 33258 to UV light (or hydrogen peroxide) leads to generation of several protonated forms of the dye. While the 1+, 2+ and 3+ forms of the dye appear to exhibit strong affinity to DNA (binding to RNA is very weak), the protonated form which exists in pH 0.5 (presumably the 4+) exhibits affinity to RNA.

Materials and Methods

Cells

MSU 1.1 human fibroblasts [8] were grown in Dulbecco's Modified Eagles Medium (Sigma-Aldrich, Poland) supplemented with 10 % fetal bovine serum, penicillin (50 units/ml) and streptomycin (50 μg/ml), in tissue culture Petri dishes (Techno Plastic Products AG, Switzerland) at 37 °C, in a humidified atmosphere of 95 % air and 5 % CO_2. Cells were grown on 20 mm-diameter coverslips (Menzel-Gläser, Germany).

Cells were fixed with 4 % formaldehyde (Electron Microscopy Sciences, USA) using standard formaldehyde fixation protocol and subsequently stored in 1 % formaldehyde solution for 1–2 weeks prior to the experiment.

Cell Staining

Preparations of fixed cells were rinsed three times with PBS, permeabilised with 70 % ethanol (30 s) and incubated with a solution of Hoechst 33258 [9–11] (2 μg/ml; Sigma-Aldrich, Poland) for 30 min at room temperature (RT).

Acquisition of Fluorescence Images

Images were recorded using Leica TCS SP5 confocal microscope (Leica Microsystems, Germany), equipped with a 63× 1.4 NA oil immersion lens. 512 × 512 pixel images (field of view 145 × 145 μm) were recorded. PMT gain was set at 860 V; confocal iris was set at 1 Airy disk. When studying the process of UV-excited dye photoconversion, coverslips with the attached fixed cells were mounted in custom made steel holders, placed in a microscope stage and imaged at RT in PBS or solutions of various pH (fixed cells). For excitation a 100 mW Ar ion gas (458 nm) and 405 nm diode (3 mW output) lasers were used. For imaging Hoechst green-emitting products, the intensity of light in the 458 laser line was adjusted to 0,95 mW. Light intensities were measured with a FieldMaxII Laser Power Meter (Coherent, USA). Fluorescent dyes were photoconverted using UV emitted by a Leica EL6000 mercury metal halide lamp, which passed through a 360/40 nm filter (11 mW).

Data Analysis

Images were analysed and processed using LAS AF Lite (Leica Microsystems, Germany) and MacBiophotonics ImageJ (http://rsbweb.nih.gov/ij/) software. The displayed images were not manipulated beyond adjusting the γ-function, as noted in the figure legends.

Mass Spectrometry (MS)

Mass spectra were collected with Agilent Technologies 6410 Triple Quad LC/MS mass spectrometer equipped with Electrospray Interface (ESI). Drying gas temperature was set at 350 °C with flow 12 l/min. Nebuliser pressure was 35 psi, capillary voltage 3,000 V. Mass spectra were collected in positive ion mode in the m/z range from 50 to 1,000. Various fragmentor voltages were checked and 10 V was selected as the best one; this provided the highest signal and the lowest fragmentation of the investigated molecules. 5 μl of each sample was injected through an automatic autosampler, a continuous flow of 1:1 mixture of A and B was set, where (A) was water with 0.01 % formic acid and (B) was acetonitryle/methanol (1:1 v/v). The flow was forced with the HPLC pump (Agilent Technologies 1260 series) with flow rate of 0.1 ml/min. The concentration of Hoechst used in mass-spectrometry experiments was 25 μM. Mass spectra were collected and analysed at the point of the highest signal using Mass Hunter software (Agilent Technologies).

For time course mass spectrometry measurements (Fig. 2c,d) Hoechst 33258 solutions were placed in a small glass container (the total volume of 2 ml) and 60 μl of the UV-illuminated solution or 1 ml for the solution of Hoechst treated with hydrogen peroxide was used. An automatic autosampler collected 5 μl of the dye solution and injected into the mass spectrometer at 30 min intervals. The photoconverted forms of Hoechst 33258 needed for these MS analyses were produced by illuminating a solution of the dye with UV on a microscope stage (Nikon Optiphot, equipped with an HBO mercury arc lamp, 330–380 emission filter and a 100x NA 1.3 objective lens). A solution of Hoechst 33258 was prepared (25 μM) and subsequently the samples of approximately 2–3 μl were placed on a microscope slide and each one was illuminated with UV for 30 s. Subsequently the drops of the illuminated dye solution were collected, pooled together and placed in a small glass container, from which the autosampler collected the samples for mass spectrometry analyses.

Solutions

Solutions of various pH (0.5–12.5) were prepared using distilled water with pH adjusted with NaOH and HCl or HCOOH and NH_3.

Spectrofluorimetry

Hoechst 33258 (10 μM) was dissolved in solutions of pH 0.5, 2.0, 3.0, 4.0, 7.4 and 11.5. Samples were placed in quartz cuvettes and analysed using Perkin Elmer LS50B spectrofluorimeter.

Results

UV- and H_2O_2-induced Generation of Protonated Forms of Hoechst 33258

We have recently described spectral characteristics of Hoechst 33258 after illumination with UV, as well as after subjecting it to highly oxidative conditions (30 % H_2O_2) [1]. In both cases the dye was converted to forms that were excited with blue light, and emitted green fluorescence (Fig. 2a,b). In order to verify and extend the preliminary studies of the chemical nature of these green-emitting forms, we performed mass spectrometry analyses of solutions of Hoechst 33258 subjected to UV or oxidising conditions. In samples containing the original and the photoconverted forms of the dye three peaks were detected by mass spectrometry. They correspond to three protonated forms of the dye: a mono-, di- and tri-cation, with their respective mass-to-charge ratios: 425.2, 213.1, 142.4 (examples of MS spectra are given below). A similar result was obtained when Hoechst 33258 was exposed to hydrogen peroxide (Fig. 2b).

Mass spectrometry analysis demonstrated that exposure to UV resulted in a significant decrease of the abundance of the detectable di-cation, a small decrease of the mono-cation, and an increase of the tri-cation (Fig. 2c). Analysis of the ratios between the abundances of different protonated forms indicate that the ratio of 3+/1+ increased, while the 2+/1+ ratio decreased significantly. It is important to note that MS determinations of the abundance of the protonated forms prior and after the UV exposure was done on 2 separate samples, thus the accuracy of a direct comparison between these abundances is limited. Moreover, the total amount of detectable photoproducts generated by UV is fairly limited too, due to their photobleaching which occurs upon exposure to UV. Thus, the actual abundance of the photoconverted forms detected by MS, following exposure to UV, was dependent not only on their generation rate, but on their susceptibility to photobleaching as well. Nevertheless, these data hint at a possibility of UV inducing a single, double and triple protonation of the neutral form and suggest that these forms of the dye are quite stable in solution. A slight increase of the abundance of the 2+ and 3+ form seen in Fig. 2c is likely a result of a slow evaporation of the sample which was maintained in the mass spectrometer. The volume of this sample was only approx. 60 μl, since it was not practical to generate

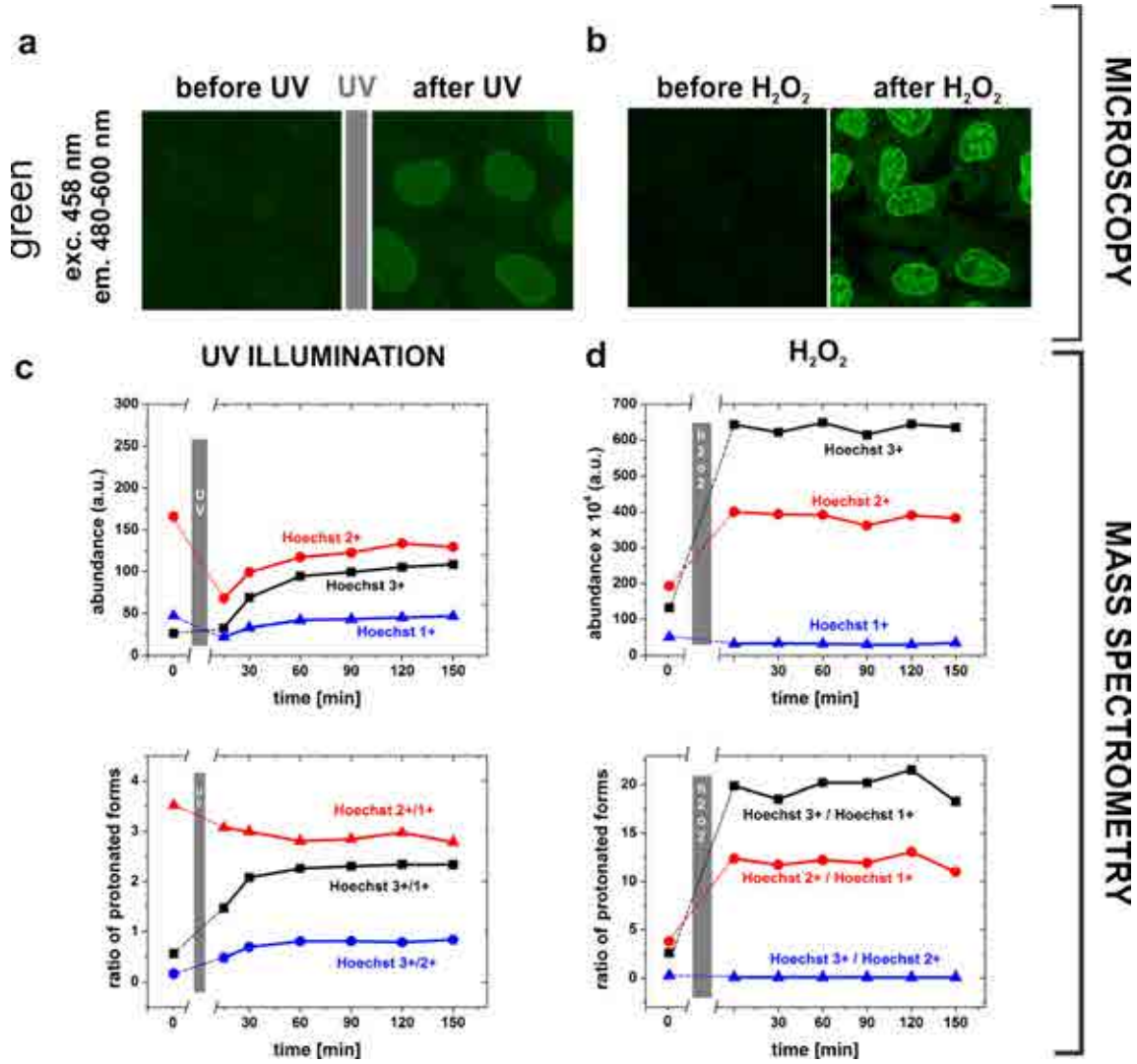

Fig. 2 Conversion of Hoechst 33258 to green-emitting forms induced by exposure to UV or hydrogen peroxide in fixed MSU 1.1 fibroblasts stained with Hoechst 33258 (2 μg/ml), detected by fluorescence confocal microscopy (a,b) and mass spectrometry (c,d). **a**, **b** – Images of the green emission of Hoechst-stained cells prior and following exposure to UV (a) or hydrogen peroxide (30 %) (b) Excitation: 458 nm, emission: 480–600 nm (as demonstrated previously [1], Figs. 2–4 and 6). The γ-function of the images in (a) was set to 0.5. **c**, **d** – Conversion and stability in time of the protonated forms of Hoechst 33258 measured by mass spectrometry. Three peaks corresponding to m/z=142.4 (Hoechst 3+), m/z=213.1 (Hoechst 2+) and m/z=425.2 (Hoechst 1+) were prominent in MS spectra. Abundances of the protonated forms of Hoechst 33258 measured after illuminating the sample with UV or after subjecting it to 4 % H_2O_2 confirm the induction of protonation and indicate that the protonated forms are stable in solution

the Hoechst photoproducts by UV in larger quantities (see Materials and Methods). Small amounts of the solution were taken from this sample at time intervals for MS analysis. The evaporation led to an increase of the concentration of the protonated forms in the sample which was maintained in the spectrometer. The volume of the sample in which Hoechst 33258 was exposed to hydrogen peroxide was much larger (1 ml), however the exposed surface was the same as in the small sample treated by UV, thus evaporation had a negligible effect on the concentration of the protonated forms of the dye in this case (Fig. 2d).

Unfortunately mass spectrometry analysis does not provide information about the abundance of the neutral form, therefore the yield of its photoconversion into a single protonated form remains unknown.

Exposing Hoechst to oxidising conditions resulted in a dramatic increase of the abundance of the 3+ and 2+ forms (Fig. 2d). The ratio of 2+/1+ and 3+/1+ increased significantly. The abundances and the ratios between different forms remained unaltered for 2.5 h after adding hydrogen peroxide to the sample (Fig. 2d). This observation is consistent with a notion that exposure to H_2O_2 induced protonation of the Hoechst molecule, resulting in high levels of di- and tri-cation. All the protonated forms appeared quite stable in water. It remains unknown, however, if oxidation also led to destruction of some of the dye molecules, for instance to breakage of

the rings or fragmentation of the molecule. Although the peaks representing degradation products were not seen on mass spectra, such a possibility cannot be excluded entirely, since small fragments of less than 100 mass-to-charge ratio were not detectable.

In our previous report we demonstrated that the equilibrium between the photoconverted, green-emitting form of the dye, and the original, blue-emitting form [1] was reached 60 min after UV exposure. In this experiment all measurements of the relative amounts of both forms were based on their fluorescence intensities. However, it is important to note that in order to induce and measure fluorescence intensity of the original and the photoconverted dye, the samples had to be exposed periodically to UV and blue exciting light. This raised a question as to the possible role of these short light exposures in further modifications of the original and the photoconverted molecules. The potential influence of these short illuminations on the production and a final concentration of the photoconverted forms can be eliminated in samples that remain and are analysed without exposure to intense light, as it is done in a mass spectrometer (Fig. 2c,d). We note that, in the MS experiments, in the absence of exposure to UV and blue exciting light, the abundance of the UV-induced photoproducts and the forms induced by exposure to hydrogen peroxide were stable for the duration of the experiment (2.5 h). This observation suggests that the forms of Hoechst 33258 that were generated by UV or H_2O_2 were stable in solution.

An issue to consider, when interpreting the MS experiments (Fig. 2c,d), is the fact that mass spectrometry detects the protonated forms of the dye, but does not directly provide any information about the neutral form, which is most likely the parental molecule in the UV- or oxidation-induced protonation processes. Hoechst 1+, 2+ and 3+ that are detected by MS most likely represent only a subpopulation of the whole population of the dye in the investigated solutions. Unfortunately, the relative concentrations of the protonated and the neutral form remain unknown. Another issue that needs to be taken into account is the fact that a large portion of Hoechst 33258 molecules may undergo irreversible photobleaching to a nonfluorescent form. The MS data alone do not provide the information if and which of the protonated forms are fluorescent, and whether other molecule rearrangements occur as a result of photobleaching. Some of these missing pieces of information can be extracted from analysis of MS and spectrofluorimetry data, as described below.

Hoechst Green and Blue Fluorescence in Various pH Environments

Blue and green fluorescence emissions of Hoechst 33258 (DNA-bound and in solution) are strongly dependent on pH (Fig. 3 and 4a,b, see also Fig. 5 and 6b, c below). Subjecting MSU 1.1 Hoechst-stained (2 μg/ml) fixed cells to environments of various pH (0.5–3.5) resulted in generation of a green fluorescence signal, which became detectable at pH 3.0, and was very prominent in a highly acidic environment (pH=0.5–2.0) (Fig. 3a). The shapes of the emission spectra of the forms of the DNA-bound Hoechst, that were excited by blue light, were measured in a confocal microscope, in environments of pH 2.0, 4.0, 6.0 and 7.4 (Fig. 3b). No green fluorescence was detected at pH 6.0 and 7.4, but a clear green emission was detected at pH 2.0. A comparison between the green emission spectra of DNA-bound Hoechst 33258 subjected to an acidic environment (pH 2.0) and the dye exposed to UV is shown in Fig. 3c. The spectra overlap well and have their maxima at approximately 540 nm, suggesting that the form (or forms) of the DNA-bound Hoechst molecule, which is generated in a highly acidic environment, exhibits the spectral properties that are very close to the form which is induced by UV illumination of Hoechst 33258 in solution.

Further confocal microscopy and mass spectrometry measurements confirmed a very strong dependence of Hoechst 33258 blue and green fluorescence emissions on acidity of the environment (Fig. 4a-d). Confocal microscopy demonstrated that, as the pH decreased from 7.4 to 4, the intensity of fluorescence of the original blue-emitting DNA-bound form increased gradually. As pH decreased further, from 3.5 to 3.0, the intensity of blue fluorescence of the DNA-bound Hoechst increased sharply and fell again as pH decreased from 2.5 to 1.5 (Fig. 4a,b). A similar pH-dependent behaviour has been demonstrated in the case of 1+ and 2+ form of the dye by mass spectrometry, in solutions of various pH (Fig. 4c,d). Their abundance also increased as pH decreased from 7.4 to 4 (1+ form) and 3 (2+ form) and fell sharply below pH 3.0 (Fig. 4d). A comparison between the spectrofluorimetry and mass spectrometry data suggests that the 1+ form is likely the one which emits blue fluorescence. It remains unclear, however, if the 2+ form emits blue or green fluorescence. It is also important to consider that the existing body of data does not allow to exclude a possibility that the protonated forms are completely nonfluorescent and the green emitting forms have no electric charge, and are, therefore, not detected by mass spectrometry. Such a possibility seems highly unlikely, however, since very small fragments of the original Hoechst 33258 molecule would not be expected to be fluorescent and exhibit affinity to DNA. One should also note that mass spectrometry experiments provide no information about the concentrations of the parental, uncharged form of Hoechst 33258, which may also exhibit blue emission.

A different pH dependence was observed for the DNA-bound green-emitting form. Fluorescence intensity, and presumably the concentration of this form, was very weak at neutral pH and increased sharply in pH range 2.5 to 0.5 (Fig. 4a,b). In mass spectrometry data a similar pH dependence was seen for the 3+ form only. It was abundant at

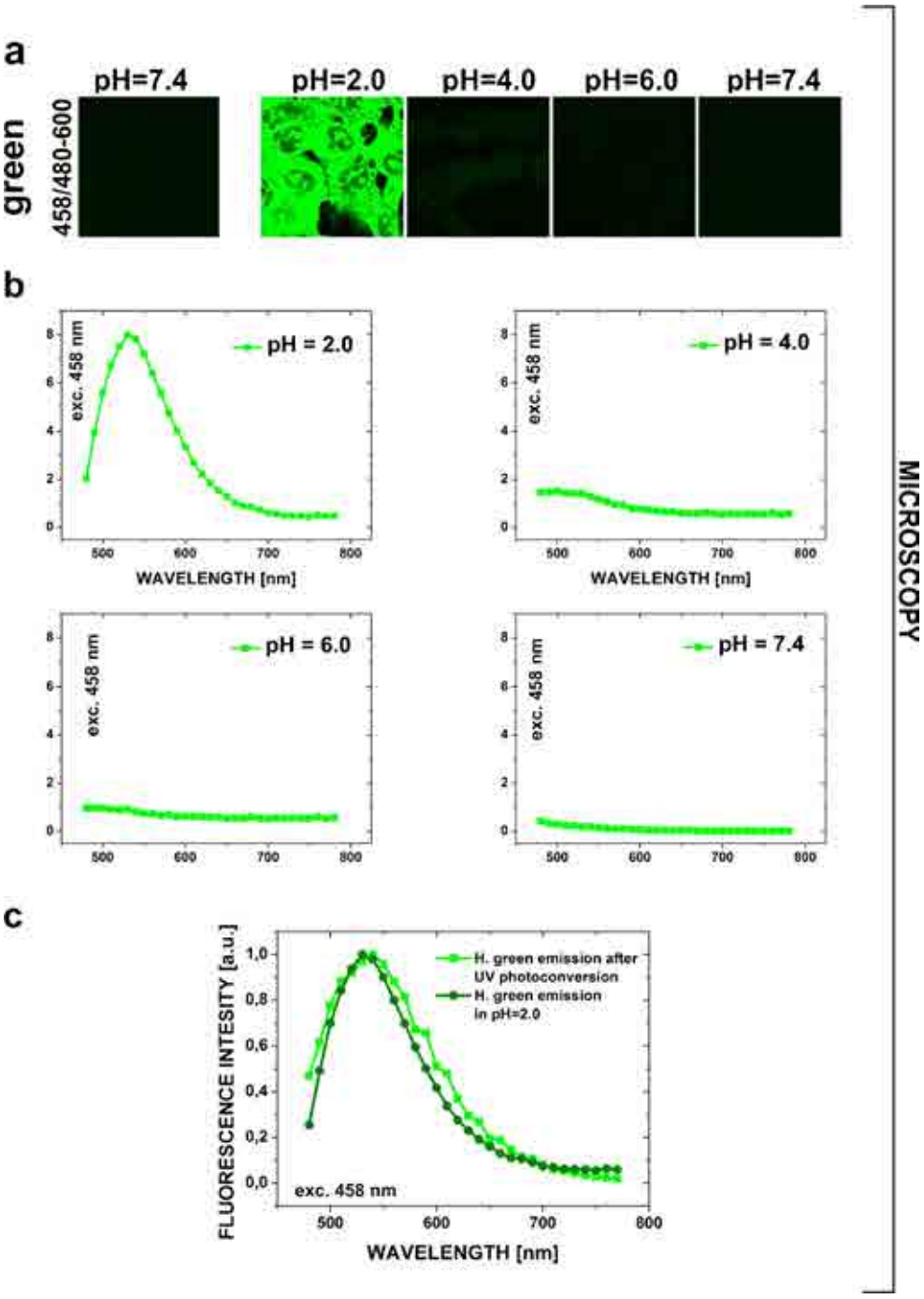

Fig. 3 Spectral properties of the green emitting form of Hoechst 33258 generated by UV or acidic conditions. **a** – DNA-bound Hoechst 33258 green fluorescence in various pH environments. Confocal microscopy images of the green emitting form (or forms) of the dye generated after subjecting MSU 1.1 fixed cells, stained with Hoechst 33258 (2 μg/ml), to solutions of various pH (2.0, 4.0, 6.0 and 7.4). **b** – Hoechst 33258 green emission curves in various pH environments. Fluorescence spectra measured in a confocal microscope after subjecting the fixed, stained cells to solutions of various acidity (pH 2.0, 4.0, 6.0, 7.4) demonstrate a weak signal at pH 4.0 and a strong green emission at pH 2.0. **c** – DNA-bound Hoechst green emission spectra recorded after exposure to UV (*squares*), and in low pH solution (*circles*). The spectra show significant similarity

pH 2.5, which was the lowest pH investigated by MS. The abundance of the 3+ form was very low at neutral pH, and increased sharply when pH decreased from 3.5 to 2.5 (Fig. 4c,d). Therefore it is possible that the green emitting form of Hoechst 33258, which is induced by a high concentration of protons at pH 2.5–3.5, may be the 3+ form. It is also possible that a 4+ form is generated at pH below 2. This form might be difficult to detect in solution, in the presence of the abundant 2+ and 3+ forms, but could become readily detectable in a microscopy experiment, due to binding and accumulation in cells. Interestingly, the staining pattern at pH 0.5–2.0 differs from the typical Hoechst 33258 staining of nuclear DNA which is seen at pH 2.0–7.4. At pH 0.5–2.0 nucleoli become brightly stained, while chromatin exhibits only very weak signals (see also Fig. 6b). Thus a possibility exists that a highly protonated form of the dye which predominates in the pH range of 0.5–2.0 has an affinity to RNA. However, the abundances of various protonated forms at pH below 2.5 remain unknown. Although we conducted mass spectrometry studies at lower pH, we noticed a strong

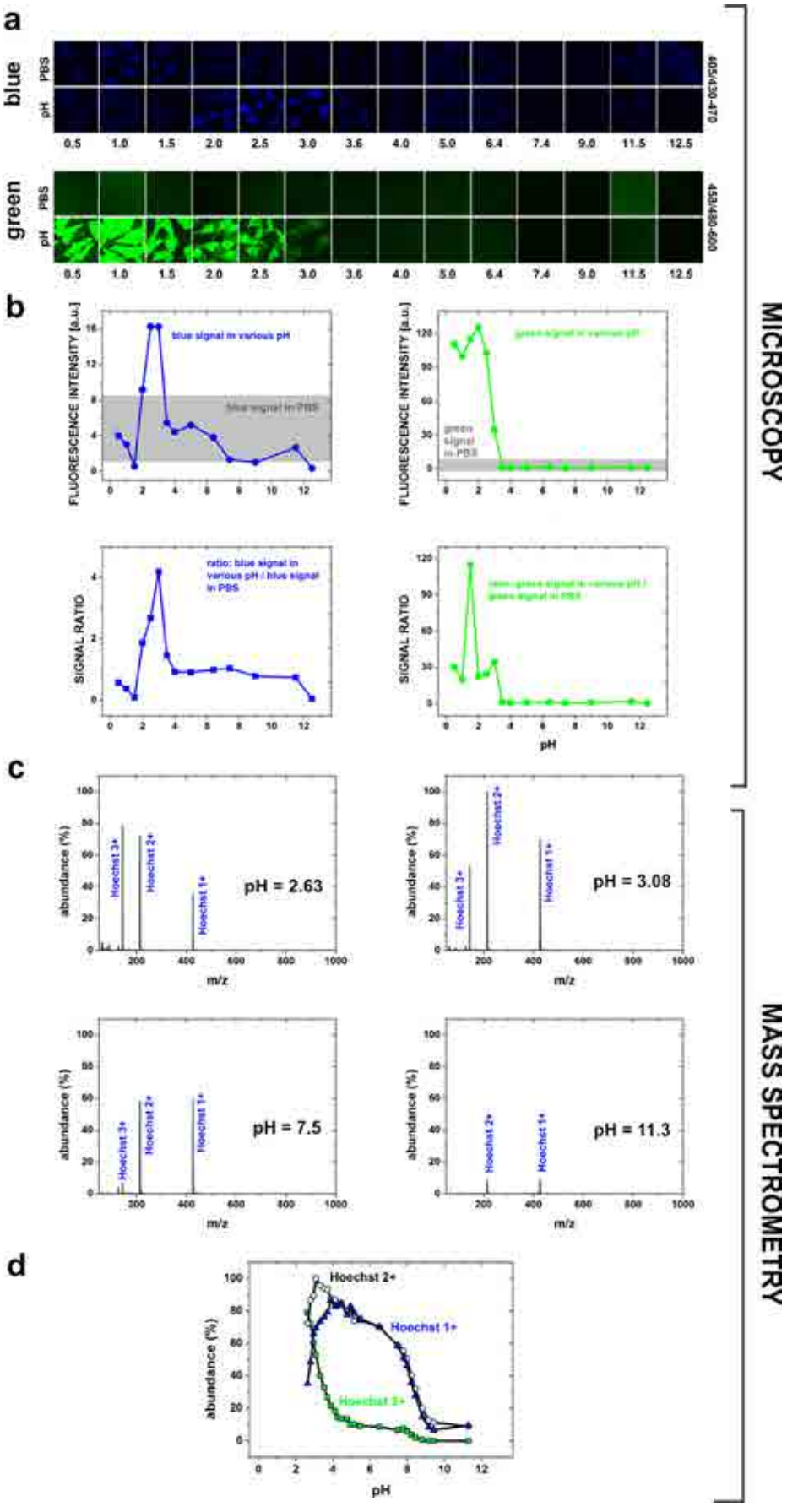

Fig. 4 Dependence of the intensities of Hoechst 33258 blue and green fluorescence, and the abundances of the protonated forms, on acidity of the environment, analysed by fluorescence confocal microscopy and mass spectrometry. **a** – Fluorescence microscopy detection of blue and green emissions of the DNA-bound Hoechst 33258, in solutions of various pH. In both sets (*blue and green*) the top rows present control images - the blue or green fluorescence of Hoechst in PBS. The γ-function of the images presenting blue fluorescence of Hoechst was set to 0.75. The bottom rows show images of the same preparations submerged in solutions of various pH. Detection conditions for blue emission – exc. 405 nm, em. 430–470 nm; green emission: exc. 458 nm, em. 480–600 nm. **b** – Intensities of green and blue fluorescence of DNA-bound Hoechst 33258 derived from fluorescence images. The maximum intensity of the green emission is detected in pH range 0.5-2.5, while the maximum intensity of the blue emission in pH range 2.5–3.0. **c** – Mass spectrometry detection of various Hoechst 33258 protonated forms in solutions of different acidity. **d** – The abundances of various protonated forms of Hoechst 33258 in solutions of various acidity, based on mass spectrometry data

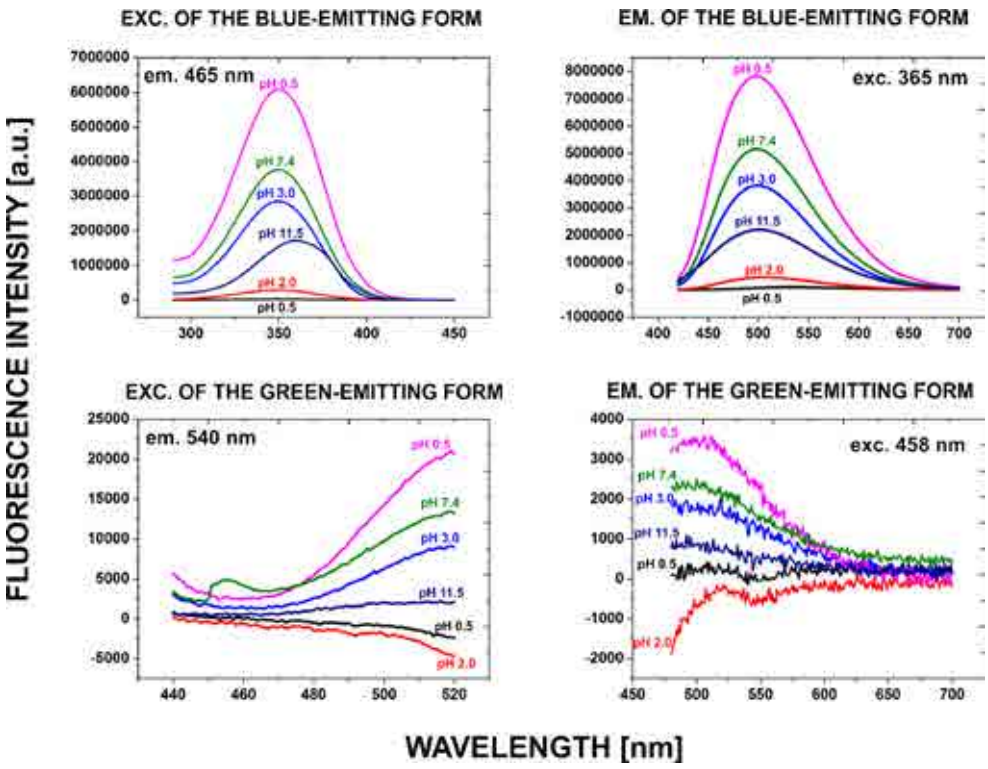

Fig. 5 Excitation and emission spectra of the original blue-emitting form of Hoechst 33258 (10 μM) and the protonated forms of the dye in solutions of different acidity (0.5, 2.0, 3.0, 4.0, 7.4 and 11.5) measured in a spectrofluorimeter. The highest intensity of the green emission is detected at pH 4.0

fragmentation of the dye molecule (data not shown). This phenomenon complicated interpretation of MS spectra recorded at low pH.

Fluorescence Spectra of the Original Blue-Emitting and the Converted Green-Emitting Forms

The spectrally resolved microscopy data of DNA-bound Hoechst (Fig. 3 *and* Fig. 4a,b) were supplemented with spectrofluorimetry data of the dye solutions of different pH (Fig. 5). Intensity of the blue emission of Hoechst 33258 (we hypothesize that this emission can be attributed to the 1+ and possibly the 2+ form) in solution reached the highest value at pH 4. This was similar to microscopy measurements that showed the strongest blue emission of DNA-bound Hoechst in the buffers of pH 2.5–3.0. Note that the pH scales of microscopy and mass spectrometry experiments do not directly correspond to each other, as discussed below.

Spectral properties of the green-emitting form were more difficult to study, as demonstrated by Fig. 5. The low pH solution of Hoechst 33258 placed in a spectrofluorimeter most likely still contained all forms of the dye (0, 1+, 2+ and 3+ and possibly even the 4+), as might be inferred from the data obtained for the DNA-bound dye (Fig. 4). Thus, the putative triple-protonated green-emitting form of Hoechst 33258 was probably only a minor subpopulation of a large pool of molecules in all protonation states. It is reasonable to expect that the predominant form of Hoechst 33258, which is represented in such a solution, is still the original blue-emitting form. Thus the unprocessed emission spectrum of the solution is a convolution of emissions of all protonated forms and contains only a small contribution from the green emitting form or forms. Spectral separation of the blue and the green emitting forms is much easier in the case of a DNA-bound dye in a microscopy experiment. In this setting the photoconverted form is concentrated on nuclear DNA. Photoconversion of the DNA-bound dye is readily detectable and the blue and green emissions can be efficiently separated by using appropriate combinations of excitation wavelengths and the emission filters.

Reversibility of the Process of Hoechst 33258 Protonation

We demonstrated previously that subjecting Hoechst 33258 to a highly oxidising environment (30 % H_2O_2) resulted in generation of a green-emitting form of the dye, and that this process was fully reversible [1] (Fig. 6a). Here we hypothesize that the 3+ (and possibly the 2+) protonated forms of Hoechst 33258 induced by the environment of pH below 4 might be similar or identical to the green emitting forms of the dye induced by UV and, possibly, by oxidising conditions as well. We also presume that the 4+ form might be generated at pH below 2.0. Thus, we have examined the reversibility of the protonation of Hoechst 33258 which was induced by low pH.

We subjected the DNA-bound dye to a highly acidic environment (pH=1.0) in turns with a neutral-pH environment

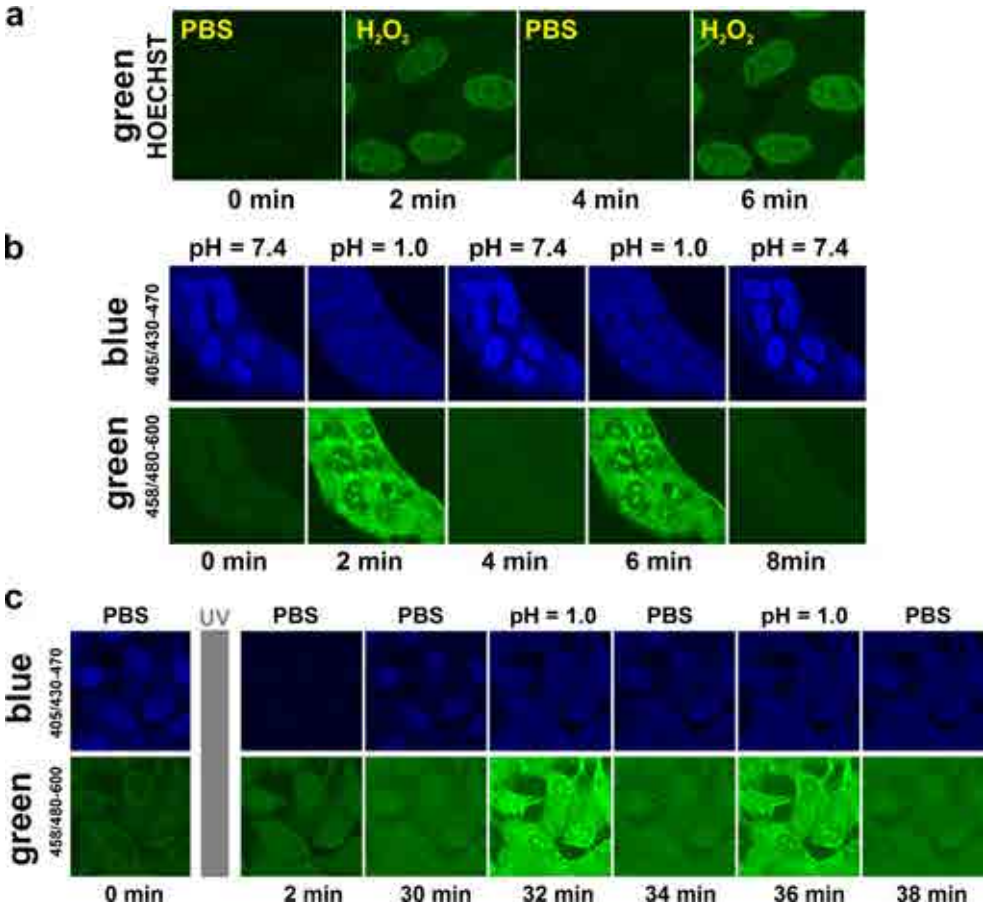

Fig. 6 Reversibility of changes of intensities of the blue and green emissions of DNA-bound Hoechst 33258 in fixed cells. **a** – Induction and disappearance of the green fluorescence emission signal during exposure of DNA-bound Hoechst 33258 to oxidising (30 % H_2O_2) and nonoxidising conditions (PBS), detected by fluorescence confocal microscopy (as shown in [1], Fig. 6). The γ-function of the images was set to 0.5. **b** – Induction and disappearance of the green fluorescence emission signal during exposure of Hoechst 33258 to low (pH=1.0) and neutral (PBS, pH 7.4) acidity environments (PBS), measured in a fluorescence confocal microscope. The γ-function of the images was set to 0.5. **c** – Acidity-induced reversible changes of the intensity of UV-induced Hoechst green fluorescence. The green emission of Hoechst was induced by UV in the same way as in the previously described experiments. Subsequently the photoconverted form of Hoechst was subjected to changes of acidity. The photoconverted, green emitting form of the dye exhibits reversible changes of the green emission, in response to changes of acidity of the environment. The γ-function of the images was set to 0.5

(pH=7.4) (Fig. 6b). As described previously, this low pH led to generation of the green emitting form which stained nucleoli rather than DNA in chromatin. Repeating this cycle of exposures to highly acidic and neutral environments resulted in appearance and disappearance of the green emitting form of the dye, suggesting that this process (i.e. generation of the protonated forms, including the putative 4+ form) was indeed fully reversible (Fig. 6b). Moreover, when cells stained with Hoechst 33258 were illuminated with UV, using a standard mercury metal arc lamp (360/40 nm emission filter, 11 mW), the green-emitting form was generated as expected (Fig. 6c). This form stained DNA in chromatin, suggesting that this was the 3+ form. When a sample treated according to this procedure was subjected to the repeated cycles of a highly acidic (pH 1.0) and neutral environment, a concomitant appearance and disappearance of Hoechst 33258 green fluorescence in nucleoli was detected. This observation and the previously described data (Fig. 4) indicate that the UV exposure as well as pH of approximately 2 to 4 may be inducing the 2+ and the 3+ form, which have affinity to DNA, while the pH 0.5–2.0 may induce the 4+ form which exhibits affinity to RNA.

Discussion

In the work described above we investigated generation of green-emitting forms of Hoechst 33258 (DNA-bound and in solution) by UV, oxidising conditions and by environments of low pH. In interpretation of our data we consider the 1+, 2+, 3+ and 4+ forms of the molecule. It is important to recognise, however, that the presence of the protophilic atoms of nitrogen in the molecule of Hoechst 33258 provides conditions for inducing many forms within a group embraced by a given net electric charge. For

instance, the fully protonated 4+ form may actually represent a mixture of several forms from among 128 possible protonation states [3]. Also, the neutral form may actually represent a molecule with one deprotonated and one protonated nitrogen atom [2]. Thus, the various protonated forms to which we refer in the text should be understood as potentially representing one of the structures described in Fig. 1 and based on [3], or other molecular structures that also yield a given net charge.

Mass spectrometry data presented in our report indicate that UV, exposure to oxidising conditions and low pH generate protonated forms of Hoechst 33258. Under the conditions we used, UV as well as oxidation appeared to induce 1+, 2+ and 3+ forms. Acidity led to generation of 1+, 2+, 3+ and possibly 4+ form as well. The protonation states that we observed were dependent on pH as would be expected.

MS and spectrally resolved data describing Hoechst 33258 in various pH environments were gathered in order to provide more information about the chemical nature of the green-emitting form (or forms) of the dye. This approach was based on an assumption that not only the parental molecule of the dye, but also the protonated forms of Hoechst 33258 emit fluorescence. In principle one should also consider a possibility of the protonated forms being nonfluorescent. In this case any attempt to link fluorescence changes (the observed shift to longer wavelength) with the protonation states would have no ground. As mentioned before, such a scenario is unlikely, since one would have to assume that all the protonated forms of Hoechst 33258 are nonfluorescent, while some other forms that carry no electric charge and are undetectable by MS would exhibit blue and green fluorescence. Such a possibility is highly improbable. Thus, in our reasoning we assume that the protonated forms are indeed fluorescent, and their spectral properties depend on their protonation state.

A comparison between the pH-dependent changes of abundances of various protonation forms of Hoechst 33258, as demonstrated by MS, and changes of fluorescence properties measured with spectrally resolved microscopy and spectrofluorimetry, leads us to postulate that the 1+ form emits blue fluorescence, while the green-emitting form induced by UV or low pH is the 3+ form (and possibly the 4+ form as well). This reasoning is based on the observation that the abundance of 3+ form detected by MS, and the intensity of fluorescence of the green form detected by spectrally resolved microscopy, increase rapidly as pH falls from approximately 4 to 2. The ranges of pH at which the increases occur are similar, however we note that the local pH in the immediate vicinity of DNA may differ slightly from the pH in the bulk of the buffer. This putative difference may mean that the DNA-bound Hoechst reside in an environment of somewhat different pH than the bulk solution i.e. different than the value given on the axis of the graph in Fig. 4. Moreover, it is not known if any quenching of fluorescence occurs in the case of DNA-bound Hoechst, and how acidity influences this process and the overall detected fluorescence intensity. While the green fluorescence can be attributed to the 3+ form with fair confidence, unfortunately, the available MS and fluorimetry data are not sufficient to assign blue or green emission to the 2+ form.

It is possible that the 4+ form was induced at pH below 2. MS studies of Hoechst 33258 in such a highly acidic environment were complicated by fragmentation of the molecule. Moreover, according to Ladinig et al. 2005 [3] the 4+ form of Hoechst becomes significantly represented only at pH<0. Therefore, in order to visualise it on MS spectra it is necessary to generate a very high concentration of this form in solution, which is technically cumbersome. In contrast, microscopy visualisation of the 4+ form is easier due to a high local concentration of this form bound to nucleic acids, and an ability to spectrally separate green and blue emissions using carefully selected excitation wavelengths and emission filters. Microscopic spectrally resolved data indicate that the form of the dye which is present at pH 0.5–2.0, that is a putative 4+ form, exhibited affinity to RNA. Conspicuously, the nucleoli of the fixed cells were brightly stained (green emission), while the areas rich in DNA emitted only very weak fluorescence. In this context it is important to mention that Hoechst 33258, as most if not all fluorescent probes used for labelling DNA, exhibits also some affinity for RNA [12]. Thus, the putative 4+ form may differ from 1+, 2+ and 3+ forms by having a higher affinity to RNA than DNA. Such a phenomenon, although unexpected, agrees with the fact that small modifications of the bis-benzimidazole molecule have been shown to result in strong changes of affinity and mode of binding to DNA [13, 14]. Interestingly, the issue of a relationship between protonation of Hoechst 33258 and a conformation of the molecule appears to remain unresolved, since minor as well as substantial conformation changes were postulated [2]. There is another factor which may have contributed to the nucleolar staining we observed. It is possible that under the acidic conditions self-quenching of fluorescence of Hoechst bound to DNA becomes very efficient, while quenching on RNA is poor. Such a phenomenon could contribute to the pattern of staining observed at pH below 2. More experimental work is required to resolve this issue. Another factor whose role is difficult to assess is denaturation of DNA at low pH, potentiated by exposure to exciting light [15]. However, we postulate that this phenomenon was not responsible for the staining pattern we observed, since acid denaturation would be expected to generate single stranded DNA. Such denatured DNA might be expected to be stained green, as RNA in nucleoli, at low pH.

Our observation of changes of the blue fluorescence emission accompanying protonation are in agreement with the previous reports, suggesting that changes in the chemical structure of Hoechst 33258 result in significant changes of the electronic charge distribution and, as a consequence, the spectral properties of the dye [5]. Also the data reported here are consistent with the view that the predominant form of Hoechst 33258 in a neutral

pH is the single-protonated form, while in a low pH environment it is the triple-protonated form [3], and at pH 4.5 Hoechst 33258 exists in a double-protonated form. Hoechst 33258 fluorescence emission spectra, excited by 365 nm, recorded at four different pH values (7, 4.5, 1.5 and 11) were reported before [5]. It is reasonable to expect that at this excitation only the emission component which we briefly refer to as 'blue' was detected. This study showed that lowering the pH value from 7 to 4.5 resulted in a significant increase in fluorescence yield of Hoechst 33258 and in a red-shift of the emission spectrum by ~22 nm. Presumably this shift was associated with generation of the 3+ protonated form of the molecule. Further lowering of the solution pH did not result in any further increase, but on the contrary, it led to a decrease of the fluorescence intensity. We have also seen an increase in the blue fluorescence of Hoechst in solution treated with solution of pH value 4.0 (Fig. 5) and Hoechst 33258 on DNA in the pH value of 3.0 (Fig. 4), nevertheless we have not noticed any increase of the blue (or green) fluorescence of Hoechst in a strongly alkaline environment. Mass spectrometry showed that in a strongly alkaline environment (pH ~11.0) Hoechst 33258 underwent strong ionisation with no prominent peaks of the protonated forms visible on MS-spectra (data not shown). Microscopy and spectrofluorimetry also confirmed that when Hoechst was subjected to a highly alkaline environment its blue fluorescence was significantly decreased (Figs. 4 and 5).

The dependence of the intensity of Hoechst 33258 blue fluorescence on pH was also reported by Görner and collaborators [16]. These experiments showed that Hoechst reached the highest intensity of the blue fluorescence around pH value 4.0. In our experiments the highest blue fluorescence intensity of Hoechst 33258 was observed near pH value of approximately 3.0 (Fig. 4). This difference may arise from the fact that in our experiments DNA-bound Hoechst was investigated while the data in the report [16] describe measurements of Hoechst 33258 in solution.

Conclusions

Upon exposure to UV DNA-bound Hoechst 33258 undergoes photoconversion to a blue-excited green-emitting form. Mass spectrometry revealed that UV, as well as exposure to oxidising conditions, result in generation of the protonated (1+, 2+, 3+ and possibly the 4+) forms of the dye. While the 1+, 2+ and 3+ forms of the dye exhibit affinity to DNA (fluorescence of nuclear DNA is strong, while RNA is very weak), the protonated form which exists in pH 0.5 (presumably the 4+) exhibits affinity to RNA.

Acknowledgments We gratefully acknowledge financial assistance of Polish National Committee for Science (UMO-2011/01/B/NZ3/00609, UMO-2013/11/B/NZ3/00189), Jagiellonian University (DS funds) and 'Doctus' scholarship awarded by Małopolska Centre of Entrepreneurship to DŻ-B. The confocal microscope was purchased through an EU structural funds grant BMZ no. POIG.02.01.00-12-064/08.

References

1. Żurek-Biesiada D, Kędracka-Krok S, Dobrucki JW (2013) UV-Activated Conversion of Hoechst 33258, DAPI, and Vybrant DyeCycle Fluorescent Dyes into Blue-Excited, Green-Emitting Protonated Forms. Cytometry A 83(5):441–51
2. Alemán C, Namba AM, Casanovas J (2005) Acid–base and electronic structure-dependent properties of Hoechst 33342. J Biomol Struct Dyn 23(1):29–36
3. Ladinig M, Leupin W, Meuwly M, Respondek M, Wirz J, Zoete V (2005) Protonation Equilibria of Hoechst 33258 in Aqueous Solution. Helv Chim Acta 88(1):53–67
4. Adhikary A, Bothe E, Jain V, von Sonntag C (2000) Pulse radiolysis of the DNA-binding bisbenzimidazole derivatives Hoechst 33258 and 33342 in aqueous solutions. Int J Radiat Biol 76(9):1157–66
5. Barooah N, Mohanty J, Pal H, Sarkar SK, Mukherjee T, Bhasikuttan AC (2011) pH and temperature dependent relaxation dynamics of Hoechst-33258: a time resolved fluorescence study. Photochem Photobiol Sci 10(1):35–41
6. Barooah N, Mohanty J, Pal H, Bhasikuttan AC (2011) Supramolecular assembly of Hoechst-33258 with cucurbit[7]uril macrocycle. Phys Chem Chem Phys 13(28):13117–26
7. Szczurek AT, Prakash K, Lee HK, Żurek-Biesiada DJ, Best G, Hagmann M, Dobrucki JW, Cremer C, Birk U (2014) Single molecule localization microscopy of the distribution of chromatin using Hoechst and DAPI fluorescent probes. Nucleus 19:5(4)
8. Morgan TL, Yang DJ, Fry DG, Hurlin PJ, Kohler SK, Maher VM, McCormick JJ (1991) Characteristics of an infinite life span diploid human fibroblast cell strain and a near-diploid strain arising from a clone of cells expressing a transfected v-myc oncogene. Exp Cell Res 197(1):125–36
9. Latt SA, Stetten G (1976) Spectral studies on 33258 Hoechst and related bisbenzimidazole dyes useful for fluorescent detection of deoxyribonucleic acid synthesis. J Histochem Cytochem 24(1):24–33
10. Stokke T, Steen HB (1986) Fluorescence spectra of Hoechst 33258 bound to chromatin. Biochim Biophys Acta 868(1):17–23
11. Weisblum B, Haenssler E (1974) Fluorometric properties of the bibenzimidazole derivative Hoechst 33258, a fluorescent probe specific for AT concentration in chromosomal DNA. Chromosoma 46(3):255–60
12. Ebrahimi SE, Bibby MC, Fox KR, Douglas KT (1995) Synthesis, DNA binding, footprinting and in vitro antitumour studies of a meta-hydroxy analogue of Hoechst 33258. Anticancer Drug Des 10(6):463–79
13. Bailly C, Colson P, Houssier C, Wang H, Bathini Y, Lown JW (1994) Mode of DNA binding of bis-benzimidazoles and related structures studied by electric linear dichroism. J Biomol Struct Dyn 12(1):173–81
14. Seaton A, Higgins C, Mann J, Baron A, Bailly C, Neidle S, van den Berg H (2003) Mechanistic and anti-proliferative studies of two novel, biologically active bis-benzimidazoles. Eur J Cancer 39(17):2548–55
15. Bernaś T, Asem EK, Robinson JP, Cook PR, Dobrucki JW (2005) Confocal fluorescence imaging of photosensitized DNA denaturation in cell nuclei. Photochem Photobiol 81(4):960–9
16. Görner H (2001) Direct and sensitized photoprocesses of bisbenzimidazole dyes and the effects of surfactants and DNA. Photochem Photobiol 73(4):339–48

PAPER 3:

Single molecule localization microscopy of the distribution of chromatin using Hoechst and DAPI fluorescent probes

RESEARCH PAPER

Nucleus 5:4, 331–340; July/August 2014; © 2014 Landes Bioscience

Single molecule localization microscopy of the distribution of chromatin using Hoechst and DAPI fluorescent probes

Aleksander T Szczurek[1,†], Kirti Prakash[1,2,†], Hyun-Keun Lee[1,3,†], Dominika J Żurek-Biesiada[4], Gerrit Best[5,6], Martin Hagmann[5,6], Jurek W Dobrucki[4], Christoph Cremer[1,2,3,5], and Udo Birk[1,3,5,*]

[1]Institute of Molecular Biology; Mainz, Germany; [2]Institute for Pharmacy and Molecular Biotechnology; University of Heidelberg; Heidelberg, Germany; [3]Department of Physics; University of Mainz; Mainz, Germany; [4]Faculty of Biochemistry, Biophysics, and Biotechnology; Jagiellonian University; Kraków, Poland; [5]Kirchhoff Institute for Physics; University of Heidelberg; Heidelberg, Germany; [6]University Hospital Heidelberg; University of Heidelberg; Heidelberg, Germany

[†]These authors contributed equally to this work.

Keywords: localization microscopy, blinking, Hoechst, DAPI, DNA, chromatin, photoconversion, super-resolution microscopy, SPDM, SMLM, dSTORM, fluorescence microscopy, nucleus

Abbreviations: SMLM, Single Molecule Localization Microscopy; DAPI, 4',6-diamidino-2-phenylindole; dSTORM, direct Stochastic Optical Reconstruction Microscopy; SPDM, Spectral Position Determination Microscopy

Several approaches have been described to fluorescently label and image DNA and chromatin in situ on the single-molecule level. These superresolution microscopy techniques are based on detecting optically isolated, fluorescently tagged anti-histone antibodies, fluorescently labeled DNA precursor analogs, or fluorescent dyes bound to DNA. Presently they suffer from various drawbacks such as low labeling efficiency or interference with DNA structure. In this report, we demonstrate that DNA minor groove binding dyes, such as Hoechst 33258, Hoechst 33342, and DAPI, can be effectively employed in single molecule localization microscopy (SMLM) with high optical and structural resolution. Upon illumination with low intensity 405 nm light, a small subpopulation of these molecules stochastically undergoes photoconversion from the original blue-emitting form to a green-emitting form. Using a 491 nm laser excitation, fluorescence of these green-emitting, optically isolated molecules was registered until "bleached". This procedure facilitated substantially the optical isolation and localization of large numbers of individual dye molecules bound to DNA in situ, in nuclei of fixed mammalian cells, or in mitotic chromosomes, and enabled the reconstruction of high-quality DNA density maps. We anticipate that this approach will provide new insights into DNA replication, DNA repair, gene transcription, and other nuclear processes.

Introduction

In order to study the functional architecture of chromatin at the nanoscale, highest resolution light microscopy of DNA in intact 3D cell nuclei should prove to be a major source of information. Several attempts to investigate chromatin nanostructure by super-resolution microscopy have been undertaken either by detecting the GFP-tagged core histones,[1-3] or by imaging fluorescently labeled DNA, using cyanine intercalators[4,5] (YOYO-1, TO-PRO-1), minor groove binders[4,5] (SYTO, PicoGreen), or by a special bleaching-based approach termed generalized single molecule high-resolution imaging with photobleaching (gSHRImP) on POPO-3 labeled DNA.[6] DNA intercalators, however, can interfere with the DNA structure.[24] Recently, super-resolution on the single molecule detection level using a DNA precursor analog, 5-ethynyl-2′-deoxyuridine (EdU), was reported, following incubation throughout a complete cell cycle.[7] EdU was labeled with a standard fluorophore using a "click" reaction. However, such long-term incorporation of DNA precursor analogs results in toxicity[8] (affecting cells before fixation) and in a variety of staining patterns.

So far, all methods for direct single molecule localization microscopy of nuclear DNA have suffered from serious drawbacks. The lack of a proper tool for accurate direct imaging of DNA nanostructures poses a major obstacle to the investigation of nuclear processes such as studies of spatial relationships between global DNA distribution and specific replication units, transcription and splicing complexes, or linker DNA and nucleosome core proteins (for a review see[9]). The recently described UV-induced photoconversion of standard DNA

*Correspondence to: Udo Birk; Email: u.birk@imb-mainz.de
Submitted: 04/04/2014; Revised: 06/06/2014; Accepted: 06/12/2014; Published Online: 06/19/2014
http://dx.doi.org/10.4161/nucl.29564

minor groove binding dyes opens new opportunities in super-resolution imaging of chromatin in situ. In combination with the aforementioned questions related to nuclear nanostructures, this UV-induced photoconversion of DNA minor groove binding dyes promotes super-resolution imaging of chromatin in situ.[10,11]

Among a wide variety of DNA stains applied in fluorescence microscopy, the DNA minor groove binders bisbenzimide Hoechst and DAPI are the two most commonly used. Both have their excitation maxima around 360 nm and their emission maxima around 460 nm. Recently it has been shown that both dyes can be readily converted from the blue-emitting state to their green-emitting derivatives upon illumination with UV[10,11] or 405 nm laser light.[11] Mass spectrometry studies demonstrated that under these circumstances Hoechst 33258 and DAPI undergo protonation.[11] Interestingly, conversion of the blue-emitting into the green-emitting forms of these dyes may be driven by hydrogen peroxide as well.[11] When excited with a 458 nm Ar^+ laser line, these photoconverted forms of Hoechst 33258 and DAPI emit green fluorescence, with the emission maxima shifted from 465 nm to 530 nm (Hoechst) and from 454 nm to 505 nm (DAPI).[11] Furthermore, the photoconverted green-emitting forms of the dyes are bleached readily under blue excitation.[11]

Here we took advantage of these exceptional features of Hoechst and DAPI dyes, and employed them in single molecule localization microscopy (SMLM)[12] of DNA in situ. A special SMLM approach, Spectral Position Determination Microscopy (SPDM) with physically modified fluorochromes,[12,13] was applied. In this SMLM variant, blinking of standard fluorophores is induced by appropriate high illumination intensities at suitable excitation wavelengths, in the presence of a chemical environment favoring the processes of both blinking and photoconversion. In this blinking-based imaging approach molecules emit fluorescent bursts[3] after stochastic recovery from a "non-emitting" form until they are bleached. Because of the possibility of multiple bursts being emitted from a single fluorophore, we use the term "signals" rather than "molecules" throughout the text. Means to eliminate such multiple detections in our experiment are described in Materials and Methods.

Interestingly, upon illumination with a high intensity 491 nm laser light, the green-emitting forms of Hoechst- or DAPI-stained DNA exhibit such stochastic blinking, which can be detected in the green-yellow channel. Thus, in a given field of view and at a given moment (under suitable illumination and environmental conditions), only a few, optically isolated molecules reside in the green-emitting fluorescent state. The emission induced by the 491 nm excitation light can be recorded until the molecules are bleached. The center of an individual fluorescent burst designates the position of a single fluorescing molecule in the object space.[12] Subsequently, other molecules stochastically undergo the transition from the blue-emitting to the green-emitting form under simultaneous illumination with 405 nm light, again to be recorded individually. This enables the optical isolation of a number of closely spaced single molecules, and assignment to a joint localization map.

Here, we report on the first successful "nanoimaging" of the positions of Hoechst and DAPI molecules, using localization microscopy of chromatin in fixed mammalian cells, with an average precision of localization of 15–25 nm. Consequently, this new approach allowed us to perform optical imaging of the local distribution of DNA in the cell nucleus and in mitotic chromosomes with a high optical and structural resolution, down to a few tens of nanometers.

Results

Under the conditions used, we could not obtain blinking-based superresolution images from the standard blue-emitting forms of the dyes. In a previous paper we noted that the signals of the green-emitting forms of both dyes, Hoechst 33258 and DAPI, are rather weak under standard experimental conditions.[11] Under these conditions the vast majority of the molecules bound to DNA remains in their blue-emitting form, except for a small fraction of the green-emitting form, which presumably remains in equilibrium with the parent form of the dye.[11] The population of molecules in this green-emitting form can be enriched by 405 nm-induced photoconversion.[11] Controlling the power of the 405 nm illumination, the number of molecules in the green-emitting form can be adjusted to fulfil the criterion of optical isolation required for localization based superresolution.

For detection of the green-emitting molecules, we used 491 nm illumination with appropriate intensities. Without 405 nm illumination, a lower blinking rate in the green-yellow emission channel was observed (see **Fig. S1**) (approximately 11 signals per frame corresponding to 0.08 signals per μm^2). Nonetheless, after the registration of 10 000 frames, the total number of approximately 110 000 detected fluorescent bursts was already sufficient to reconstruct an image based on molecule position information (see example in **Fig. S1**). Then, the 405 nm excitation was switched on, and in the following 10 000 frames, a substantially higher number of optically isolated fluorescence signals was recorded in the same sample region. Hence, at a given number of frames registered, the structural resolution was further enhanced due to a higher number of detected molecules. Subsequently, the 405 nm laser line was used in all further experiments resulting in a continuous replenishment of the population of the green-emitting photoproducts during the measurement.[11] The different illumination modes using two lasers at 405 nm and 491 nm are compared in **Figure 1**. The emission spectra of the original (blue) and the photoconverted (green) forms of Hoechst or DAPI overlap significantly (**Fig. 2G**; **Fig. S2**). We selected a detection band in the green-yellow range (585–675 nm) to minimize crosstalk from the long-wavelength emission tail of the blue-emitting form.

Furthermore, our imaging protocol allows for significantly extended measurement times. The main reason for this is the fact that 491 nm light is only marginally absorbed by the original (blue) forms of the dyes (absorption maxima: Hoechst; λ_{exc} = 355 nm, DAPI; λ_{exc} = 364 nm). After the localization measurement including 405 nm illumination, the fluorescence intensity of the Hoechst 33258 blue-emitting form dropped to 89 ± 4% normalized to 100% prior to the experiment, while in the case without

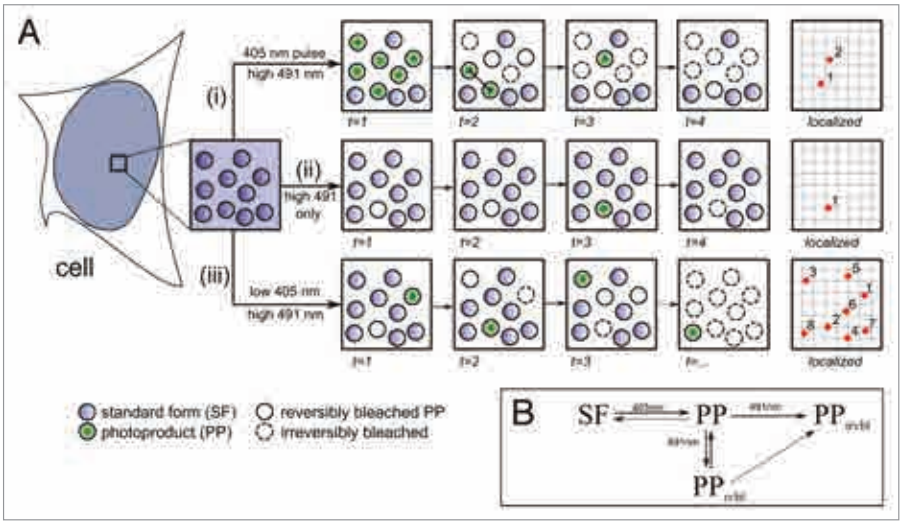

Figure 1. A putative scheme suggesting a photophysical mechanism for single molecule localization microscopy of photoconverted DNA minor groove binders, proposed on the basis of our experimental observations. Enlarged insets in (**A**) indicate DNA-bound dye molecules in a small subdiffractional area (rectangle) where only one fluorescent burst can be discerned per frame (t = 1, 2, 3, ...). Depiction of the effects of several modes of illumination: (i) High intensity 491 nm light applied after an intense 405 nm pulse: photoconverted molecules "blink" for several minutes after the pulse (in absence of the 405 nm excitation), indicating the existence of a light induced, non-emitting, reversibly bleached state; immediate saturation at the beginning of acquisition (t = 1) prevents the extraction of most single molecule signals. Closely spaced signals registered in the same frame are extracted incorrectly as a single point emitter due to diffraction (t = 2). Position coordinates are assigned to the fluorescent bursts detected in the green-yellow channel (red dots). (ii) When only high intensity 491 nm illumination is applied on the sample, blinking is rarely observed due to the low content of natively present green-emitting form of the dyes. This results in rather few localized signals in the green-yellow channel (**Fig. S1**). Spontaneous conversion of molecules to the green form might be possible; however we have no experimental proof. (iii) Simultaneous illumination of the sample with high intensity illumination at 491 nm plus low intensity illumination with 405 nm light as described in Materials and Methods. This approach allows not only an immediate registration of the blinking photoproduct after stochastic recruitment upon 405 nm illumination, but also the concomitant preservation of photophysical properties of the standard form. Time of acquisition may be freely expanded in order to register a large number of molecules in several tens of thousands of frames (t = …). We anticipate that Hoechst and DAPI can easily be applied to localization microscopy involving sequential pulse photoconversion (405 nm) and pulse excitation (491 nm). (**B**) Proposed schemes of photoinduced reactions: SF, Standard Form; PP, green-emiting photoproduct; PP_{rvbl} , Reversibly bleached photoproduct; PP_{irvbl}, Irreversibly bleached photoproduct. The reverse reaction of photoconversion can be proposed on grounds of a chemical equilibrium. Direct transition from the reversibly bleached state to the irreversibly bleached state can, e.g., be caused by photooxidation or photolysis.

405 nm illumination the fluorescence intensity decreased to 88 ± 5% (n = 10 cells, the detailed protocol is described in Materials and Methods). A related approach, simultaneously utilizing two laser lines (for excitation and for induction of the blinking-"on"-state), was already described for other fluorophores and was named STORM[14]/dSTORM.[15] In contrast, in our protocol the two laser lines are used for generation and excitation plus reversible bleaching of the photoproduct (DAPI and Hoechst).

In order to perform single molecule localization microscopy experiments based on blinking of the green-emitting photoconverted form, the imaging buffer composition must be carefully adjusted in order to obtain a suitable blinking rate (frequency of switching between the non-emitting state and the state in which they emit fluorescent bursts, become detected and later localized). We observed a strong dependence of the blinking behavior in the green-yellow channel on the oxygen content of the embedding medium, when excited with 491 nm light (**Fig. S3**). Oxygenation was modified by an oxygen scavenging system consisting of glucose oxidase and catalase in glycerol. We then determined the optimal concentrations of these enzymes (see Materials and Methods for details) and were able to obtain a 50-fold increase in the number of fluorescent burst signals detected, and a 200-fold increase in comparison to PBS (for detailed effects of the imaging buffer, see **Supplementary Materials** and **Fig. S3**). The optimized embedding medium was then used for all further experiments and resulted in the optical isolation and detection of numerous blinking molecules that stochastically emitted fluorescence bursts (for further information see **Fig. S3**).

We examined three bisbenzimide dyes (DAPI, and two forms of Hoechst) for use in localization microscopy of DNA with the aforementioned imaging protocol. We found that DAPI was less efficient for SMLM than Hoechst dyes, possibly due to higher crosstalk between blue-emitting and green-emitting forms which resulted in lower signal-to-noise ratio for single fluorescent molecules (**Fig. 2G**; **Fig. S2**). Thus, we favor Hoechst dyes for SMLM rather than using DAPI. Both Hoechst and DAPI exhibit a similar qualitative behavior under different illumination schemes as summarized in **Figure 1**. The use of these effects for SMLM is assessed experimentally in the following.

An application of the principle of blinking of bisbenzimide dyes is shown in **Figure 2**. It illustrates that a careful adjustment of the intensities of the 405 nm and the 491 nm lasers along with suitable imaging buffers and camera settings enabled precise localization of Hoechst 33258 molecules bound to DNA in the nucleus of a HeLa cell. All structural features of the widefield fluorescence image of the original, blue-emitting form of the dye (emission filter 470[70]) (**Fig. 2C**) are readily visible also in the localization microscopy image (**Fig. 2A**); however, the latter provides much better contrast and optical/structural resolution with much more recognizable details (**Fig. 2**, **Fig. S4**). Note that our acquisition system is optimized for SMLM measurements in terms of pixel size. Therefore, the widefield images presented as raw data are not optimal. In line with previous SPDM studies of histone H2B stably expressed with GFP,[1] the nucleus shows a pattern of higher chromatin density regions adjacent to the nuclear envelope (**Fig. 2B and F**) and around the nucleoli (**Fig. 2D**), likely representing heterochromatin. An expected lower signal density of the photoconverted form of the dye is detected in the euchromatic regions, in agreement with the wide field image.

Furthermore, we applied our photoproduct-based localization microscopy method to "nanoimaging" of mitotic chromosomes, having a higher chromatin density than in interphase. To perform highly efficient DNA localization imaging under these conditions, it was necessary not only to adjust the intensities of both laser lines (491 nm and 405 nm), but to adjust the dye concentration as well, taking into account the resulting signal density of the structure of interest. Typically, in densely labeled objects, we observed a significantly reduced precision of signal acquisition and localization due to a high fluorescence background. Hence, we used a much lower concentration of Hoechst 33342 to acquire satisfactory SMLM images of the highly condensed mitotic chromosomes. A comparison between images recorded in the conventional resolution widefield mode and in the single molecule localization mode based on the Hoechst 33342 photoproduct explicitly demonstrates that the density of DNA in a condensed chromosome is non-uniform at the nanoscale, and small regions of higher and lower DNA density can be readily recognized (**Fig. 3**). Such microdomains of different DNA densities have been anticipated in metaphase chromosomes on the basis of transmission[16] and scanning electron microscopy data,[17] as well as near-field optical microscopy.[18] Small chromatin subdomains are also predicted in chromatin coarse grain models.[19] In the case of the localization images obtained here, dense chromatin clusters are readily distinguishable in the density map in **Figure 3D**.

The mean localization accuracy in this experiment (which quantifies the precision of position estimation in localization microscopy and hence impairs the achieved optical resolution) was estimated to be approximately 14 nm using the same evaluation algorithm as in **Figure 3**, in contrast to ca. 25 nm in the case of data obtained in intact nuclei stained with Hoechst 33342. We ascribe this difference to the lower background intensities (the absence of out-of-focus contributions) and to a short distance between the imaged object and the coverslip (possibly resulting in less detectable optical aberrations originating from differences in refractive indices). Both are due to the drastically reduced sample thickness in the case of mitotic chromosomes as compared with an interphase nucleus. However, using a different statistical noise model for the changed imaging conditions (for details see Materials and Methods), the localization precision was estimated to be 45 nm (see **Fig. 3**) (46 nm when the Thompsons' assumptions were followed[20]). Similar values for the localization precision were also obtained in localization microscopy experiments using fluorescent proteins.[21]

Discussion

It is generally accepted that nuclear chromatin is organized on several levels of compaction. While the structure of the nucleosome is well known, the higher levels of chromatin organization are a matter of continuous debate. It is also broadly believed that these structures are difficult to preserve on the nanoscale. Thus, a promising approach to study chromatin structure must include careful fixation of the whole cell rather than attempts to isolate chromatin in a native state for further studies. Electron spectroscopic imaging has opened a new avenue to localize precisely certain elements, such as phosphorus or nitrogen inside a cell nucleus.[22] However, the labeling specificity on a level of compounds, rather than elements, can be easily implemented using fluorescence microscopy. Nevertheless, until recently the optical resolution of conventional fluorescence microscopy (~200 nm in the image plane and ~600 nm axially) has been far too low to precisely study the nanostructure of chromatin. The recent progress of super-resolution optical methods such as STED, SIM, and SMLM (PALM, STORM, SPDM, GSDIM, and a number of related techniques; for review see Cremer and Masters[23]) generated the methodological basis for 3-dimensional imaging of chromatin nanostructures. The localization microscopy described in this report, based on "nanoimaging" of minor groove binding DNA dyes, constitutes the next step in this direction.

Localization microscopy of a low molecular weight fluorescent dye, which is tightly bound to DNA, offers potential advantages over the techniques that have been proposed so far. Super-resolution imaging of chromatin based on detection of the core histones is promising, but is also affected by the limited access of an antibody or detachment of histones during replication, transcription or repair. The possibility to study the DNA conformation on the nanoscale may provide key information regarding the accessibility of chromatin to these factors. Another possibility is to label the total DNA directly by means of introducing DNA precursor analogs, a technique which is expected to be limited by the toxicity of the modified nitrogen base,[8] but which could effectively be combined with our protocol. In our experiments, cells were first fixed in a way that preserves the original configuration and structure to a high degree, and then fluorescently labeled, constituting a viable option in high resolution imaging. For successful localization microscopy experiments, the fluorescence emission rate of the single molecule emitters must be high, and the blinking rate of these emitters must

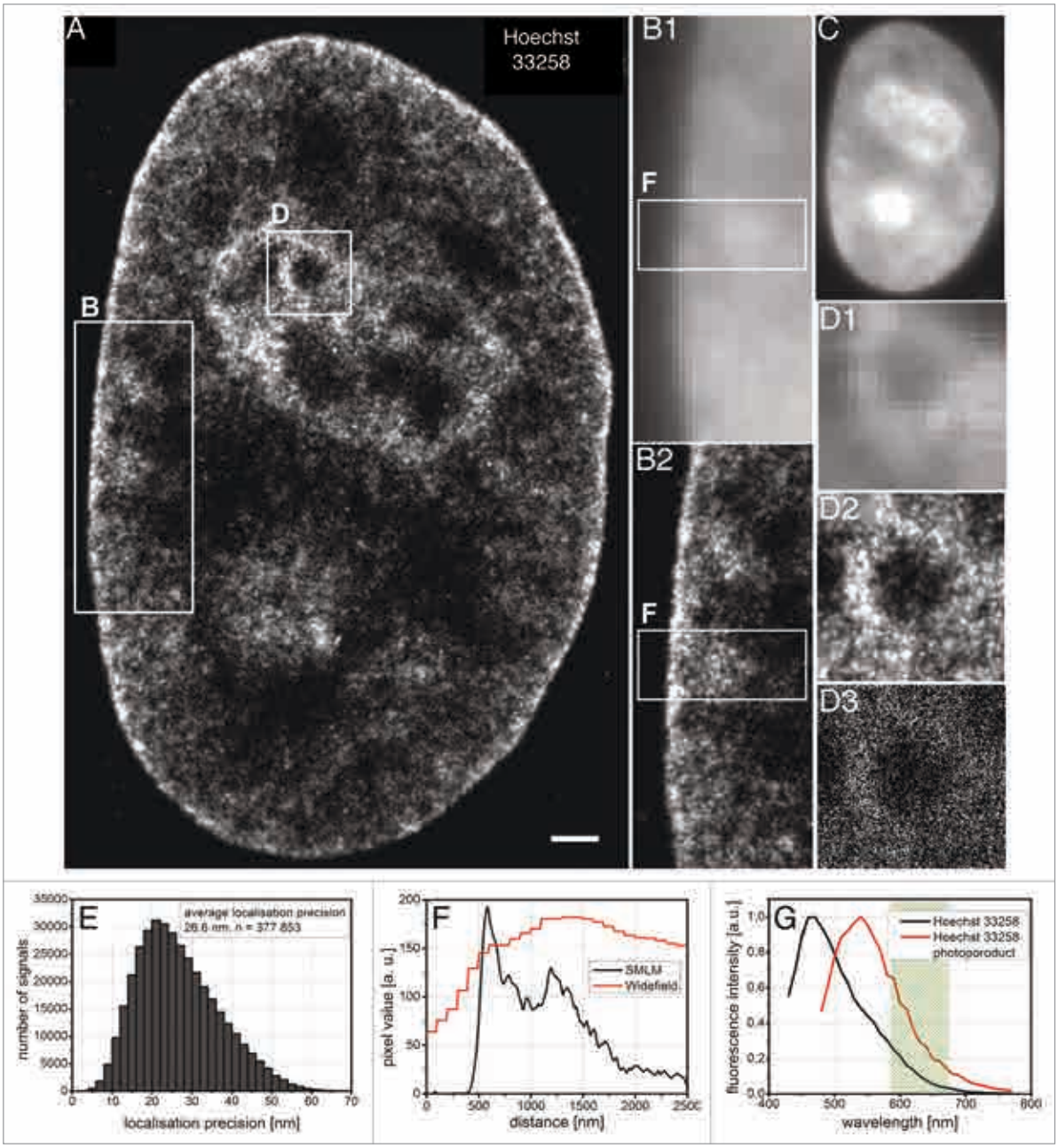

Figure 2. Structure of HeLa cell nucleus imaged by means of single molecule localization microscopy of the Hoechst 33258 photoproduct. Image acquired with high intensity laser excitation 491 nm combined with low intensity 405 nm light. (**A**) Localization microscopy of an optical plane through the entire nucleus allowed identification of approximately 400 000 signals. Localized points were blurred with the respective localization precision. Scale bar represents 1 µm. (**B**) Magnifications of a heterochromatic region in the vicinity of the nuclear envelope: (B1) widefield mode, (B2) photoproduct-based localization mode. Inserts correspond to 2.7 µm × 6.5 µm. (**C**) Raw data of a widefield preaquisition of the regular Hoechst form (λ_{exc} = 405 nm, λ_{em} = 450–490 nm). (**D**) Magnified inserts of a 1.8 µm × 1.8 µm region embracing a nucleolus: (D1) widefield mode, γ = 3, (D2) photoproduct signal positions blurred with the corresponding localization precision; (D3) point representations of localized signals. (**E**) The histogram of localization precision reveals an average value of roughly 27 nm, corresponding to an optical two-point resolution of individual molecules of about 70 nm. (**F**) Plot profile through the heterochromatic region indicated in (**B**) using widefield (red) and localization microscopy (black). (**G**) Emission spectra of DNA bound Hoechst 33258 (λ_{exc} = 405 nm, black) and its photoproduct (λ_{exc} = 458 nm, red) obtained with a confocal microscope equipped with an adjustable emission spectra (10 nm step size) as described previously.[11] The transmission band of the fluorescence emission filter used in the SMLM acquisitions is marked in green.

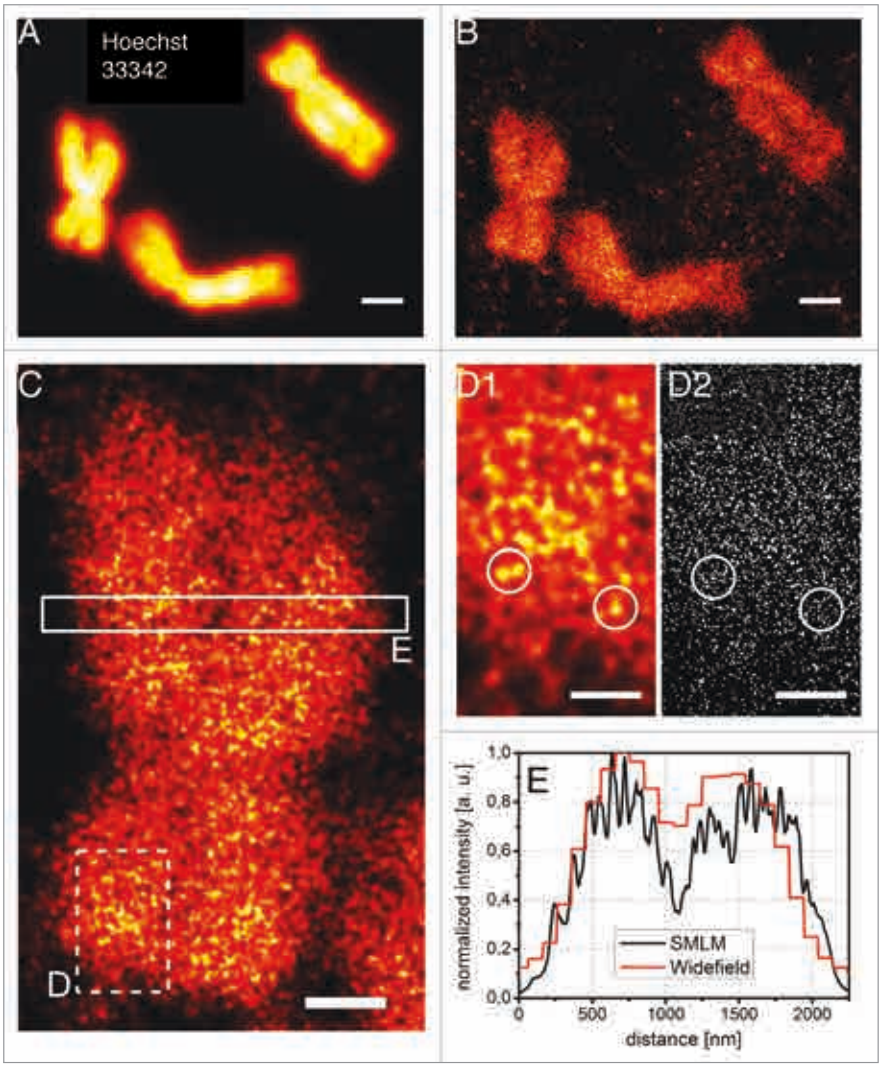

Figure 3. Single molecule localization microscopy of mitotic chromosomes stained with Hoechst 33342. Comparison of (**A**) the widefield image (raw data, collected in 450–490 nm range) and (**B**) the localization image of chromatin assessed by application of low intensity 405 nm together with high intensity 491 nm light shows the superiority of the latter. The localization image (**B**) depicts the density map of chromosomes obtained from blinking Hoechst 33342 photoproduct molecules. Common background signals stem from cellular debris containing DNA, possibly originating from detached chromatin fibers and mitochondria. Scale bar corresponds to 1 µm. (**C**) Density map assessed by means of triangulation performed on the data set acquired in the photoproduct SMLM measurement of a single chromosome. Scale bar represents 500 nm. (**E**) Plot profile through both chromatids for widefield and localization images taken from the rectangular region indicated in (**C**). Enlarged inserts indicated with the dashed line on (**C**): (**D1**) enlarged fragment of the density map, (**D2**) point representation of the data set processed for density maps, circles indicate examples of signal clusters. Scale bar in (**D**) is 200 nm. In (**E**) a spatial modulation of the signal below the diffraction limit is observed. Emission spectra of Hoechst 33342 and its photoproduct are available in **Figure S3A**.

provide for optical isolation, i.e., a sparse distribution of a few detected molecules in any acquired frame. These preconditions have been fulfilled so far by YOYO-1 and YO-PRO-1 cyanine dyes intercalating between DNA bases.[4,5] These dyes were applied to high quality localization imaging of small DNA structures such as bacterial chromosomes or single chromatin fibers, however with lesser success to eukaryotic nuclei.[5] The influence of intercalation between DNA bases on the overall structure of chromatin in a cell fixed by crosslinking methods is expected to be low, but needs to be investigated. Moreover, a prospect of imaging the structure of chromatin in live cells ought to be explored. It has been shown that DNA intercalators disturb interactions between the linker histone (H1) and DNA, while minor groove binders do not have such an effect.[24] Histone H1 is a key factor in the control of chromatin higher order structures. Removal of a fraction of the H1 population from the DNA results in chromatin aggregation and disturbs the nuclear structure entirely. Thus DNA intercalators do not hold promise for super-resolution imaging of DNA in live cells. In contrast, DNA minor groove binders do not interfere with the interaction between histone H1 and DNA in vivo, and do not cause chromatin aggregation and various subsequent adverse effects.[24]

As we have demonstrated in this report, three popular DNA minor groove binding dyes, Hoechst 33258, Hoechst 33342, and DAPI, can be used to reconstruct localization microscopy images of DNA by exploiting the phenomenon of their UV-induced photoconversion.[10,11] The localization microscopy images presented here depict regions of high and low DNA concentration at molecular optical resolution: on average, the smallest detectable distance between two individual Hoechst/DAPI molecules can be estimated by converting the localization accuracy to the width of the probability distribution of the position of the detected molecule (which equals ca. 2.3 times the localization accuracy achieved),[25] namely approximately 50 nm. This method of imaging cell nuclei outperforms previous conventional (**Fig. S5**)

and localization-based methods in terms of resolution, sampling rate of the labeled DNA containing structure, photostability of the dyes, and simplicity of application in any laboratory without need of additional complex evaluation software as previously reported.[6] Moreover, preliminary data (not shown) suggest that combination with other SMLM compliant dyes (e.g., Alexa, Atto, etc.) is possible and in the near future shall provide a novel tool for investigations of DNA associated proteins.

In our study, we have shown that the method is capable to produce nanoscale images of the nuclear DNA distribution using standard dyes, without the need to introduce foreign genes (e.g., for GFP) or base analogs (as e.g., EdU). The single molecule localization data sets will allow a large variety of quantitative evaluations (e.g., radial density analysis[26]), as well as tests of numerical models of the mammalian genome. It may be noted that the large DNA density fluctuations (up to almost two orders of magnitude) observed on the nanoscale (see **Fig. S4**) are not in contradiction to mutually disjunct chromosome territories (potentially giving rise to a specific interchromatin compartment). Both numerical model calculations and experimental evidence indicate that such chromosome territories (except a relatively small border zone of typically a few hundred nanometers) result in nuclear zones of very low DNA density. Such zones are clearly observed in the localization images presented here. We expect that future quantitative SMLM studies will allow measurements of the extent of the interchromatin domain compartment at substantially higher resolution than conventional fluorescence microscopy.

The reconstructed images obtained by means of localization microscopy have pointillistic features, hence, discrimination of fine details depends on the density and precision of position estimation of the molecules detected.[27] A somatic cell genome consists of 6×10^9 base pairs,[28] which comprises roughly 10^8–10^9 putative binding sites for DNA minor groove binding dyes.[29] Assuming a nuclear volume of ~300 μm^3 (ellipsoid with a lateral radius of 6 µm and an axial thickness of 4 µm) and an observation volume of ~50 μm^3 (acquisition of the central cross-section in an optical section of ~0.5 µm thickness), approximately one sixth of these binding sites are present in the observed volume, corresponding to about 2×10^7 to 2×10^8 putative minor groove binding sites. At the present state of the art, the yield of the localization method described here allowed the identification of approximately 10^6 signals (assuming fluorescent bursts to represent individual molecules) with a concomitant loss of only 10% of fluorescence intensity after an acquisition series, which is quite difficult to achieve in localization microscopy (**Fig. S3C**). This means that even the one million of localized dye binding sites which we detected in our experiments still constitutes only a minor fraction of all the dye molecules in this region. It should be noted that the fraction of dye molecules remaining in the blue-emitting state for the entire acquisition time did not contribute to our localization images. However, it is also important to note that if one million of molecules are detected in a nuclear area of 100 μm^2 (and 500 nm thickness) the number of detected molecules amounts to 100 × 100 per 1 μm^2 in the image. This also means that the projected image of this slice of the nucleus contains on average one localized molecule every 10 nm in the image (the distances in 3D space are obviously larger). Therefore, it seems reasonable to state that extending the amount of data collected (i.e., recording a larger number of fluorescence bursts) will eventually enable 3-dimensional super-resolution microscopy of chromatin on the single molecule level. Thus, we anticipate that this approach holds promise for solving structure and function questions that were not accessible to optical microscopy so far. Additionally, such microscopic data will provide the basis for quantitative evaluations of the distribution of chromatin also with the help of computer models of chromatin organization.

The method can be developed further and several questions still need to be answered. These include the importance of the AT-rich sequence preference of the three dyes used here for imaging of the entire nuclear chromatin.[30,31] Studies of Hoechst 33258 in solution revealed that the fluorescence emission intensity in the presence of GC containing sequences is only half of that in the presence of AT repetitions.[30] The latter are most often involved in the formation of heterochromatin and the different emissivity presumably leads to an overestimation of heterochromatin signal density and an underestimation in euchromatic regions.

Undoubtedly, many of the photophysical effects in SMLM of DNA binding dyes are still far from understood. Developing this technology requires better comprehension of the photoconversion mechanisms and of the blinking behavior for Hoechst dyes and DAPI. Their green-emitting forms appear to be more susceptible to light-induced changes, one of which being the exploited formation of a reversibly non-emitting form (**Fig. 1**; see also **Fig. S2A**). Such a non-emitting state was already reported for many standard fluorophores such as Alexa dyes or fluorescent proteins.[1,12,32-34] One could also anticipate that, upon 405 nm illumination, the investigated dyes are converted into several chemically different forms that may interact, so cooperative effects underlying the process of blinking cannot be excluded.[35] Apart from this, the effect of the 405 nm line on the blinking behavior of the green-emitting form of the dyes needs to be investigated further (for detailed discussion see **Supplementary Materials**). In our results, multiple detection of the same fluorophore due to reoccurring blinking cannot be excluded, resulting in an overestimation of the number of molecules detected. If such multiple blinking events occur frequently for each molecule, the detected signals will form a Gaussian distribution around the center position indicating the true fluorophore position. Due to the high labeling density we could not investigate such a distribution in our experiments, however on some individual fluorophores we recognized multi-blinking behavior.

As we have shown in this report, oxygen has a major influence on the blinking characteristics of green-emitting photoproducts of DNA dyes (**Fig. S3**), and only the utilization of oxygen-depleted media may facilitate blinking rates suitable for SMLM. Interestingly, once an oxygen scavenging system is employed, blinking becomes apparent only in a narrow window of oxygen concentration. We attribute this fact to the necessity of establishing an optimal proportion between the populations of irreversibly bleached photoproduct molecules (involving oxygen[36]) and molecules moved toward some transient non-emitting state upon

high intensity 491 nm illumination (**Fig. 1**). The addition of the triplet state quencher mercaptoethylamine (MEA),[37] previously used in dSTORM switching buffers,[15] led to a nearly 40-fold loss in the number of fluorescence bursts detected (**Fig. S3**). Future photophysical studies will hopefully reveal the nature of blinking of fluorescent molecules such as the DNA-binding dyes Hoechst and DAPI.

We anticipate that the use of the DNA-minor-groove binders presented here for super-resolution localization microscopy will be of great value in furthering our knowledge about pivotal nuclear processes such as DNA replication, transcription, or repair. Moreover, the results described here are highly relevant to the contemporary challenge to acquire precise information about local DNA compaction on the single gene level (potentially in combination with fluorescence in situ hybridization, TALEN,[38] and the CRISPR/Cas system[39] as recently used in superresolution microscopy), and to obtain super-resolution spatial maps of the whole genome. So far, a major limitation in the development of super-resolution methods for imaging of DNA is the still insufficient knowledge about the photophysical and chemical mechanisms of 'blinking'. We believe that a deeper understanding herein will pave the way for true "nanoscopy" of DNA and other nuclear structures down to a few nanometers.

Materials and Methods

Cell culture and sample preparation

HeLa cervical cancer cells were grown on 0.17 mm thick coverslips in 6-well plates filled with Dulbecco's Modified Eagles Medium supplemented with 10% (v/v) fetal bovine serum in 37 °C and high humidity. After 15 min fixation with 4% formaldehyde and following permeabilization using 0.5% Triton X-100, the cells were washed with phosphate buffered saline (PBS) and treated for 1 h with a 0.5 ml solution of aqueous RNase A (0.2 mg/ml, 37 °C). Afterwards, the DNA was stained for 30 min with 1 ml aqueous solution of either Hoechst 33258 (0.2 µg/ml), Hoechst 33342 (0.1 µg/ml), or DAPI (4',6-diamidino-2-phenylindole, 0.2 µM), added directly to the 6-well plate. Such low concentrations should not provide unforeseen effects on the binding mode.[40] Subsequently, cells were washed with PBS, then embedded in a solution consisting of glycerol with 10% imaging buffer (stock comprising 0.25 mg/ml Glucose oxidase, 0.02 mg/ml Catalase, 0.05 g/ml glucose in PBS), and immediately sealed with nailpolish. Measurements were performed instantly. For chromosome spreads we performed mitotic block on HeLa cells using vinblastine (126 µM for 4 h) followed by washing with medium. Afterwards the medium with mitotic cells was collected to 14 cm^3 flask and centrifuged (150 g, 5 min). Subsequently, the cell pellet was resuspended in 5 ml 75 mM KCl water solution for 10 min. Next, we added 5 ml fixative (3: 1 glacial acetic acid: methanol). After centrifugation (150 g, 5 min) cells were resuspended in ice cold fixative. This step was repeated at least 4 times. A cell suspension with 6 ng/ml Hoechst 33258 was dropped on a coverslip in horizontal position and air-dried until the fixative evaporated. Further sample preparation proceeded as mentioned above. All reagents were obtained from Sigma-Aldrich, Germany.

SPDM setup and measurements

The basic principle of the SMLM technique used here has been described in detail.[12,13] Under appropriate physicochemical conditions, the fluorophores are driven into a long-lived "reversibly bleached"/"dark" state by high intensity illumination, followed by their stochastic recovery to the fluorescent state (SPDM with physically modified fluorophores, in the following abbreviated as SPDM). Single fluorophores returning to the fluorescent state remain fluorescing only for a short period of time until they bleach permanently or return to a reversible "dark state" again. This process of switching between different absorption and/or emission states has been termed "blinking" and allows for the optical isolation and localization of single molecules with super-resolution precision (raw images available in **Fig. S2**). The calculated localization accuracy[20] (σ) is dependent on the number of detected photons (N), background noise per pixel (b), width of the point spread function (s), and pixel size (a) in the image plane and detection efficiency:

$$\sigma^2 = \frac{s^2 + a^2/12}{N} + \frac{8\pi s^4 b^2}{a^2 N^2}$$

The structural resolution in localization microscopy (R) depends on the mean localization precision of individual molecules ($< \sigma >$) and the mean distance of detected molecules, d (reflecting a quality of sampling the structure of interest):

$$R = \sqrt{(2.35 < \sigma >)^2 + (2d)^2}$$

The SPDM method as described by Lemmer et al. 2008[12] did not utilize a secondary light source for conversion or activation of fluorophores and relied solely on suitable embedding media and adjusted laser parameters (wavelength and intensity) of a single laser light source. Using suitably high illumination intensities combined with a high number of registered frames, the use of the 491 nm excitation laser alone was in principle sufficient to obtain SPDM images of the green-emitting photoproducts. For the dyes presented in this report, however, it was advantageous to also use a low intensity illumination at 405 nm in addition to high intensity illumination at 491 nm; this allowed us to increase the number of signals detected by continuously recruiting green-emitting photoproduct molecules during the measurement. Similar enhancements have been obtained in other cases also by dSTORM.[15]

For measurements, we used the custom built SMI-Vertico microscope.[13] Both spectrally distinct forms of Hoechst dyes and DAPI were illuminated with 0.002 kW/cm^2 by a 405 nm diode laser (Kvant Ltd) and with 1.5 kW/cm^2 by a 491 nm DPSS laser (Cobolt AB, Sweden). The fluorescence was detected using a 1.4 NA oil immersion objective (HCX PL APO, 63×, Leica Microsystems GmbH) and a high quantum efficiency CCD camera (SensiCam QE, PCO Imaging). To achieve the high laser intensity necessary for the localization mode, an additional achromatic lens (f = 500mm, Chroma GmbH) was used to

focus the beam. The emitted fluorescence was registered after passing through the band-pass emission filters 470(40) (Thorlabs GmbH) and 630(90) (Semrock) for the 405 nm laser and 491 nm laser, respectively. The detailed optical setup is shown in **Figure S6**.

During the experiments, raw image data stacks typically consisting of 20 000 images were recorded with an integration time of 65 ms. In these image stacks, the total number of separate fluorescent bursts identified per optical section of about 500 nm thickness through a cell nucleus ranged from about 400 000 to 2 000 000, depending on the cell line used.

To detect and localize these single bursts, we used two different algorithms written in MATLAB (The Mathworks Inc). For the images of the interphase cell nuclei we used the fastSPDM software as described by Grüll et al.[41] which is based on a center of gravity (CG) determination of the single molecule data. The software is particularly focused on high processing speed by efficient programming and possible application of field programmable gate arrays (FPGA).[41] Single molecule fluorescence bursts that were localized in several subsequent frames within the radius given by the localization accuracy were rejected by the software with only one position counted in order to avoid multiple localizations of the same fluorophore. However, a single fluorophore may emit fluorescence bursts again at later times during the measurement. Due to the stochastic nature of the fluorescent bursts, present algorithms are very limited in rejecting such temporally distant events of the same molecule; so far this constitutes an unresolved problem in the SMLM imaging method.

For the chromosome images we applied an adjusted algorithm, which uses a more complex method for the background estimation as well as a more realistic noise model and is therefore computationally more intense. Also, a more robust detection routine for closely spaced signals was included in the alternative algorithm. The localization of single events was based on CG determination of the signal weighed according to the maximum likelihood principle. A more detailed description of the algorithm is beyond the scope of this paper and shall be discussed in a subsequent publication. The raw images of the chromosomes contained, due to their condensed nature, higher local densities of blinking signals and also a strongly fluctuating background signal. The more robust alternative detection algorithm was found to be better suited for the chromosome images than fastSPDM, whereas both methods delivered very similar results for the interphase nucleus images. For reconstruction of the latter we have therefore used the previously published fastSPDM algorithm.

The long acquisition times resulted in considerable mechanical drift of the stage. We corrected the lateral drift taking advantage of the underlying structure visible in a raw image sequence (averaged over 10 subsequent frames for one sample image) and calculating the auto-correlation between sample images and fitting two (for x and y) eighth order Fourier series to the acquired data to obtain the drift vectors.

Density maps of the DNA distribution in chromosomes were obtained using a triangulation procedure. Such an approach of visualization involves iterative, multiplied reconstruction of SMLM images and was described before.[42] **Figure 3** was reconstructed using 100 iterations.

Disclosure of Potential Conflicts of Interest

No potential conflict of interest was disclosed.

Acknowledgments

We gratefully acknowledge the colleagues at IMB who supported us with reagents. In particular, we would like to thank Wolf Gebhardt, George Reid, Miguel Almeida, Stefan Redl, Rene Ketting, Juri Kazakevych, and Natalia Soshnikova for the reagents. Special thanks to Wolf Gebhardt and Heinz Eipel for many interesting discussions and to Vijay Tiwari for proof-reading the manuscript. This work was supported by the Boehringer Ingelheim Foundation and Polish National Center for Science (2011/01/B/NZ3/00609). A Doctoral Scholarship Doctus from the European Union, awarded to D.Z-B. is gratefully acknowledged. The support of University Hospital Heidelberg (Prof S. Dithmar) to G.B. and M.H. is also gratefully acknowledged.

Authors' Contributions

K.P., C.C., and U.B. initiated the project. A.S., H-K.L., K.P., and D.Z-B. designed the experiments. A.S. prepared the samples and performed the single-molecule measurements. H-K.L., K.P., C.C., and U.B. developed and constructed the SPDM microscopy apparatus used in the super-resolution microscopy laboratory (Cremer-Lab) of the IMB. K.P., G.B., M.H., and U.B. contributed to the software used to data analysis. D.Z. performed the confocal experiments. K.P., A.S., H-K.L., G.B., and M.H. performed the data analysis. C.C., J.D., and U.B. supervised the work. All authors contributed in writing of the manuscript.

Supplemental Materials

Supplemental materials may be found here:
www.landesbioscience.com/journals/nucleus/article/29564

References

1. Markaki Y, Gunkel M, Schermelleh L, Beichmanis S, Neumann J, Heidemann M, Leonhardt H, Eick D, Cremer C, Cremer T. Functional nuclear organization of transcription and DNA replication: a topographical marriage between chromatin domains and the interchromatin compartment. Cold Spring Harb Symp Quant Biol 2010; 75:475-92; PMID:21467142; http://dx.doi.org/10.1101/sqb.2010.75.042
2. Matsuda A, Shao L, Boulanger J, Kervrann C, Carlton PM, Kner P, Agard D, Sedat JW. Condensed mitotic chromosome structure at nanometer resolution using PALM and EGFP- histones. PLoS One 2010; 5:e12768; PMID:20856676; http://dx.doi.org/10.1371/journal.pone.0012768
3. Cremer C, Kaufmann R, Gunkel M, Pres S, Weiland Y, Müller P, Ruckelshausen T, Lemmer P, Geiger F, Degenhard S, et al. Superresolution imaging of biological nanostructures by spectral precision distance microscopy. Biotechnol J 2011; 6:1037-51; PMID:21910256; http://dx.doi.org/10.1002/biot.201100031
4. Flors C. DNA and chromatin imaging with super-resolution fluorescence microscopy based on single-molecule localization. Biopolymers 2011; 95:290-7; PMID:21184489; http://dx.doi.org/10.1002/bip.21574
5. Schoen I, Ries J, Klotzsch E, Ewers H, Vogel V. Binding-activated localization microscopy of DNA structures. Nano Lett 2011; 11:4008-11; PMID:21838238; http://dx.doi.org/10.1021/nl2025954

6. Simonson PD, Rothenberg E, Selvin PR. Single-molecule-based super-resolution images in the presence of multiple fluorophores. Nano Lett 2011; 11:5090-6; PMID:22003850; http://dx.doi.org/10.1021/nl203560r
7. Zessin PJM, Finan K, Heilemann M. Super-resolution fluorescence imaging of chromosomal DNA. J Struct Biol 2012; 177:344-8; PMID:22226957; http://dx.doi.org/10.1016/j.jsb.2011.12.015
8. Zhao H, Halicka HD, Li J, Biela E, Berniak K, Dobrucki J, Darzynkiewicz Z. DNA damage signaling, impairment of cell cycle progression, and apoptosis triggered by 5-ethynyl-2′-deoxyuridine incorporated into DNA. Cytometry A 2013; 83:979-88; PMID:24115313; http://dx.doi.org/10.1002/cyto.a.22396
9. Rouquette J, Cremer C, Cremer T, Fakan S. Functional nuclear architecture studied by microscopy: present and future. Int Rev Cell Mol Biol 2010; 282:1-90; PMID:20630466; http://dx.doi.org/10.1016/S1937-6448(10)82001-5
10. Piterburg M, Panet H, Weiss A. Photoconversion of DAPI following UV or violet excitation can cause DAPI to fluoresce with blue or cyan excitation. J Microsc 2012; 246:89-95; PMID:22288651; http://dx.doi.org/10.1111/j.1365-2818.2011.03591.x
11. Zurek-Biesiada D, Kedracka-Krok S, Dobrucki JW. UV-activated conversion of Hoechst 33258, DAPI, and Vybrant DyeCycle fluorescent dyes into blue-excited, green-emitting protonated forms. Cytometry A 2013; 83:441-51; PMID:23418106; http://dx.doi.org/10.1002/cyto.a.22260
12. Lemmer P, Gunkel M, Baddeley D, Kaufmann R, Urich A, Weiland Y, Reymann J, Müller P, Hausmann M, Cremer C. SPDM: light microscopy with single-molecule resolution at the nanoscale. Appl Phys B 2008; 93:1-12; http://dx.doi.org/10.1007/s00340-008-3152-x
13. Reymann J, Baddeley D, Gunkel M, Lemmer P, Stadter W, Jegou T, Rippe K, Cremer C, Birk U. High-precision structural analysis of subnuclear complexes in fixed and live cells via spatially modulated illumination (SMI) microscopy. Chromosome Res 2008; 16:367-82; PMID:18461478; http://dx.doi.org/10.1007/s10577-008-1238-2
14. Rust MJ, Bates M, Zhuang X. Sub-diffraction-limit imaging by stochastic optical reconstruction microscopy (STORM). Nat Methods 2006; 3:793-5; PMID:16896339; http://dx.doi.org/10.1038/nmeth929
15. Heilemann M, van de Linde S, Schüttpelz M, Kasper R, Seefeldt B, Mukherjee A, Tinnefeld P, Sauer M. Subdiffraction-resolution fluorescence imaging with conventional fluorescent probes. Angew Chem Int Ed Engl 2008; 47:6172-6; PMID:18646237; http://dx.doi.org/10.1002/anie.200802376
16. Adolph KW, Kreisman LR, Kuehn RL. Assembly of chromatin fibers into metaphase chromosomes analyzed by transmission electron microscopy and scanning electron microscopy. Biophys J 1986; 49:221-31; PMID:3955172; http://dx.doi.org/10.1016/S0006-3495(86)83636-0
17. Harrison CJ, Jack EM, Allen TD, Harris R. Investigation of human chromosome polymorphisms by scanning electron microscopy. J Med Genet 1985; 22:16-23; PMID:4039005; http://dx.doi.org/10.1136/jmg.22.1.16
18. Winkler R, Perner B, Rapp A, Durm M, Cremer C, Greulich K-O, Hausmann M. Labelling quality and chromosome morphology after low temperature FISH analysed by scanning far-field and near-field optical microscopy. J Microsc 2003; 209:23-33; PMID:12535181; http://dx.doi.org/10.1046/j.1365-2818.2003.01101.x
19. Tark-Dame M, van Driel R, Heermann DW. Chromatin folding--from biology to polymer models and back. J Cell Sci 2011; 124:839-45; PMID:21378305; http://dx.doi.org/10.1242/jcs.077628
20. Thompson RE, Larson DR, Webb WW. Precise nanometer localization analysis for individual fluorescent probes. Biophys J 2002; 82:2775-83; PMID:11964263; http://dx.doi.org/10.1016/S0006-3495(02)75618-X
21. Gunkel M, Erdel F, Rippe K, Lemmer P, Kaufmann R, Hörmann C, Amberger R, Cremer C. Dual color localization microscopy of cellular nanostructures. Biotechnol J 2009; 4:927-38; PMID:19548231; http://dx.doi.org/10.1002/biot.200900005
22. Bazett-Jones DP, Li R, Fussner E, Nisman R, Dehghani H. Elucidating chromatin and nuclear domain architecture with electron spectroscopic imaging. Chromosome Res 2008; 16:397-412; PMID:18461480; http://dx.doi.org/10.1007/s10577-008-1237-3
23. Cremer C, Masters BR. Resolution enhancement techniques in microscopy. Eur Phys J H 2013; 38:281-344; http://dx.doi.org/10.1140/epjh/e2012-20060-1
24. Wojcik K, Dobrucki JW. Interaction of a DNA intercalator DRAQ5, and a minor groove binder SYTO17, with chromatin in live cells--influence on chromatin organization and histone-DNA interactions. Cytometry A 2008; 73:555-62; PMID:18459157; http://dx.doi.org/10.1002/cyto.a.20573
25. Kaufmann R, Lemmer P, Gunkel M, Weiland Y, Müller P, Hausmann M, Baddeley D, Amberger R, Cremer C. SPDM: single molecule superresolution of cellular nanostructures. In: Enderlein J, Gryczynski ZK, Erdmann R, editors. Proceedings of the SPIE. 2009. page 71850J–71850J–19
26. Bohn M, Diesinger P, Kaufmann R, Weiland Y, Müller P, Gunkel M, von Ketteler A, Lemmer P, Hausmann M, Heermann DW, et al. Localization microscopy reveals expression-dependent parameters of chromatin nanostructure. Biophys J 2010; 99:1358-67; PMID:20816047; http://dx.doi.org/10.1016/j.bpj.2010.05.043
27. Allen JR, Ross ST, Davidson MW. Single molecule localization microscopy for superresolution. J Opt 2013; 15:094001; http://dx.doi.org/10.1088/2040-8978/15/9/094001
28. Hattori M; International Human Genome Sequencing Consortium. Finishing the euchromatic sequence of the human genome. Nature 2004; 431:931-45; PMID:15496913; http://dx.doi.org/10.1038/nature03001
29. Loontiens FG, Regenfuss P, Zechel A, Dumortier L, Clegg RM. Binding characteristics of Hoechst 33258 with calf thymus DNA, poly[d(A-T)], and d(CCGGAATTCCGG): multiple stoichiometries and determination of tight binding with a wide spectrum of site affinities. Biochemistry 1990; 29:9029-39; PMID:1702995; http://dx.doi.org/10.1021/bi00490a021
30. Weisblum B, Haenssler E. Fluorometric properties of the bibenzimidazole derivative Hoechst 33258, a fluorescent probe specific for AT concentration in chromosomal DNA. Chromosoma 1974; 46:255-60; PMID:4136742; http://dx.doi.org/10.1007/BF00284881
31. Aymami J, Nunn CM, Neidle S. DNA minor groove recognition of a non-self-complementary AT-rich sequence by a tris-benzimidazole ligand. Nucleic Acids Res 1999; 27:2691-8; PMID:10373586; http://dx.doi.org/10.1093/nar/27.13.2691
32. Baddeley D, Jayasinghe ID, Cremer C, Cannell MB, Soeller C. Light-induced dark states of organic fluochromes enable 30 nm resolution imaging in standard media. Biophys J 2009; 96:L22-4; PMID:19167284; http://dx.doi.org/10.1016/j.bpj.2008.11.002
33. Baddeley D, Crossman D, Rossberger S, Cheyne JE, Montgomery JM, Jayasinghe ID, Cremer C, Cannell MB, Soeller C. 4D super-resolution microscopy with conventional fluorophores and single wavelength excitation in optically thick cells and tissues. PLoS One 2011; 6:e20645; PMID:21655189; http://dx.doi.org/10.1371/journal.pone.0020645
34. Huber O, Brunner A, Maier P, Kaufmann R, Couraud PO, Cremer C, Fricker G. Localization microscopy (SPDM) reveals clustered formations of P-glycoprotein in a human blood-brain barrier model. PLoS One 2012; 7:e44776; PMID:22984556; http://dx.doi.org/10.1371/journal.pone.0044776
35. Zurek-Biesiada D., Waligórski P. DJ. Mass spectrometry and fluorimetry analysis of blue-excited green-emitting protonated forms of Hoechst 33258 generated by exposure to ultraviolet light (submitted). 2014
36. Bernas T, Zarebski M, Dobrucki JW, Cook PR. Minimizing photobleaching during confocal microscopy of fluorescent probes bound to chromatin: role of anoxia and photon flux. J Microsc 2004; 215:281-96; PMID:15312193; http://dx.doi.org/10.1111/j.0022-2720.2004.01377.x
37. Song L, Varma CA, Verhoeven JW, Tanke HJ. Influence of the triplet excited state on the photobleaching kinetics of fluorescein in microscopy. Biophys J 1996; 70:2959-68; PMID:8744334; http://dx.doi.org/10.1016/S0006-3495(96)79866-1
38. Boch J, Scholze H, Schornack S, Landgraf A, Hahn S, Kay S, Lahaye T, Nickstadt A, Bonas U. Breaking the code of DNA binding specificity of TAL-type III effectors. Science 2009; 326:1509-12; PMID:19933107; http://dx.doi.org/10.1126/science.1178811
39. Anton T, Bultmann S, Leonhardt H, Markaki Y. Visualization of specific DNA sequences in living mouse embryonic stem cells with a programmable fluorescent CRISPR/Cas system. Nucleus 2014; 5:163-72; PMID:24637835; http://dx.doi.org/10.4161/nucl.28488
40. Adhikary A, Buschmann V, Müller C, Sauer M. Ensemble and single-molecule fluorescence spectroscopic study of the binding modes of the bis-benzimidazole derivative Hoechst 33258 with DNA. Nucleic Acids Res 2003; 31:2178-86; PMID:12682368; http://dx.doi.org/10.1093/nar/gkg308
41. Gruell F, Kirchgessner M, Kaufmann R, Hausmann M, Kebschull U. Accelerating Image Analysis for Localization Microscopy with FPGAs. In: 2011 21st International Conference on Field Programmable Logic and Applications. IEEE; 2011. page 1–5
42. Baddeley D, Cannell MB, Soeller C. Visualization of localization microscopy data. Microsc Microanal 2010; 16:64-72; PMID:20082730; http://dx.doi.org/10.1017/S143192760999122X

PAPER 3. SUPPLEMENTARY MATERIALS:

Single molecule localization microscopy of the distribution of chromatin using Hoechst and DAPI fluorescent probes

Supplemental Material to:

Aleksander T Szczurek, Kirti Prakash, Hyun-Keun Lee, Dominika J Żurek-Biesiada, Gerrit Best, Martin Hagmann, Jurek W Dobrucki, Christoph Cremer, and Udo Birk

Single molecule localization microscopy of the distribution of chromatin using Hoechst and DAPI fluorescent probes

Nucleus 2014; 5(4)
http://dx.doi.org/10.4161/nucl.29564

http://www.landesbioscience.com/journals/nucleus/article/29564/

Single molecule localization microscopy of the distribution of chromatin using Hoechst and DAPI fluorescent probes

SUPPLEMENTARY MATERIALS

Aleksander T.Szczurek[1,*], Kirti Prakash[1,2,*], Hyun-Keun Lee[1,3*], Dominika J. Żurek-Biesiada[4], Gerrit Best[5,6], Martin Hagmann[5,6], Jurek W. Dobrucki[4], Christoph Cremer[1,2,3,5] and Udo Birk[1,3,5,+]

[1]Institute of Molecular Biology, Mainz, Germany,

[2]Institute for Pharmacy and Molecular Biotechnology, University of Heidelberg, Heidelberg, Germany,

[3]Department of Physics, University of Mainz, Mainz, Germany

[4]Faculty of Biochemistry, Biophysics and Biotechnology, Jagiellonian University, Kraków, Poland,

[5]Kirchhoff Institute for Physics, University of Heidelberg, Heidelberg, Germany,

[6]University Hospital Heidelberg, University of Heidelberg, Heidelberg, Germany,

[*]these authors contributed equally, [+]corresponding author

---

Content:

1. Excitation mode of the DNA dyes

For successful localization measurements in the SMLM technique, in general, single, optically isolated bursts of fluorescence are required for image reconstruction. Either substantially overlapping or too crowded signals will lead to a loss of positioning information (for details see Materials and Methods). Therefore, we optimized the 405 nm illumination intensity in order to identify as many resolvable signals (fluorescence bursts) of photoproduct molecules per frame as possible. A high 405 nm intensity (10 mW beam) applied to the sample caused saturation of the signal in the green-yellow channel, when intense 491 nm light (88 mW beam) was applied simultaneously. This stems from the fact that the number/density of molecules transferred from the blue-emitting to the green-emitting form upon illumination with 405 nm laser light became too high to be effectively read-out using 491 nm excitation with subsequent single molecule position fitting. When the intensity of the 405 nm laser was appropriately reduced, chromatin structures stained with the photoproduct became visible at an enhanced resolution in the reconstructed localization images. Eventually, using a very low power for the 405 nm excitation (0.05 mW beam), well isolated single molecule fluorescent bursts became prominent (Supplementary Figures S1, S2). Such a strategy takes advantage of the 405 nm-independent stochastic renewal of the fluorescent state (at 491 nm excitation) of the green-emitting form photoproduct upon high intensity 491 nm illumination, since we still observed blinking of photoproduct after switching off 405 nm illumination.

It is worth mentioning that a detectable pool of a green-emitting photoproducts of the investigated dyes seems to be present even without performing stochastic photoconversion with 405 nm light[1]. Instead of using this light to carry out photoconversion one could increase the green-emitting photoproduct population by adjusting the composition of the embedding media. This means that it appears possible to eliminate 405 nm light (used for photoconversion so far) from our imaging protocol, and perform single excitation wavelength localization microscopy as originally reported in the single wavelength SMLM: SPDM approach.[2]

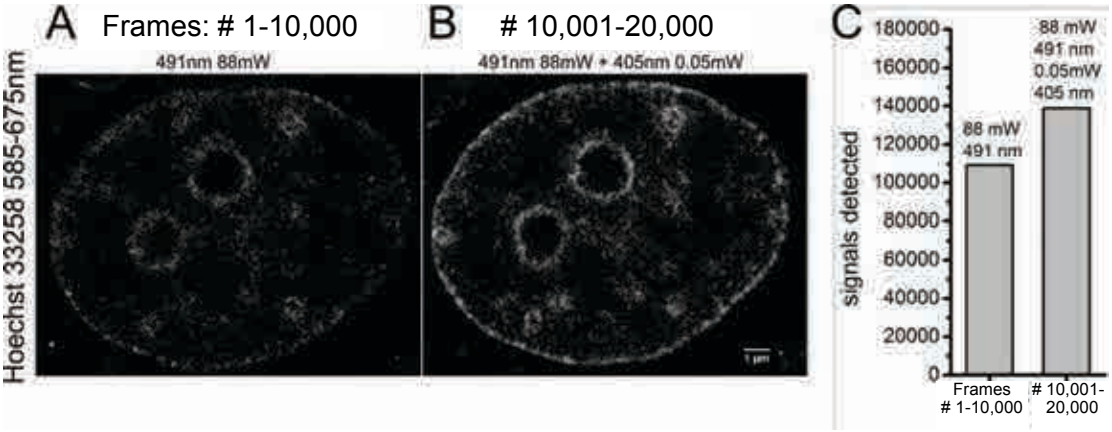

Supplementary Figure S1. The influence of illumination wavelengths on blinking rates of Hoechst 33258 bound to DNA in a typical HeLa cell nucleus. **(A)** In the first 10,000 frames, fluorescence was excited with a high illumination intensity with a single laser wavelength (491 nm only), and the fluorescence was detected in the green-yellow channel (585 - 675 nm), as described in the original SPDM approach.[2,3] In the cell nucleus shown here, a total of about 110,000 individual molecule signals were detected. **(B)** Enhancement of the blinking rate per frame by induced photoconversion from the blue-emitting form to the green-emitting form of Hoechst 33258. After exposing the sample to a single 491 nm excitation illumination for 10,000 frames (and continuously acquiring images), an additional low intensity 405 nm illumination was applied (illumination intensity ca. 1,800x lower than that of the simultaneous 491 nm illumination) again acquiring 10,000 frames. This enabled us to record approximately 30,000 additional molecule signals (corresponding to an increase of about 30% compared to the single wavelength excitation approach). Usually the majority of signals during the measurement were detected at the beginning of the acquisition (see e.g. Supplementary Fig. S3C), due to the fact that the green-emitting photoproduct is originally in equilibrium with the standard form.[1] The signal positions were blurred with the respective localization precision. **(C)** Number of detected fluorescent bursts; left column: total number of signals detected using 491 nm illumination alone (frames 1 - 10,000; an image reconstructed from these signals is shown in A); right column: total number of signals detected subsequently in the same cell using 491 nm excitation together with an additional low intensity 405 nm illumination (frames 10,001 – 20,000; reconstructed image depicted in B).

As shown in Supplementary Figure S2, the fluorescence emission spectra of the original (blue-emitting) and the green-emitting form can be separated optimally in the green-yellow detection range. In general, a large red-shift facilitates the extraction of blinking signals from the background, thus in this respect the Hoechst dyes outperformed DAPI consistently.

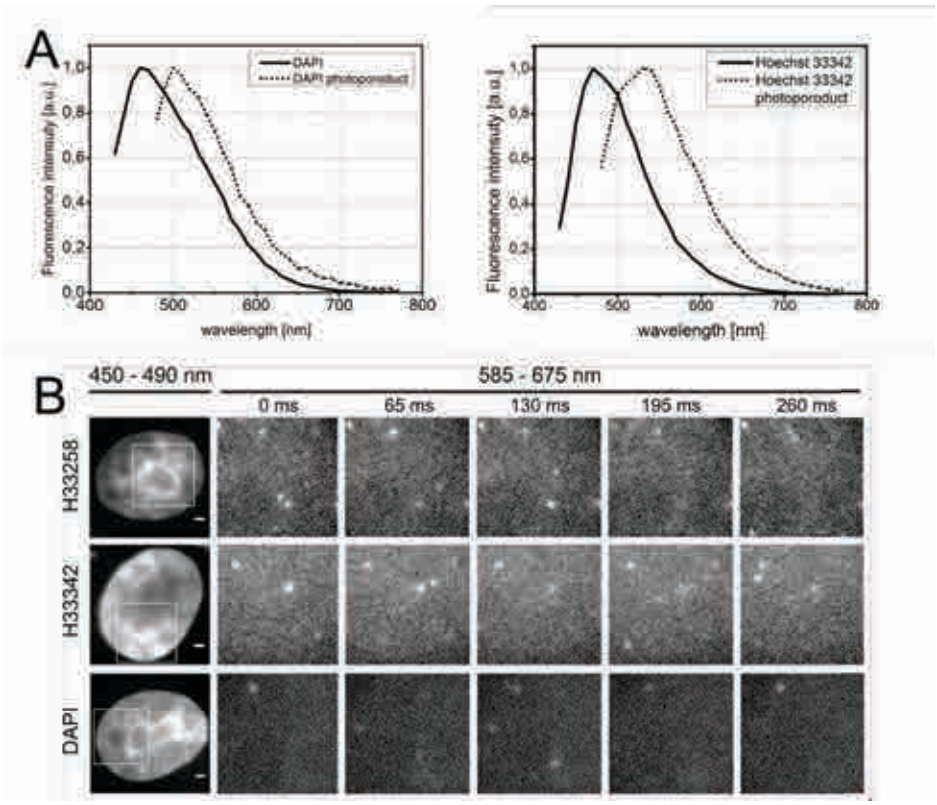

Supplementary Figure S2. **(A)** Normalized emission spectra of DAPI and Hoechst 33342. The regular form was excited with 405 nm laser light. The green-emitting photoproducts were excited with the 458 nm line of an Argon laser. Spectra were constructed using a confocal microscope with adjustable detection spectra (step size 10 nm) as described in Żurek-Biesiada et al. 2013.[1] **(B)** Sequence of frames (raw image data) demonstrating single blinking molecules of Hoechst 33258 (first row), Hoechst 33342 (second row) and DAPI (third row) bound to nuclear DNA of HeLa cells. These images were obtained in widefield mode using 405 nm excitation and a 470(40) emission filter. Blinking was observed upon simultaneous illumination with both low intensity 405 nm laser and high intensity from a 491 nm laser. Cells were embedded in glycerol and 5% of imaging buffer (the composition and the imaging protocol are described in Materials and Methods). Scale bar 1 μm. The magnified inserts represent 5.6 μm x 5.6 μm fields of view.

2. Influence of the buffer composition

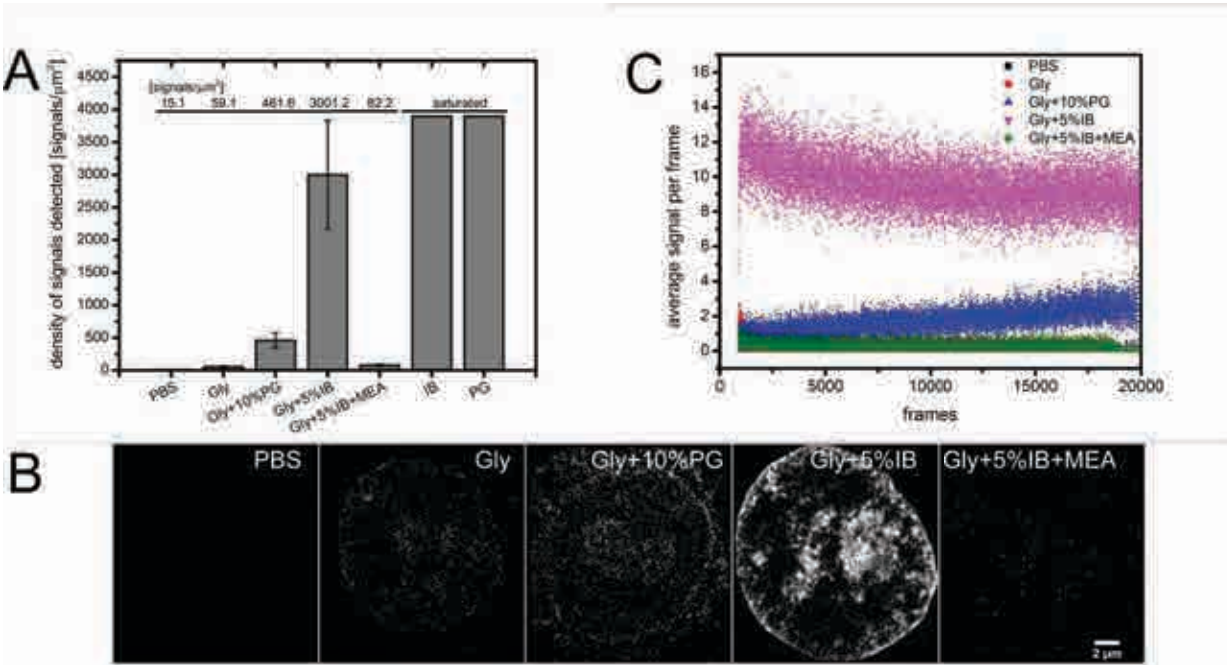

Supplementary Figure S3. The influence of the embedding media on blinking characteristics of the green-emitting photoproduct of Hoechst 33258. After staining the cells with the dye (0.1 µg/ml) for 30 min the following media were tested: PBS, glycerol, glycerol with 10% Prolong Gold® (PG), glycerol with 5% imaging buffer (IB, oxygen scavenging system, concentrations given in Materials and Methods), glycerol with 5% imaging buffer containing 50 mM mercaptoethylamine MEA (oxygen scavenging system and a primary thiol, reported previously by Heilemann and coauthors[4]), imaging buffer scavenging oxygen and Prolong Gold®. Due to signal saturation and stabilisation of fluorescence, no blinking was observed in the last two media. HeLa cell nuclei were imaged using 88 mW 491 nm excitation combined with 0.05 mW 405 nm excitation. The resulting images were obtained by recording 20,000 frames with 65 ms integration time. **(A)** The signal density is given in fluorescent bursts per unit area of cell nuclei. The mean values and standard deviation were calculated for 10 cells. **(B)** Typical images acquired in various buffer compositions. **(C)** The number of signals extracted per frame, averaged over 10 cells. For the sake of clarity, error bars are omitted. The first few frames were automatically discarded due to high overlapping of single molecule signals.

We investigated the influence of the following additives on the blinking rate: PBS, glycerol, oxygen scavenger, commercial antifade agents and thiols. For this purpose we employed the imaging protocol described in Materials and Methods. PBS and glycerol alone provide insufficient conditions for reconstructing images of nuclei due to fast bleaching (Supplementary Fig. S3). No fluorescence bursts could be detected after recording several image frames. In the case of glycerol supplemented with a small amount of Prolong Gold® standard antifade (Life Technologies, compatible with fluorescent probes such as Alexa Fluor® dyes and fluorescent proteins[56]), we detected much more fluorescence bursts. However, Prolong Gold® also gave rise to numerous cytoplasmic signals of increasing frequency (Supplementary Fig. S3). Nonetheless, a 10% dilution of Prolong Gold® in glycerol

suppressed bleaching. Our data suggest that a crucial role in blinking regulation of bisbenzimide dyes and DAPI is played by oxygen rather than the primary thiol. Blinking of Hoechst 33258 became prominent when the oxygen concentration was reduced. Such conditions were provided by using a medium containing glycerol with 5% imaging buffer (glucose oxidase and catalase system). Higher concentrations of imaging buffer were also tested (10, 20, 30 and 100%) but have not provided better results (data not shown, we cannot rule out the possibility in which slightly higher concentrations could be used successfully in combination with a 491 nm laser illumination intensity higher than what is available in our setup). We suppose that in such a system a decreased probability of interaction with oxygen might be a major factor also influencing blinking. However, once β-mercaptoethylamine (MEA; 50 mM final concentration) was added to such a buffer, the blinking rate was reduced. It is possible that MEA interacts with oxygen, and, as a result, oxidation of its thiol group and formation of disulfide bonds occurs.[7] Moreover, MEA is known to act as a triplet state quencher[8]. Any specific thiol reaction with the dye molecules, similar to the previously reported reactivity of cyanine dyes, can most likely be excluded.[9] Furthermore, in an oxygen-depleted environment (100% imaging buffer system or Prolong Gold®) fluorescence is stabilised and hardly any bleaching of both forms occurs, i.e. no single molecule signals could be extracted. Since oxygen is regarded as the major cause of photobleaching,[10] we anticipate that adjusting the oxygen content helps to establish the optimal ratio between irreversible and reversible photobleaching of the photoproducts.

3. Considerations on non-emitting state formation

'Blinking' based localization microscopy procedures requires the transfer from a non-emitting (or non-detectable) to a fluorescence emitting state and back to a non-emitting state ('dark' state). A suggestion regarding the mechanism of non-emitting state formation in Hoechst dyes was put forward by Cosa and colaborators.[11] They proposed a model in which Hoechst 33258 undergoes an intramolecular proton transfer between the phenol group and the bisbenzimide nitrogen under UV illumination. As a result, an additional protonated centre may arise at the expense of the phenol group of Hoechst 33258 which may become susceptible to de-excitation in a non-radiative manner. Interestingly, previous mass spectrometry experiments demonstrated that UV illumination of DNA dyes in solution gives rise to the additional peak in the mass-to-charge spectrum, which can be attributed to the extra-protonated form of Hoechst 33258.[1] However, this explanation of the 'dark' state formation seems unlikely in the light of our finding that Hoechst 33342 (phenol group replaced with ethyl group) and DAPI (no phenol group) also undergo photoconversion and blinking.

One may argue, however, that such a non-emitting state does not exist, and only the reaction which is a reversal of photoconversion, occurs. In such a case the green-emitting form, while exposed to a high intensity illumination of 491 nm light, would be expected to regain the initial spectral properties and return to the blue-emitting, standard form. Further studies on photophysical properties of bisbenzimide DNA dyes should test this hypothesis.

4. Hoechst 33258 fluorescence intensity profiles

In Supplementary Figure S4, four example profiles taken across a reconstructed localization image are shown. The profiles depicted (1-4) have a length of 1,000 nm and have been averaged across a width of 100 nm. Positions of the profiles taken are indicated in the reconstructed image.

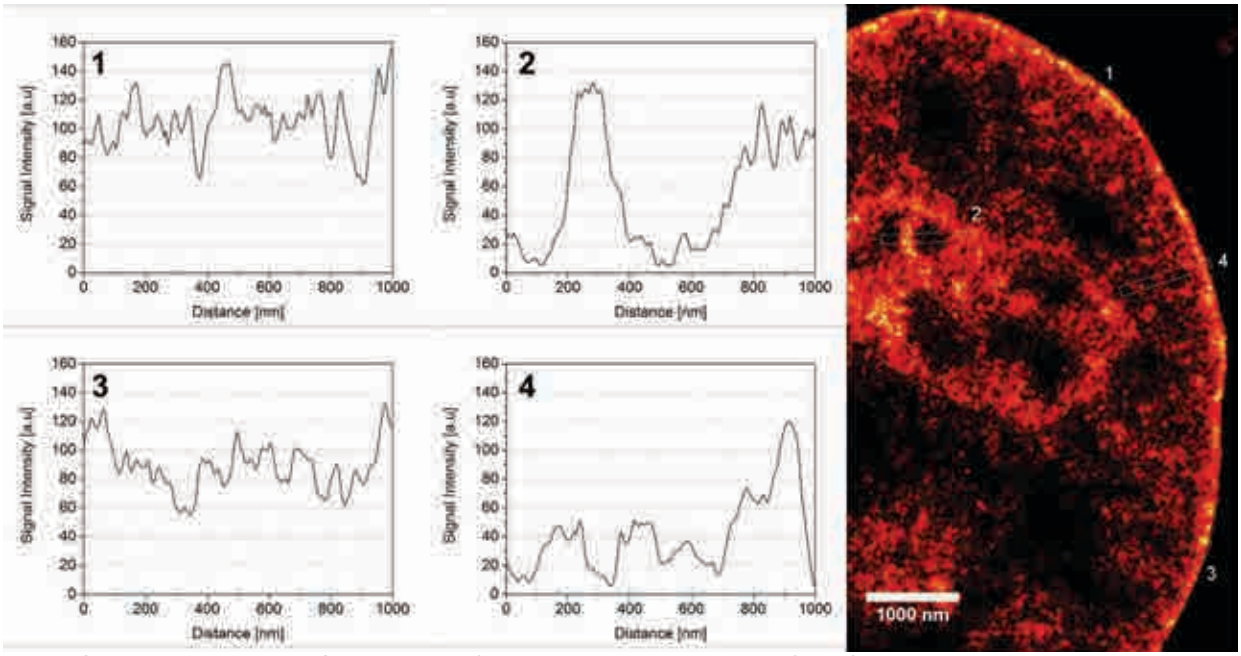

Supplementary Figure S4. Examples of 1000 nm long intensity plot profiles of Hoechst 33258 integrated across various sites within a HeLa cell nucleus (a width of 100 nm). The plot profiles are based on data taken from Fig. 2. The profiles were based on the individual localization data after Gaussian blurring with the respective localization precision.

5. Comparison of fluorescence microscopy techniques

A direct comparison of the same cell in SMLM, widefield and confocal laser scanning microscopy not available due to difficulties in relocating the same cell in independent microscope systems. In Supplementary Figure S5, we provide a comparison of similar cell nuclei from the three imaging devices.

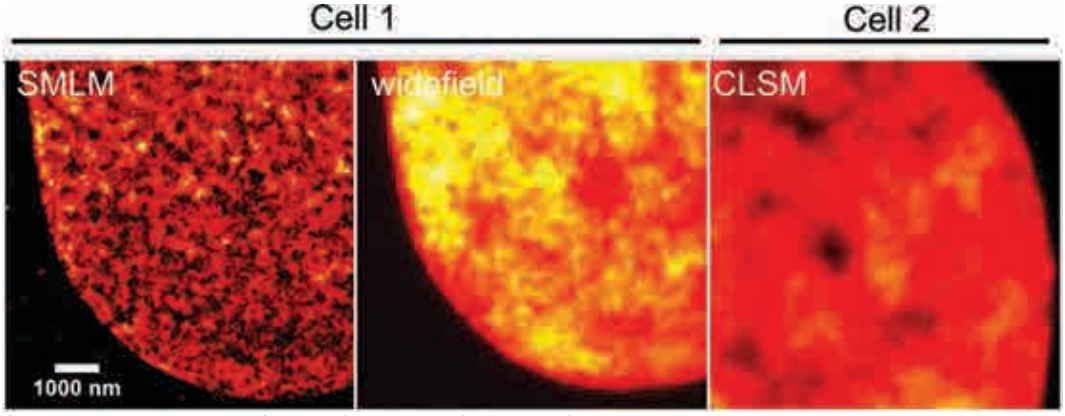

Supplementary Figure S5. Performance of various fluorescence microscopy approaches in independent measurements: Cell 1, image of human fibroblast acquired using widefield microscopy and then localization microscopy (SMLM), Cell 2, image of a secondary VERO-B4 monkey fibroblast taken using confocal light scanning microscopy (CLSM) - an approach providing best resolution in standard fluorescence microscopy. Cells were stained with Hoechst 33258.

6. Optical setup

The basic optical setup (Vertico-SPDM microscope) has been described previously.[3] The laser beam enters the microscope after reflection from mirrors M1 - M6. Both laser beams (wavelengths: 405 nm and 491 nm) are combined using a long pass dichroic mirror (DM, ZT405RDC®, Chroma), which transmits wavelengths above 405 nm. The collimator composed of achromatic lenses (CL1, f = 30 mm, CL2, f = 200 mm) expands the beam 5x. The irises (I1 - I5) are used during alignment. The beam is focused into the backfocal plane of a 63x 1.4 NA objective by an achromatic lens (CdL, f = 60 mm) after reflection from the beam splitter (BS, quad-band dichroic mirror®, Chroma). The fluorescent light emitted from the sample passes first the beam splitter and then the emission filter (FF01-630/92, Semrock) mounted on a filter wheel (FW). Subsequently, the light is focused by a tube lens (TL, f = 200 mm) onto the CCD chip of a highly sensitive 12 bit black-and-white camera (CAM). In order to implement the localization mode, for high laser illumination intensity, a localization lens (LL, f = 500 mm) is inserted in the optical pathway, decreasing the illuminated area in the sample plane to a Gaussian spot of roughly 60 µm diameter at full width at full maximum.

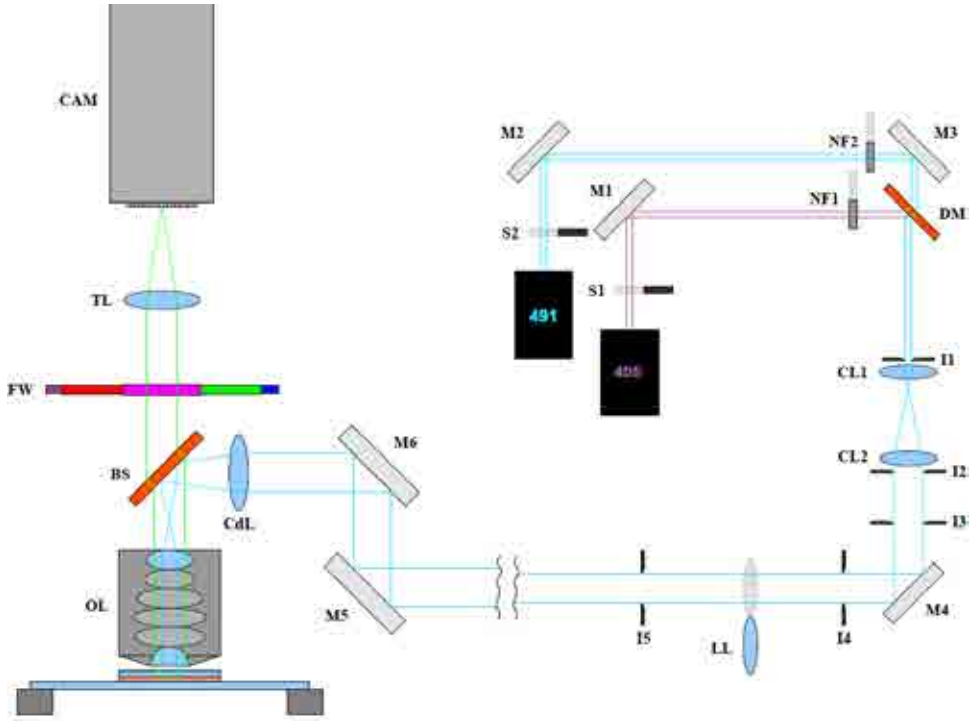

Supplementary Figure S6. Optical setup for localization microscopy measurements. For a description of the parts, see section 6: Optical setup.

References for supplementary materials

1. Zurek-Biesiada D, Kędracka-Krok S, Dobrucki JW. UV-activated conversion of Hoechst 33258, DAPI, and Vybrant DyeCycle fluorescent dyes into blue-excited, green-emitting protonated forms. Cytometry A 2013; 83:441–51.

2. Lemmer P, Gunkel M, Baddeley D, Kaufmann R, Urich A, Weiland Y, Reymann J, Müller P, Hausmann M, Cremer C. SPDM: light microscopy with single-molecule resolution at the nanoscale. Appl Phys B 2008; 93:1–12.

3. Reymann J, Baddeley D, Gunkel M, Lemmer P, Stadter W, Jegou T, Rippe K, Cremer C, Birk U. High-precision structural analysis of subnuclear complexes in fixed and live cells via spatially modulated illumination (SMI) microscopy. Chromosome Res 2008; 16:367–82. 8

4. Heilemann M, van de Linde S, Schüttpelz M, Kasper R, Seefeldt B, Mukherjee A, Tinnefeld P, Sauer M. Subdiffraction-resolution fluorescence imaging with conventional fluorescent probes. Angew Chem Int Ed Engl 2008; 47:6172–6.

5. Kaufmann R, Müller P, Hildenbrand G, Hausmann M, Cremer C. Analysis of Her2/neu membrane protein clusters in different types of breast cancer cells using localization microscopy. J Microsc 2011; 242:46–54.

6. Gunkel M, Erdel F, Rippe K, Lemmer P, Kaufmann R, Hörmann C, Amberger R, Cremer C. Dual color localization microscopy of cellular nanostructures. Biotechnol J 2009; 4:927–38.

7. Hamilton GA, Buckthal DJ, Mortensen RM, Zerby KW. Reactions of cysteamine and other amine metabolites with glyoxylate and oxygen catalyzed by mammalian D-amino acid oxidase. Proc Natl Acad Sci U S A 1979; 76:2625–9.

8. Song L, Varma CA, Verhoeven JW, Tanke HJ. Influence of the triplet excited state on the photobleaching kinetics of fluorescein in microscopy. Biophys J 1996; 70:2959–68.

9. Dempsey GT, Bates M, Kowtoniuk WE, Liu DR, Tsien RY, Zhuang X. Photoswitching mechanism of cyanine dyes. J Am Chem Soc 2009; 131:18192–3.

10. Bernas T, Zarebski M, Cook PR, Dobrucki JW. Minimizing photobleaching during confocal microscopy of fluorescent probes bound to chromatin: role of anoxia and photon flux. J Microsc 2004; 215:281–96.

11. Cosa G, Focsaneanu KS, McLean JR, McNamee JP, Scaiano JC. Photophysical properties of fluorescent DNA-dyes bound to single- and double-stranded DNA in aqueous buffered solution. Photochem Photobiol 2001; 73:585–99.

CHAPTER 3. FUTURE PERSPECTIVES

As the conventional microscopic methods do not allow obtaining imaging resolution better than 180 nm in the lateral (xy) plane, and 500 nm in the axial (z) plane [2], the nearest future of microscopy lies in further development of super-resolution microscopic techniques. As for now, super-resolution microscopy has brought about major progress in visualisation of biological specimens, nevertheless, it still struggles with some major shortcomings.

The biggest problem of single molecule localisation microscopy is the length of the image acquisition. Assuming that around 60-70 single fluorescent bursts are registered for one image frame, and the satisfactory number of fluorescence bursts, to successfully reconstruct a high-quality super-resolution image of a cell nucleus, revolves around 1 million, then one needs around 17 000 image frames to collect such measurement. If frames are taken at 50 ms interval, registering of 17 000 frames would take around 15 minutes. In reality this time is longer, since first of all, the applied fluorophores undergo some irreversible bleaching, and with time fluorescence bursts become weaker and rarer (hence, it is preferable to lengthen the measurement). Second of all, computers that are used for software operation are far from being perfect, and the limited RAM memory along with lack of perfection of the operating systems, as well as, for example, slow data saving processing, extends the theoretical 15 minutes to a much longer time. Therefore, in average, including sample stabilisation, image acquisition, data saving and processing, one needs around one hour or an hour and a half to collect a high quality super-resolution image of a slice of a cell nucleus. For such an extended time the biggest threat to the acquisition of the image is the physical drift of the microscope stage or the sample. The drift in the xy plane would result in blurring of the image, while the drift in the z plane would result in losing the focus, and hence, blurring of the image as well. Figure 3.1 shows a super-resolution image of a cell nucleus that is the result of a microscopic stage drift during the image acquisition.

There are various algorithms used for correction of the drift, and Figure 3.1B,D shows the same image as in Figure 3.1A,C after applying a drift correction algorithm. The drift was corrected using algorithms based on cross-correlation (as described in [203]) or underlying structure (as described for DNA SMLM imaging in PAPER 3). Nevertheless, if not essential, one should avoid additional mathematical processing of the microscopic data.

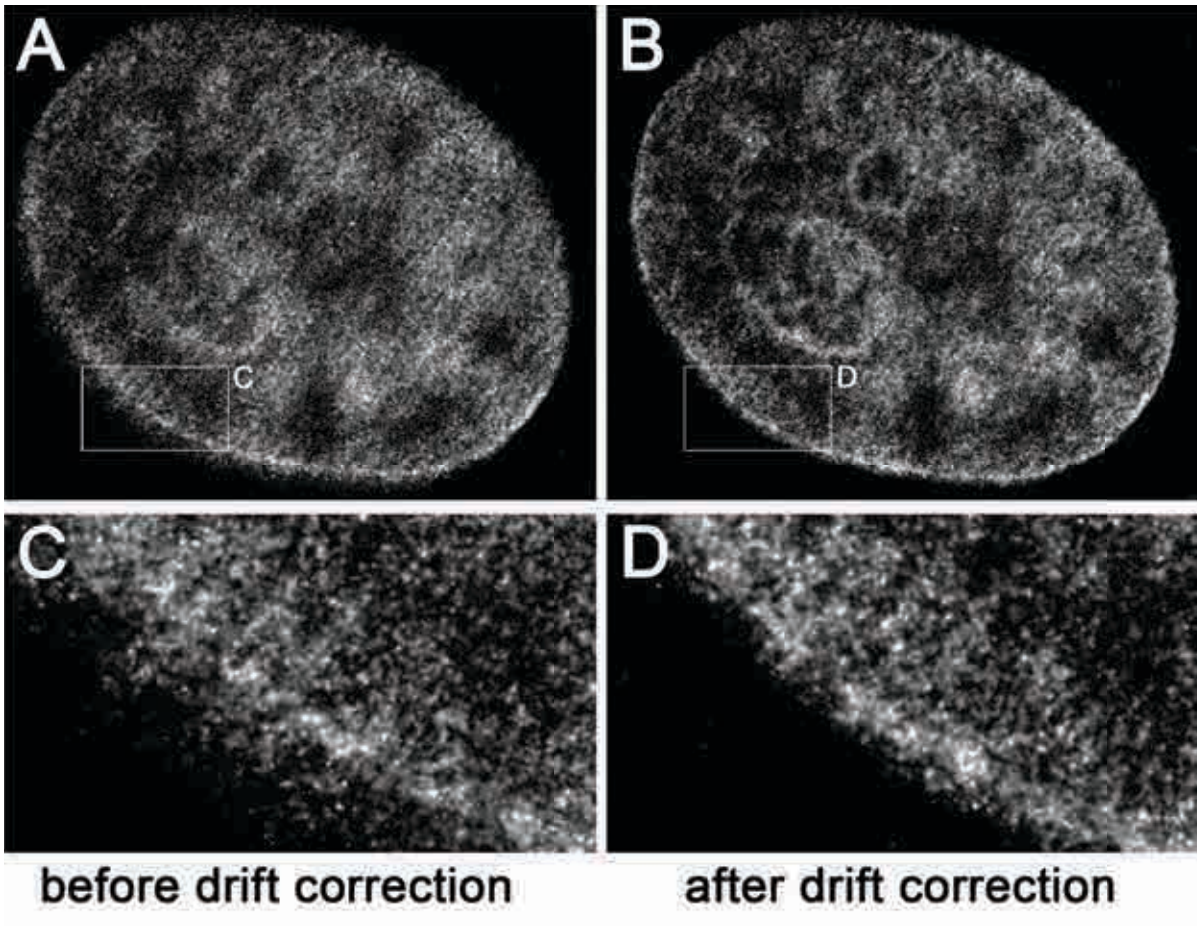

Figure 3.1 A comparison of super-resolution images of a cell nucleus before (A,C) and after (B,D) drift correction [Żurek-Biesiada et al., unpublished].

Long image acquisition is also one of the main shortcomings to super-resolution live cell imaging. Even though live cell super-resolution imaging has been already performed [26–30, 143, 204–206], the obtained results are still far from satisfactory. Living cells are in motion, and if such movement takes place during the measurement, the collected image becomes blurry. An example of application of live cell PALM was presented in [206], however, this study was facilitated by the slow motion of the investigated adhesion-complexes. For a perfect imaging method it is crucial to maximise the number of the collected photons per unit of time. In other words, image acquisition should be fast enough to facilitate collection of a sufficient number of single molecule fluorescent bursts before the specimen moves. Manley et al. [205] have reported that a high number of photons collected during the PALM measurement was possible using EosFP, which is a very bright FP.

Another issue regarding live cell imaging is the energy carried by the laser used in SMLM. In an approach where the majority of the fluorescent molecules should be irreversibly bleached, one needs to use laser beams of a sufficiently high power. Using beams of high intensity may be harmful to living organisms. Unfortunately, most of the current super-resolution methods apply laser powers that are still considerably high. Therefore, a need for bright fluorophores that do not require very high laser power outputs is constantly growing.

This doctoral thesis is focused on the process of photoconversion of DAPI, Hoechst dyes and Vybrant® DyeCycle™ Violet. However, other, unpublished data [Żurek-Biesiada et al., unpublished] strongly suggest that the UV-activated conversion might be a common feature of most, if not all UV-excited dyes. Figure 3.2 presents images of several UV-excited fluorescent dyes immobilised in a polyvinyl polymer [207], and later subjected to the process of photoconversion. DAPI (DAPI) (exc./em. 340/454 nm) [132,208], Hoechst 33258 (H33258) (exc./em. 355/465 nm) [99,209,210], Hoechst 33342 (H33342) (exc./em. 350/461 nm) [211,212], and Vybrant® DyeCycle™ Violet Stain (VdcV) (exc./em. 369/437 nm) [213] are used for DNA staining. 5-dimethyloaminonaphthalene-1sulfonyl aziridine (dansyl aziridine) (DA) (exc./em. 340/543) [214] reacts with methionine residue in troponin C. N-iodoacetyl-n'-(5-sulfo-1-naphthyl)ethylenediamine (Et) (exc./em. 336/490 nm) [215] binds to myosin. 1,6-Diphenyl-1,3,5-hexatriene (DPH) (exc./em. 350/452 nm) [216, 217] is used for staining biomembranes. Alexa Fluor® 405 (A405) (exc./em. 401/421 nm) [218] is an amine-reactive derivative of Cascade Blue dye produced by LifeTechnologies. Fluorescence spectra of the original forms of the investigated dyes and their respective photoproducts are presented in Figure 3.2B.

The only fluorescent dye for which a spectral change has not been observed was DPH. However, DPH is different from other dyes used in this experiment in that its molecule has no nitrogen or other atoms that could be protonated. Figure 3.2C presents chemical structures of the investigated dyes. The structure of Vybrant® DyeCycle™ Violet remains unknown.

For VdcV super-resolution imaging can be performed using single excitation wavelength (blue light). However, in the case of Hoechst dyes or DAPI this imaging needs to be performed using two different excitation wavelengths. One laser is used to convert DAPI/Hoechst dyes into their green-emitting forms and the second excitation is used to image their respective photoproducts. This means that for the entire length of the measurement a continuous UV or 405 nm illumination needs to be present. During the measurements (conducted for the purpose of this thesis), even though this additional 405 nm illumination was present at very low power, significant imaging problems were encountered. The objective lenses exposed to a continuous illumination with 405 nm light were damaged. The light was absorbed by the objective lenses changing the structure of the lenses and leaving a visible mark in the spot where the beam was focused. This unfortunate phenomenon led to destruction of several objective lenses, which excluded the possibility that only one of the used objective lenses was defective. Therefore, employing and developing dyes that are excited with light of low output power, and preferably light of longer wavelength (and thus lower photon energy), is crucial in order to avoid damage of the imaging equipment.

Raw data collected during one SMLM measurement contained images of the subsequent fluorescent bursts of the applied fluorophores. Later, these data were processed using a specialised algorithm, which calculates the exact positions of the fluorescent molecules. A basic approach to this precise localisation of single molecules has been described in [42], and various methods of data representation have been so far developed

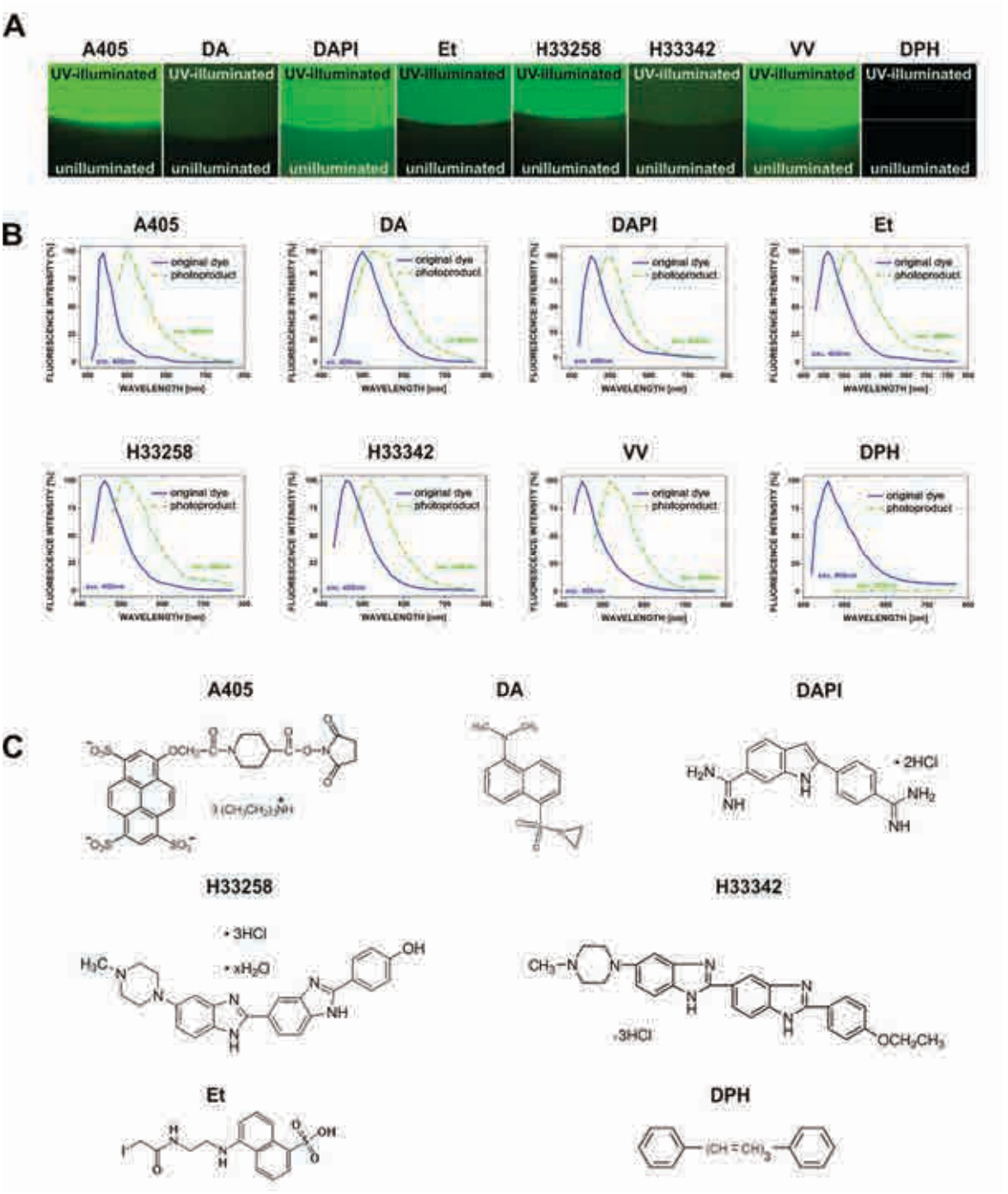

Figure 3.2 UV-activated conversion of various UV-excited fluorescent dyes [Żurek-Biesiada et al., unpublished]. **A** – Photoconversion of Alexa 405 (A405), Dansyl Aziridine (DA), DAPI (DAPI), N-iodoacetyl-n'-(5-sulfo-1-naphthyl)ethylenediamine (Et), Hoechst 33258 (H33258), Hoechst 33342 (H33342), Vybrant® DyeCycle™ Violet Stain (VdcV). The polymers with immobilised dyes were illuminated with UV (360/40 nm filter) emitted by a mercury metal halide lamp (Leica EL6000, beam intensity 11 mW, 60 s exposure). DPH (DPH) did not undergo the process of photoconversion **B** – Emission spectra of the original dyes of Alexa 405 (A405), Dansyl Aziridine (DA), DAPI (DAPI), N-iodoacetyl-n'-(5-sulfo-1-naphthyl)ethylenediamine (Et), Hoechst 33258 (H33258), Hoechst 33342 (H33342), Vybrant® DyeCycle™ Violet Stain (VdcV) and DPH (DPH) doped in a polymer block, and their respective photoproducts. Excitation for the original dyes was at 405 nm and their photoproducts at 458 nm. **C** – Chemical structures of Alexa 405 (A405), Dansyl Aziridine (DA), DAPI (DAPI), N-iodoacetyl-n'-(5-sulfo-1-naphthyl)ethylenediamine (Et), Hoechst 33258 (H33258), Hoechst 33342 (H33342), Vybrant® DyeCycle™ Violet Stain (VdcV) and DPH (DPH).

(e.g. Gaussian blurring, triangulation etc. [219, 220]). Depending on the algorithm, the output super-resolution image may vary significantly. Figure 3.3 presents super-resolution images of a polytene chromosome reconstructed using two different algorithms (Figure 3.3A), i.e. fastSPDM [219] and (Figure 3.3B) advancedSPDM (described in PAPER3). The difference in the localisation precision of the output images produced by these two algorithms is significant. The fastSPDM algorithm produced much better localisation accuracy (approx. 18 nm) and much higher contrast in the output images, but as it is shown in the inset (Figure 3.3C), it did also produce a grating pattern, resulting from the action of algorithm itself. At the same time, advancedSPDM did not produce grating, but it provided much lower contrast and worse localisation precision (approx. 50 nm), producing an image, which is more blurry (Figure 3.3D). Therefore, a search for the perfect algorithm is still continuing.

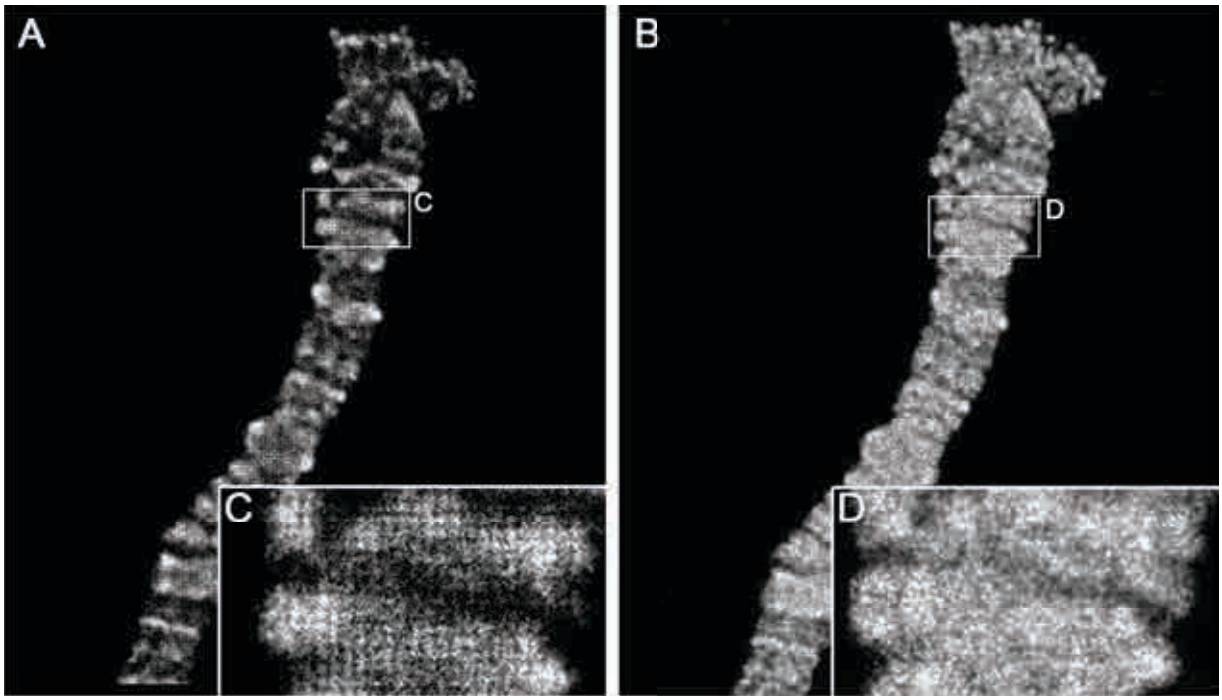

Figure 3.3 Images of a polytene chromosome (stained with VdcV at 400 nM) reconstructed using two different algorithms [Żurek-Biesiada et al., unpublished]. A – An image reconstructed with fastSPDM algorithm. The action of the fastSPDM algorithm produced grating. With high-density DNA staining (2470 single molecules/μm^2) grating became prominent. The mean localisation precision of this image was 18 nm. **B** – An image reconstructed with advancedSPDM algorithm. The action of the advancedSPDM algorithm did not produce grating. The mean localisation precision of this image was 50 nm.

Another issue worth discussing is the quantitative analysis of the visualised single molecules in the acquired images. The interesting question that might be asked is how many of the molecules that are attached to DNA really undergo the phenomenon of *blinking*? To illustrate this issue the following approximation can be made. Diploid human genome consists of 6 x 10^9 base pairs. Binding of Hoechst 33258 to DNA is complex and depends strongly on the length and sequence of DNA, as well as the presence of DNA-associated proteins. Many examples of Hoechst 33258 stoichiometry have already been proposed. For example, a model where 1 Hoechst 33258 molecule binds per 100

base pairs [221], or a model in which 1,2,3,4, or 6 molecules of Hoechst 33258 bind per 5 A-T base pairs [222] were described. In another study a binding ratio of [H33258]/[DNA bp] of 0.05, 0.15, or 0.20 was proposed [111]. Adhikary et al. 2003 state that an optimal binding [H33258]/[DNA bp] ratio is 0.05. In the case of this ratio Hoechst 33258 binds to a minor groove of DNA (and does not partly intercalate at C-G reach regions, as in the case of higher binding ratios). At this ratio Hoechst 33258 shows the highest increase in its fluorescence quantum yield upon binding to DNA. Therefore, for the purpose of calculating the proportion of Hoechst molecules detected in localisation microscopy experiments described in this dissertation, the model which assumes [H33258]/[DNA bp] binding ratio of 0.05 was used. Assuming that such staining conditions were reached, there could be roughly 300 millions of Hoechst 33258 molecules (300 x 10^6) in one cell nucleus. Our experimental data suggest that 1 million (10^6) single molecule fluorescent bursts registered in a SMLM measurement is a sufficient number of individual fluorescent signals to reconstruct a super-resolution image of a slice of a cell nucleus [52]. Therefore, if 300 x 10^6 molecules of Hoechst 33258 are bound to DNA in a cell nucleus, and 10^6 single molecule fluorescent bursts are detected, only 0.33% of the DNA-bound Hoechst 33258 molecules are used to form an image. Hence the question arises as to what one really sees in the SMLM images of DNA? Which part of the chromatin structure is really visualised, and how much information (and regarding what) is being lost? What is the real definition of resolution then? Further, if one wanted to visualise exactly the structure of the cell nucleus, and for example, one DNA thread diameter would be represented by one pixel in the image, then how big the computer screens would have to be in order to present all the details?

Super-resolution has significantly improved the lateral and axial resolution of the imaging samples. A resolution of 50-70 nm in all three dimensions has already been achieved [33, 223, 224]. Nevertheless, this result is still far from the nanometre resolution. Better resolution means more details visible in the images, and this means better understanding of biology. That is why, the search for the perfect fluorophore along with perfect imaging environment has just begun. Maximisation of the number of emitted photons per time unit is highly needed along with minimisation of the *background* level.

Vybrant® DyeCycle™ Violet

The last paper presented in this doctoral dissertation PAPER 3 is an example of a successful exploitation of the DNA-binding dyes, DAPI and Hoechst 33258/33342, in super-resolution microscopy of the DNA structures. However, I would like to point out that another paper, entitled *Localization microscopy of DNA in situ using Vybrant® DyeCycleTM Violet Fluorescent Probe* (author list: Żurek-Biesiada D, Szczurek A, Prakash K, Mohana GK, Lee HK; Roignant JY, Birk U, Dobrucki JW, Cremer C.) [52], has been recently submitted to revision. This paper is focused on application of the fluorescent dye Vybrant® DyeCycleTM Violet in single molecule localisation microscopy.

Vybrant® DyeCycleTM Violet allows visualisation of the DNA structures and obtaining high-resolution images. There are several advantages that put VdcV before DAPI

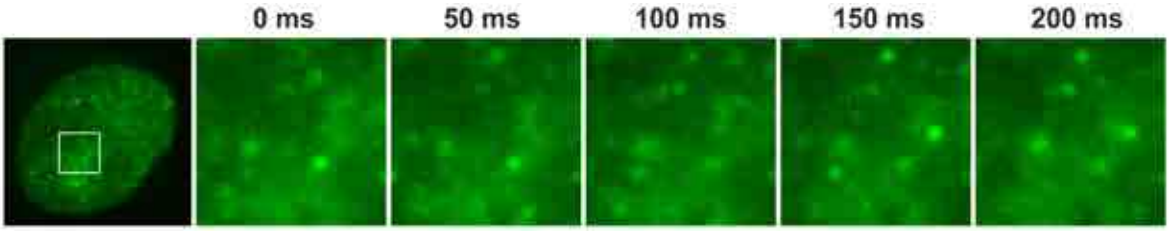

Figure 3.4 Single molecule fluorescent bursts. Single molecule fluorescent bursts detected in green-yellow emission range (585 - 675 nm) during a typical experiment using high intensity single wavelength excitation (50 mW, 491 nm). The green-emitting molecules of VdcV (conc. 500 nM) are reversibly bleached and stochastically reappear in the detection channel of the SPDM microscope. Note that some of the molecules appear bright with much longer lifetime than the integration time of the camera.

and Hoechst dyes. First of all, VdcV does not require double excitation during image acquisition. For this dye, single laser excitation (i.e. blue light) is sufficient to collect a super-resolution image, which excludes the need for using 405 nm or UV laser, and thus, minimises the damage inflicted on the objective lenses. This happens because even before UV-excitation, the amount of the green-emitting product of VdcV is significant, which excludes the need for a prior photoconversion of the dye [52]. Second of all, VdcV produces brighter and clearer single molecule fluorescent bursts, which allows for their better optical isolation (see Figure 3.4). Thus, higher localisation precision can be achieved. Figure 3.5 presents a histogram of localisation precision of the fluorescent signals collected during image acquisition of the nucleus presented in Figure 3.6. The mean localisation precision was 17 nm, which corresponds to spatial resolution of about 40-50 nm in the specimen plane. This result is four to five times better than in the case of conventional microscopy. With this dye, up to 5 x 10^6 single molecule localisation bursts were collected [Żurek-Biesiada et al., unpublished]. Because the green-emitting form of the dye emits brighter signals in comparison to Hoechst dyes and DAPI, VdcV requires lower power lasers during image acquisition [52]. Further, VdcV is cell permeable, which along with the diminished laser powers, makes it a potentially good candidate for future super-resolution imaging of living cells.

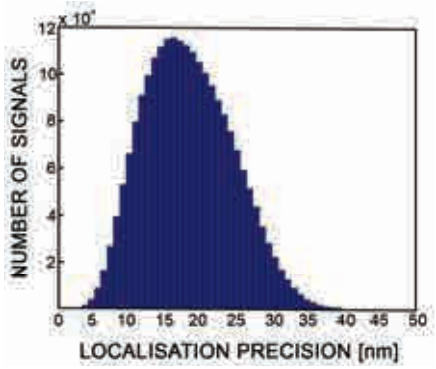

Figure 3.5 The histogram of localisation precision of cell nucleus from Figure 3.6. The histogram of localisation precision reveals an average value of roughly 17 nm, corresponding to an optical two-point resolution of individual molecules of about 40-50 nm.

Figure 3.6 presents a super-resolution image of a cell nucleus collected by means of SMLM. The super-resolution image in comparison to widefield image of the same cell nucleus has significantly improved contrast, and hence resolution. The full report on VdcV and its application in super-resolution microscopy has been provided in the submitted paper [52].

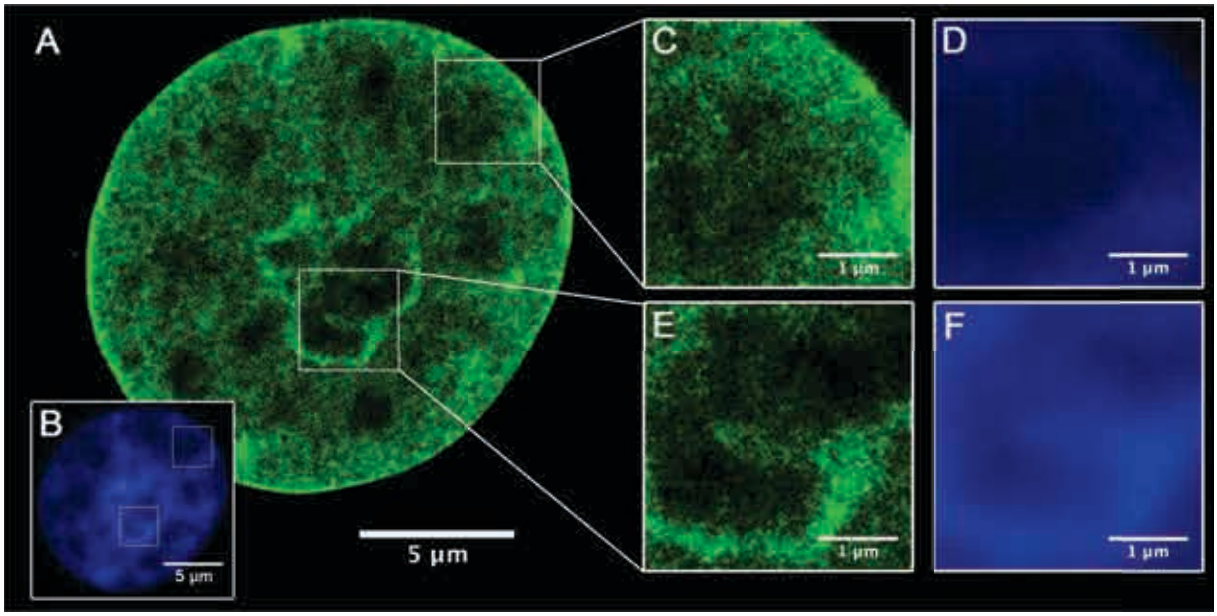

Figure 3.6 Super-resolution image of an optical slice of a nucleus. **A** - Super-resolution image of an optical slice of a nucleus of a Vero-B4 cell stained with 1 μM Vybrant® DyeCycle™ Violet, **B** – an image of the same nucleus acquired in a widefield microscope (exc. 405 nm, 450 μW, em. 450 – 490 nm).

CONCLUSIONS

Investigations into photophysics of the UV-excited DNA-binding dyes open new avenues of research into structure and function of the cell nucleus. In the light of the currently existing research all of the investigated DNA-binding dyes, i.e. DAPI, Hoechst 33258/33342, and Vybrant® DyeCycle™ Violet, have proven to be excellent candidates for super-resolution imaging of sub-diffraction DNA structures. Under UV/405nm illumination they convert to blue-excited green-emitting photoproducts, which exhibit *blinking* behaviour that can be exploited in single molecule localisation microscopy. Because the dyes bind directly to DNA, high-density labelling with high accuracy of localisation precision is possible. Also, Hoechst 33342 and VdcV are good candidates for future investigation of live specimens, as they pass through intact cell membranes easily. Investigation of the photophysical behaviour of these dyes facilitated significantly the application of the process of their photoconversion in super-resolution microscopy, as well as, brought to light new facts about their binding behaviour. Only good understanding of the photophysical properties of the investigated dyes enabled their successful application in super-resolution techniques. Further research would include explaining the mechanism of reaching the *dark* state by the dyes (to better control the *blinking* environment), explaining the photoconversion mechanism of DAPI, Hoechst 33258/33342 or VdcV, and learning the structure of VdcV as well as its binding mode to DNA. Conducting research like the one described in this doctoral dissertation contributes to the overall development of the methods of super-resolution microscopy. The methods are still fairly young, and still require many improvements in the future. Nevertheless, each experiment, each newly created dye, or each even small improvement in the equipment setting, even though sometimes not appreciated at the time of creation, contributes significantly to the overall evolution of the methods. The molecular world is still poorly understood in many aspects, and the possibility of just looking into the nanostructures with sophisticated equipment is utterly tempting and interesting. One hundred years ago no one even dreamed about reaching an imaging resolution better than 200-300 nm. Who knows where the science of biological imaging will be in the next 100 years?

References

[1] **Abbe E.** 1873. *Beiträge zur Theorie des Mikroskops und der mikroskopischen Wahrnehmung. Archiv für mikroskopische Anatomie.* Archiv für mikroskopische Anatomie. 9:413-418

[2] **Pawley J.** 1995. *Handbook of Biological Confocal Microscopy.* Plenum, New York, 1995

[3] **Sheppard CJ and Wilson T.** 1981. *The theory of the direct-view confocal microscope.* J Microsc; 124(Pt 2):107-17

[4] **Minsky M.** 1988. *Memoir on inventing the confocal scanning microscope.* Scanning 10, 128–138

[5] **Brakenhoff GJ, van der Voort HT, van Spronsen EA, Linnemans WA, Nanninga N.** 1985. *Three-dimensional chromatin distribution in neuroblastoma nuclei shown by confocal scanning laser microscopy.* Nature; 317(6039):748-9

[6] **Cremer C and Cremer T.** 1978. *Considerations on a laser-scanning-microscope with high resolution and depth of field.* Microsc Acta; 81(1):31-44

[7] **Hell S and Stelzer E.** 1992a. *Properties of a 4Pi confocal fluorescence microscope.* J. Opt.Soc. Am. A; Vol. 9, Issue 12, pp. 2159-2166

[8] **Hell S and Stelzer E.** 1992b. *Fundamental improvement of resolution with a 4Pi-confocal fluorescence microscope using two-photon excitation.* Volume 93, Issues 5–6, pp. 277–282

[9] **Hell SW and Nagorni M.** 1998. *4Pi confocal microscopy with alternate interference.* Opt Lett; 23(20):1567-9

[10] **Gustafsson MG, Agard DA, Sedat JW.** 1999. *I^5M: 3D widefield light microscopy with better than 100 nm axial resolution.* J Microsc; 195(Pt 1):10-6

[11] **Konig K.** 2000. *Multiphoton microscopy in life sciences.* J Microsc; 200(Pt 2):83-104

[12] **Axelrod D.** 1981. *Cell-substrate contacts illuminated by total internal reflection fluorescence.* J Cell Biol; 89(1):141-5

[13] **Axelrod D.** 2001. *Total internal reflection fluorescence microscopy in cell biology.* Traffic; 2(11):764-74.

[14] **Agard DA and Sedat JW.** 1983. *Three-dimensional architecture of a polytene nucleus.* Nature; 302(5910):676-81

[15] **McNally JG, Karpova T, Cooper J, Conchello JA.** 1999. *Three-dimensional imaging by deconvolution microscopy.* Methods; 19(3):373-85

[16] **Wallace W, Schaefer LH, Swedlow JR.** 2001. *A workingperson's guide to deconvolution in light microscopy.* Biotechniques; 31(5):1076-8, 1080, 1082 passim

[17] **Knoll M.** 1935. *Aufladepotentiel und Sekundaremission elektronenbestrahlter Korper.* Z tech. Phys. 16, 467-475

[18] **Gustafsson MG.** 2000. *Surpassing the lateral resolution limit by a factor of two using structured illumination microscopy.* J Microsc; 198(Pt 2):82-7

[19] **Gustafsson MG, Shao L, Carlton PM, Wang CJ, Golubovskaya IN, Cande WZ, Agard DA, Sedat JW.** 2008. *Three-dimensional resolution doubling in wide-field fluorescence microscopy by structured illumination.* Biophys J; 94(12):4957-70

[20] **Hell SW and Wichmann J.** 1994. *Breaking the diffraction resolution limit by stimulated emission: stimulated-emission-depletion fluorescence microscopy.* Opt Lett; 19(11):780-2

[21] **Hell SW.** 2007. *Far-field optical nanoscopy.* Science; 316(5828):1153-8

[22] **Kittel RJ, Wichmann C, Rasse TM, Fouquet W, Schmidt M, Schmid A, Wagh DA, Pawlu C, Kellner RR, Willig KI, Hell SW, Buchner E, Heckmann M, Sigrist SJ.** 2006. *Bruchpilot promotes active zone assembly, Ca2+ channel clustering, and vesicle release.* Science; 312(5776):1051-4

[23] **Sieber JJ, Willig KI, Heintzmann R, Hell SW, Lang T.** 2006. *The SNARE motif is essential for the formation of syntaxin clusters in the plasma membrane.* Biophys J; 90(8):2843-51

[24] **Willig KI, Rizzoli SO, Westphal V, Jahn R, Hell SW.** 2006. *STED microscopy reveals that synaptotagmin remains clustered after synaptic vesicle exocytosis.* Nature; 440(7086):935-9

[25] **Donnert G, Keller J, Wurm CA, Rizzoli SO, Westphal V, Schönle A, Jahn R, Jakobs S, Eggeling C, Hell SW.** 2007. *Two-color far-field fluorescence nanoscopy.* Biophys J; 92(8):L67-9

[26] **Hein B, Willig KI, Hell SW.** 2008. *Stimulated emission depletion (STED) nanoscopy of a fluorescent protein-labeled organelle inside a living cell.* Proc Natl Acad Sci U S A; 105(38):14271-6

[27] **Hein B, Willig KI, Wurm CA, Westphal V, Jakobs S, Hell SW.** 2010. *Stimulated emission depletion nanoscopy of living cells using SNAP-tag fusion proteins.* Biophys J; 98(1):158-63

[28] **Nagerl UV, Willig KI, Hein B, Hell SW, Bonhoeffer T.** 2008. *Live-cell imaging of dendritic spines by STED microscopy.* Proc Natl Acad Sci U S A; 105(48):18982-7

[29] **Westphal V, Rizzoli SO, Lauterbach MA, Kamin D, Jahn R, Hell SW.** 2008. *Video-rate far-field optical nanoscopy dissects synaptic vesicle movement.* Science; 320(5873):246-9

[30] **Eggeling C, Ringemann C, Medda R, Schwarzmann G, Sandhoff K, Polyakova S, Belov VN, Hein B, von Middendorff C, Schönle A, Hell SW.** 2009. *Direct observation of the nanoscale dynamics of membrane lipids in a living cell.* Nature; 457(7233):1159-62

[31] **Opazo F, Punge A, Bückers J, Hoopmann P, Kastrup L, Hell SW, Rizzoli SO.** 2010. *Limited intermixing of synaptic vesicle components upon vesicle recycling.* Traffic; 11(6):800-12

[32] **Donnert G, Keller J, Medda R, Andrei MA, Rizzoli SO, Lührmann R, Jahn R, Eggeling C, Hell SW.** 2006. *Macromolecular-scale resolution in biological fluorescence microscopy.* Proc Natl Acad Sci U S A; 103(31):11440-5

[33] **Schmidt R, Wurm CA, Jakobs S, Engelhardt J, Egner A, Hell SW.** 2008. *Spherical nanosized focal spot unravels the interior of cells.* Nat Methods; 5(6):539-44

[34] **Willig KI, Harke B, Medda R, Hell SW.** 2007. *STED microscopy with continuous wave beams.* Nat Methods; 4(11):915-8

[35] **Vicidomini G, Moneron G, Han KY, Westphal V, Ta H, Reuss M, Engelhardt J, Eggeling C, Hell SW.** 2011. *Sharper low-power STED nanoscopy by time gating.* Nat Methods; 8(7):571-3

[36] **Vicidomini G, Moneron G, Eggeling C, Rittweger E, Hell SW.** 2012. *STED with wavelengths closer to the emission maximum.* Opt Express; 20(5):5225-36

[37] **Moffitt JR, Osseforth C, Michaelis J.** 2011. *Time-gating improves the spatial resolution of STED microscopy.* Opt Express; 19(5):4242-54

[38] **Moerner WE, Kador L.** 1989. *Optical detection and spectroscopy of single molecules in a solid.* Phys Rev Lett; 62(21):2535-2538

[39] **Orrit M, Bernard J.** 1990. *Single pentacene molecules detected by fluorescence excitation in a p-terphenyl crystal.* Phys Rev Lett; 65(21):2716-2719

[40] **Ha T.** 2001a. *Single-molecule fluorescence resonance energy transfer.* Methods; 25(1):78-86

[41] **Ha T.** 2001b. *Single-molecule fluorescence methods for the study of nucleic acids.* Curr Opin Struct Biol; 11(3):287-92

[42] **Thompson RE, Larson DR, Webb WW.** 2002. *Precise nanometer localization analysis for individual fluorescent probes.* Biophys J; 82(5):2775-83

[43] **Bornfleth H, Satzler K, Eils R, Cremer C.** 1998. *High-precision distance measurements and volume-conserving segmentation of objects near and below the resolution limit in three-dimensional confocal fluorescence microscopy.* J. Microsc; 189:118–136

[44] **Lemmer P, Gunkel M, Weiland Y, Muller P, Baddeley D, Kaufmann R, Urich A, Eipel H, Amberger R, Hausmann M, Cremer C.** 2009. *Using conventional fluorescent markers for far-field fluorescence localization nanoscopy allows resolution in the 10-nm range.* J Microsc; 235(2):163-71

[45] **Cremer C, Kaufmann R, Gunkel M, Pres S, Weiland Y, Müller P, Ruckelshausen T, Lemmer P, Geiger F, Degenhard S, Wege C, Lemmermann NA, Holtappels R, Strickfaden H, Hausmann M.** 2011. *Superresolution imaging of biological nanostructures by spectral precision distance microscopy.* Biotechnol J; 6(9):1037-51

[46] **Rust MJ, Bates M, Zhuang X.** 2006. *Sub-diffraction-limit imaging by stochastic optical reconstruction microscopy (STORM).* Nat Methods; 3(10):793-5

[47] **Betzig E, Patterson GH, Sougrat R, Lindwasser OW, Olenych S, Bonifacino JS, Davidson MW, Lippincott-Schwartz J, Hess HF.** 2006. *Imaging intracellular fluorescent proteins at nanometer resolution.* Science; 313(5793):1642-5

[48] **Hess ST, Girirajan TP, Mason MD.** 2006. *Ultra-high resolution imaging by fluorescence photoactivation localization microscopy.* Biophys J; 91(11):4258-72

[49] **Cremer C.** 1999. *Principles of Spectral Precision Distance confocal microscopy for the analysis of molecular nuclear structure.* Handbook of Computer Vision and Applications; Ch. 41., Vol. 3, Academic Press San Diego, New York: 839-857

[50] *http://www.nobelprize.org/nobel_prizes/chemistry/laureates/2014/*
Access: 16.10.2014

[51] *http://www.nobelprize.org/nobel_prizes/chemistry/laureates/2008/*
Access: 14.01.2015

[52] **Zurek-Biesiada D, Szczurek A, Prakash K, Mohana GK, Lee HK; Roignant JY, Birk U, Dobrucki JW, Cremer C.** 2015. *Vybrant® DyeCycleTM Violet Fluorescent Probe.* Submitted

[53] **Han J, Burgess K.** 2010. *Fluorescent indicators for intracellular pH.* Chem Rev;110(5):2709-28

[54] **Grynkiewicz G, Poenie M, Tsien RY.** 1985. *A new generation of Ca2+ indicators with greatly improved fluorescence properties.* J Biol Chem; 260(6):3440-50

[55] **Ando R, Hama H, Yamamoto-Hino M, Mizuno H, Miyawaki A.** 2002. *An optical marker based on the UV-induced green-to-red photoconversion of a fluorescent protein.* Proc Natl Acad Sci U S A; 99(20):12651-6

[56] **Pakhomov AA, Martynova NY, Gurskaya NG, Balashova TA, Martynov VI.** 2004. *Photoconversion of the chromophore of a fluorescent protein from Dendronephthya sp.* Biochemistry (Mosc); 69(8):901-8

[57] **Gurskaya NG, Verkhusha VV, Shcheglov AS, Staroverov DB, Chepurnykh TV, Fradkov AF, Lukyanov S, Lukyanov KA.** 2006. *Engineering of a monomeric green-to-red photoactivatable fluorescent protein induced by blue light.* Nat Biotechnol; 24(4):461-5

[58] **Subach OM, Patterson GH, Ting LM, Wang Y, Condeelis JS, Verkhusha VV.** 2011. *A photoswitchable orange-to-far-red fluorescent protein, PSmOrange.* Nat Methods; 8(9):771-7

[59] **van de Linde S, Loschberger A, Klein T, Heidbreder M, Wolter S, Heilemann M, Sauer M.** 2011. *Direct stochastic optical reconstruction microscopy with standard fluorescent probes.* Nat Protoc; 6(7):991-1009

[60] **Baddeley D, Jayasinghe ID, Cremer C, Cannell MB, Soeller C.** 2009. *Light-induced dark states of organic fluochromes enable 30 nm resolution imaging in standard media.* Biophys J; 96(2):L22-4

[61] **Yildiz A, Forkey JN, McKinney SA, Ha T, Goldman YE, Selvin PR.** 2003. *Myosin V walks hand-over-hand: single fluorophore imaging with 1.5-nm localization.* Science; 300(5628):2061-5

[62] **Heilemann M, van de Linde S, Mukherjee A, Sauer M.** 2009. *Super-resolution imaging with small organic fluorophores.* Angew Chem Int Ed Engl; 48(37):6903-8

[63] **Fernandez-Suarez M, Ting AY.** 2008. *Fluorescent probes for super-resolution imaging in living cells.* Nat Rev Mol Cell Biol; 9(12):929-43

[64] **Patterson GH, Lippincott-Schwartz J.** 2002. *A photoactivatable GFP for selective photolabeling of proteins and cells.* Science; 297(5588):1873-7

[65] **Subach FV, Patterson GH, Manley S, Gillette JM, Lippincott-Schwartz J, Verkhusha VV.** 2009. *Photoactivatable mCherry for high-resolution two-color fluorescence microscopy.* Nat Methods; 6(2):153-9

[66] **Chudakov DM, Verkhusha VV, Staroverov DB, Souslova EA, Lukyanov S, Lukyanov KA.** 2004. *Photoswitchable cyan fluorescent protein for protein tracking.* Nat Biotechnol; 22(11):1435-9

[67] **Matsuda T, Miyawaki A, Nagai T.** 2008. *Direct measurement of protein dynamics inside cells using a rationally designed photoconvertible protein.* Nat Methods; 5(4):339-45

[68] **Wiedenmann J, Ivanchenko S, Oswald F, Schmitt F, Rocker C, Salih A, Spindler KD, Nienhaus GU.** 2004. *EosFP, a fluorescent marker protein with UV-inducible green-to-red fluorescence conversion.* Proc Natl Acad Sci U S A; 101(45):15905-10

[69] **Nienhaus GU, Nienhaus K, Holzle A, Ivanchenko S, Renzi F, Oswald F, Wolff M, Schmitt F, Rocker C, Vallone B, Weidemann W, Heilker R, Nar H, Wiedenmann J.** 2006. *Photoconvertible fluorescent protein EosFP: biophysical properties and cell biology applications.* Photochem Photobiol; 82(2):351-8

[70] **McKinney SA, Murphy CS, Hazelwood KL, Davidson MW, Looger LL.** 2009. *A bright and photostable photoconvertible fluorescent protein.* Nat Methods; 6(2):131-3

[71] **Habuchi S, Tsutsui H, Kochaniak AB, Miyawaki A, van Oijen AM.** 2008. *mKikGR, a monomeric photoswitchable fluorescent protein.* PLoS One; 3(12):e3944

[72] **Adam V, Lelimousin M, Boehme S, Desfonds G, Nienhaus K, Field MJ, Wiedenmann J, McSweeney S, Nienhaus GU, Bourgeois D.** 2008. *Structural characterization of IrisFP, an optical highlighter undergoing multiple photo-induced transformations.* Proc Natl Acad Sci U S A; 105(47):18343-8

[73] **Kremers GJ, Hazelwood KL, Murphy CS, Davidson MW, Piston DW.** 2009. *Photoconversion in orange and red fluorescent proteins.* Nat Methods; 6(5):355-8

[74] **Heilemann M, Margeat E, Kasper R, Sauer M, Tinnefeld P.** 2005. *Carbocyanine dyes as efficient reversible single-molecule optical switch.* J Am Chem Soc; 127(11):3801-6

[75] **Folling J, Belov V, Kunetsky R, Medda R, Schönle A, Egner A, Eggeling C, Bossi M, Hell SW.** 2007. *Photochromic rhodamines provide nanoscopy with optical sectioning.* Angew Chem Int Ed Engl; 46(33):6266-70

[76] **Gee KR, Weinberg ES, Kozlowski DJ.** 2001. *Caged Q-rhodamine dextran: a new photoactivated fluorescent tracer.* Bioorg Med Chem Lett; 11(16):2181-3

[77] **Bates M, Huang B, Dempsey GT, Zhuang X.** 2007. *Multicolor super-resolution imaging with photoswitchable fluorescent probes.* Science; 317(5845):1749-53

[78] **Irvine SE, Staudt T, Rittweger E, Engelhardt J, Hell SW.** 2008. *Direct light-driven modulation of luminescence from Mn-doped ZnSe quantum dots.* Angew Chem Int Ed Engl; 47(14):2685-8

[79] **Chen I, Ting AY.** 2005. *Site-specific labeling of proteins with small molecules in live cells.* Curr Opin Biotechnol; 16(1):35-40

[80] **Lin MZ, Wang L.** 2008. *Selective labeling of proteins with chemical probes in living cells.* Physiology (Bethesda); 23:131-41

[81] **Chudakov DM, Belousov VV, Zaraisky AG, Novoselov VV, Staroverov DB, Zorov DB, Lukyanov S, Lukyanov KA.** 2003b. *Kindling fluorescent proteins for precise in vivo photolabeling.* Nat Biotechnol; 21(2):191-4

[82] **Chudakov DM, Lukyanov S, Lukyanov KA.** 2007. *Tracking intracellular protein movements using photoswitchable fluorescent proteins PS-CFP2 and Dendra2.* Nat Protoc; 2(8):2024-32

[83] **Habuchi S, Dedecker P, Hotta J, Flors C, Ando R, Mizuno H, Miyawaki A, Hofkens J.** 2006. *Photo-induced protonation/deprotonation in the GFP-like fluorescent protein Dronpa: mechanism responsible for the reversible photoswitching.* Photochem Photobiol Sci; 5(6):567-76

[84] **Ando R, Flors C, Mizuno H, Hofkens J, Miyawaki A.** 2007. *Highlighted generation of fluorescence signals using simultaneous two-color irradiation on Dronpa mutants.* Biophys J; 92(12):L97-9

[85] **Stiel AC, Trowitzsch S, Weber G, Andresen M, Eggeling C, Hell SW, Jakobs S, Wahl MC.** 2007. *1.8 A bright-state structure of the reversibly switchable fluorescent protein Dronpa guides the generation of fast switching variants.* Biochem J; 402(1):35-42

[86] **Tsutsui H, Karasawa S, Shimizu H, Nukina N, Miyawaki A.** 2005. *Semi-rational engineering of a coral fluorescent protein into an efficient highlighter.* EMBO Rep; 6(3):233-8

[87] **Burnette DT, Sengupta P, Dai Y, Lippincott-Schwartz J, Kachar B.** 2011. *Bleaching/blinking assisted localization microscopy for superresolution imaging using standard fluorescent molecules.* Proc Natl Acad Sci U S A; 108(52):21081-6

[88] **Flors C, Ravarani CN, Dryden DT.** 2009. *Super-resolution imaging of DNA labelled with intercalating dyes.* Chemphyschem; 10(13):2201-4

[89] **Akerman B and Tuite E.** 1996. *Single- and double-strand photocleavage of DNA by YO, YOYO and TOTO.* Nucleic Acids Res; 24(6): 1080–1090

[90] **Piterburg M, Panet H, Weiss A.** 2012. *Photoconversion of DAPI following UV or violet excitation can cause DAPI to fluoresce with blue or cyan excitation.* J Microsc; 246(1):89-95

[91] **Jez M, Bas T, Veber M, Kosir A, Dominko T, Page R, Rozman P.** 2012. *The hazards of DAPI photoconversion: effects of dye, mounting media and fixative, and how to minimize the problem.* Histochem Cell Biol; 139(1):195-204

[92] **Bontemps J, Houssier C, Fredericq E.** 1975. *Physico-chemical study of the complexes of "33258 Hoechst" with DNA and nucleohistone.* Nucleic Acids Res; 2(6): 971–984

[93] **Comings DE.** 1975. *Mechanisms of chromosome banding. VIII. Hoechst 33258-DNA interaction.* Chromosoma; 52(3):229-43

[94] **Latt SA.** 1973. *Microfluorometric detection of deoxyribonucleic acid replication in human metaphase chromosomes.* Proc Natl Acad Sci U S A; 70(12):3395-9

[95] **Latt SA and Wohlleb JC.** 1975. *Optical studies of the interaction of 33258 Hoechst with DNA, chromatin, and metaphase chromosomes.* Chromosoma; 52(4):297-316

[96] **Fornander LH, Wu L, Billeter M, Lincoln P, Norden B.** 2013. *Minor-groove binding drugs: where is the second Hoechst 33258 molecule?* J Phys Chem B; 117(19):5820-30

[97] **Stokke T and Steen HB.** 1986a. *Binding of Hoechst 33258 to chromatin in situ.* Cytometry; 7(3):227-34

[98] *http://tools.lifetechnologies.com/content/sfs/manuals/mp21486.pdf*
Access: 14.04.2015

[99] **Latt SA and Stetten G.** 1976. *Spectral studies on 33258 Hoechst and related bisbenzimidazole dyes useful for fluorescent detection of deoxyribonucleic acid synthesis.* J Histochem Cytochem; 24(1):24-33

[100] **Kalninsh KK and Pestov DV.** 1994. *Absorption and fluorescence spectra of the probe Hoechst 33258.* J. Photochem. Photobiol. A: Chem; 83:39-47

[101] **Muller W and Gautier F.** 1975. *nteractions of heteroaromatic compounds with nucleic acids. A - T-specific non-intercalating DNA ligands.* Eur J Biochem; 54(2):385-94

[102] **Aymami J, Nunn CM, Neidle S.** 1999. *DNA minor groove recognition of a non-self-complementary AT-rich sequence by a tris-benzimidazole ligand.* Nucleic Acids Res; 27(13):2691-8

[103] **Pal SK, Zhao L, Zewail AH.** 2003. *Water at DNA surfaces: ultrafast dynamics in minor groove recognition.* Proc Natl Acad Sci U S A; 100(14):8113-8

[104] **Banerjee D and Kumar Pal S.** 2006. *Ultrafast charge transfer and solvation of DNA minor groove binder: Hoechst 33258 in restricted environments.* Chemical Physics Letters; 432:257–262

[105] **Portugal J, Waring MJ.** 1988. *Assignment of DNA binding sites for 4',6-diamidine-2-phenylindole and bisbenzimide (Hoechst 33258). A comparative footprinting study.* Biochim Biophys Acta; 949(2):158-68

[106] **Bailly C, Colson P, Henichart JP, Houssier C.** 1993. *The different binding modes of Hoechst 33258 to DNA studied by electric linear dichroism.* Nucleic Acids Res; 21(16):3705-9

[107] **Embrey KJ, Searle MS, Craik DJ.** 1993. *Interaction of Hoechst 33258 with the minor groove of the A + T-rich DNA duplex d(GGTAATTACC)2 studied in solution by NMR spectroscopy.* Eur J Biochem; 211(3):437-47

[108] **Abu-Daya A, Brown PM, Fox KR.** 1995. *DNA sequence preferences of several AT-selective minor groove binding ligands.* Nucleic Acids Res; 23(17): 3385–3392

[109] **Moon JH, Kim SK, Sehlstedt U, Rodger A, Norden B.** 1996. *DNA structural features responsible for sequence-dependent binding geometries of Hoechst 33258.* Biopolymers; 38(5):593-606

[110] **Guan Y, Shi R, Li X, Zhao M, Li Y.** 2007. *Multiple binding modes for dicationic Hoechst 33258 to DNA.* J Phys Chem B; 111(25):7336-44

[111] **Adhikary A, Buschmann V, Muller C, Sauer M.** 2003. *Ensemble and single-molecule fluorescence spectroscopic study of the binding modes of the bisbenzimidazole derivative Hoechst 33258 with DNA.* Nucleic Acids Res; 31(8):2178-86

[112] **Goerner H.** 2001. *Direct and sensitized photoprocesses of bis-benzimidazole dyes and the effects of surfactants and DNA.* Photochem Photobiol; 73(4):339-48

[113] **Daxhelet GA, Coene MM, Hoet PP, Cocito CG.** 1989. *Spectrofluorometry of dyes with DNAs of different base composition and conformation.* Anal Biochem; 179(2):401-3

[114] **Morozkin ES, Laktionov PP, Rykova EY, Vlassov VV.** 2003. *Fluorometric quantification of RNA and DNA in solutions containing both nucleic acids.* Anal Biochem; 322(1):48-50

[115] **Downs TR, Wilfinger WW.** 1983. *Fluorometric quantification of DNA in cells and tissue.* Anal Biochem; 131(2):538-47

[116] **Cesarone CF, Bolognesi C, Santi L.** 1979. *Improved microfluorometric DNA determination in biological material using 33258 Hoechst.* Anal Biochem; 100(1):188-97

[117] **Stout DL, Becker FF.** 1982. *Fluorometric quantitation of single-stranded DNA: a method applicable to the technique of alkaline elution.* Anal Biochem; 127(2):302-7

[118] **Chen AY, Yu C, Gatto B, Liu LF.** 1993. *DNA minor groove-binding ligands: a different class of mammalian DNA topoisomerase I inhibitors.* Proc Natl Acad Sci U S A; 90(17):8131-5

[119] **McHugh MM, Woynarowski JM, Sigmund RD, Beerman TA.** 1989. *Effect of minor groove binding drugs on mammalian topoisomerase I activity.* Biochem Pharmacol; 38(14):2323-8

[120] **Woynarowski AM, McHugh M, Sigmund RD, Bee TA.** 1988. *Modulation of Topoisomerase II Catalytic Activity by DNA Minor Groove Binding Agents Distamycin, Hoechst 33258, and 4',6-Diamidine-2-phenylindole.* Molecular Pharmacology; 35:177-182

[121] **Soderlind KJ, Gorodetsky B, Singh AK, Bachur NB, Miller GG, Lown JW.** 1999. *Bisbenzimidazole anticancer agents: targeting human tumor helicases.* Anti-Cancer Drug Des; 14:19- 36

[122] **Disney MD, Stephenson R, Wright TW, Haidaris CG, Turner DH, Gigliotti F.** 2005. *Activity of Hoechst 33258 against Pneumocystis carinii f. sp. muris, Candida albicans, and Candida dubliniensis.* Antimicrob Agents Chemother; 49(4):1326-30

[123] **Denison L, Haigh A, D'Cunha G, Martin RF.** 1992. *DNA ligands as radioprotectors: molecular studies with Hoechst 33342 and Hoechst 33258.* Int J Radiat Biol; 61(1):69-81

[124] **Harapanhalli RS, Howell RW, Rao DV.** 1994. *Bis-benzimidazole dyes, Hoechst 33258 and Hoechst 33342: radioiodination, facile purification and subcellular distribution.* Nucl Med Biol; 21(4):641-7

[125] **Singh SP, Jayanth VR, Chandna S, Dwarakanath BS, Singh S, Adhikari JS, Jain V.** 1998. *Radioprotective effects of DNA ligands Hoechst-33342 and 33258 in whole body irradiated mice.* Indian J Exp Biol; 36(4):375-84

[126] **Lyubimova NV, Coultas PG, Yuen K, Martin RF.** 2001. *In vivo radioprotection of mouse brain endothelial cells by Hoechst 33342.* Br J Radiol; 74(877):77-82

[127] **Adhikary A, Bothe E, Jain V, Von Sonntag C.** 2000. *Pulse radiolysis of the DNA-binding bisbenzimidazole derivatives Hoechst 33258 and 33342 in aqueous solutions.* Int J Radiat Biol; 76(9):1157-66

[128] **Chen TR.** 1977. *In situ detection of mycoplasma contamination in cell cultures by fluorescent Hoechst 33258 stain.* Exp Cell Res; 104(2):255-62.

[129] **Kapuscinski J and Skoczylas B.** 1978. *Fluorescent complexes of DNA with DAPI 4',6-diamidine-2-phenyl indole.2HCl or DCI 4',6-dicarboxyamide-2-phenylindole.* Nucleic Acids Res; 5(10):3775-99

[130] **Manzini G, Xodo L, Barcellona ML, Quadrifoglio F.** 1985a. *Interaction of 4'-6-diamidino-2-phenylindole 2HCl with synthetic and natural deoxy- and ribonucleic acids.* Journal of Biosciences; Volume 8, Issue 3-4, pp 699-711

[131] **Kapuscinski J and Szer W.** 1979. *Interactions of 4', 6-diamidine-2-phenylindole with synthetic polynucleotides.* Nucleic Acids Res; 6(11): 3519–3534

[132] **Kapuscinski J.** 1995. *DAPI: a DNA-specific fluorescent probe.* Biotech Histochem; 70(5):220-33

[133] *http://www.sigmaaldrich.com/catalog/product/sigma/d9542*
Access: 14.04.2015

[134] **Manzini G, Xodo L, Barcellona ML, Quadrifoglio F.** 1985b. *nteraction of DAPI with double-stranded ribonucleic acids.* Nucleic Acids Res; 13(24): 8955–8967

[135] **Tanious FA, Veal JM, Buczak H, Ratmeyer LS, Wilson WD.** 1992. *DAPI (4',6-diamidino-2-phenylindole) binds differently to DNA and RNA: minor-groove binding at AT sites and intercalation at AU sites.* Biochemistry; 31(12):3103-12

[136] **Kubista M, Akerman B, Norden B.** 1987. *haracterization of interaction between DNA and 4',6-diamidino-2-phenylindole by optical spectroscopy.* Biochemistry; 26(14):4545-53

[137] **Zink D, Sadoni N, Stelzer E.** 2002. *Visualizing chromatin and chromosomes in living cells.* Methods; 29(1):42-50

[138] **Russell WC, Newman C, Williamson DH.** 1975. *A simple cytochemical technique for demonstration of DNA in cells infected with mycoplasmas and viruses.* Nature; 253(5491):461-2

[139] **Mildner B and Chandra P.** 1979. *Molecular mechanism of action of diamidinephenylindole (DAPI). II. Effect of DAPI on the template activity of DNA and polydeoxynucleotides in the DNA-polymerase system from bacteria, eukaryotic cells and RNA tumor viruses.* Cell Mol Biol Incl Cyto Enzymol; 25(6):399-407

[140] **Janas T and Yarus M.** 2003. *Visualization of membrane RNAs.* RNA; 9(11):1353-61.

[141] **Flors C.** 2010a. *DNA and chromatin imaging with super-resolution fluorescence microscopy based on single-molecule localization.* Biopolymers; 95(5):290-7

[142] **Bohn M, Diesinger P, Kaufmann R, Weiland Y, Muller P, Gunkel M, von Ketteler A, Lemmer P, Hausmann M, Heermann DW, Cremer C.** 2010. *Localization microscopy reveals expression-dependent parameters of chromatin nanostructure.* Biophys J; 99(5):1358-67

[143] **Wombacher R, Heidbreder M, van de Linde S, Sheetz MP, Heilemann M, Cornish VW, Sauer M.** 2010. *Live-cell super-resolution imaging with trimethoprim conjugates.* Nat Methods; 7(9):717-9

[144] **Weiland Y, Lemmer P, Cremer C.** 2010. *Combining FISH with localisation microscopy: Super-resolution imaging of nuclear genome nanostructures.* Chromosome Res; 19(1):5-23

[145] **Schermelleh L, Carlton PM, Haase S, Shao L, Winoto L, Kner P, Burke B, Cardoso MC, Agard DA, Gustafsson MG, Leonhardt H, Sedat JW.** 2008. *Subdiffraction multicolor imaging of the nuclear periphery with 3D structured illumination microscopy.* Science; 320(5881):1332-6

[146] **Persson F, Bingen P, Staudt T, Engelhardt J, Tegenfeldt JO, Hell SW.** 2011. *Fluorescence nanoscopy of single DNA molecules by using stimulated emission depletion (STED).* Angew Chem Int Ed Engl; 50(24):5581-3

[147] **Ribeiro SA, Vagnarelli P, Dong Y, Hori T, McEwen BF, Fukagawa T, Flors C, Earnshaw WC.** 2010. *super-resolution map of the vertebrate kinetochore.* Proc Natl Acad Sci U S A; 107(23):10484-9

[148] **Gunkel M, Erdel F, Rippe K, Lemmer P, Kaufmann R, Hormann C, Amberger R, Cremer C.** 2009. *Dual color localization microscopy of cellular nanostructures.* Biotechnol J; 4(6):927-38

[149] **Matsuda A, Shao L, Boulanger J, Kervrann C, Carlton PM, Kner P, Agard D, Sedat JW.** 2010. *Condensed mitotic chromosome structure at nanometer resolution using PALM and EGFP- histones.* PLoS One; 5(9):e12768

[150] **Salic A, Mitchison TJ.** 2008. *A chemical method for fast and sensitive detection of DNA synthesis in vivo.* Proc Natl Acad Sci U S A; 105(7):2415-20

[151] **Zessin PJ, Finan K, Heilemann M.** 2012. *Super-resolution fluorescence imaging of chromosomal DNA.* J Struct Biol; 177(2):344-8

[152] **Flors C.** 2010b. *Photoswitching of monomeric and dimeric DNA-intercalating cyanine dyes for super-resolution microscopy applications.* Photochem Photobiol Sci; 9(5):643-8

[153] **Benke A, Manley S.** 2012. *Live-cell dSTORM of cellular DNA based on direct DNA labeling.* Chembiochem; 13(2):298-301

[154] **Schoen I, Ries J, Klotzsch E, Ewers H, Vogel V.** 2011. *Binding-activated localization microscopy of DNA structures.* Nano Lett; 11(9):4008-11

[155] **Glazer AN, Rye HS.** 1992. *Stable dye-DNA intercalation complexes as reagents for high-sensitivity fluorescence detection.* Nature; 359(6398):859-61

[156] **Simonson PD, Rothenberg E, Selvin PR.** 2011. *Single-molecule-based super-resolution images in the presence of multiple fluorophores.* Nano Lett; 11(11):5090-6

[157] **Sharonov A, Hochstrasser RM.** 2006. *Wide-field subdiffraction imaging by accumulated binding of diffusing probes.* Proc Natl Acad Sci U S A; 103(50):18911-6

[158] **Bates M, Blosser TR, Zhuang X.** 2005. *Short-range spectroscopic ruler based on a single-molecule optical switch.* Phys Rev Lett; 94(10):108101

[159] **Conley NR, Biteen JS, Moerner WE.** 2008. *Cy3-Cy5 covalent heterodimers for single-molecule photoswitching.* J Phys Chem B; 112(38):11878-80

[160] **Smith DA, Holliger P, Flors C.** 2012. *Reversible fluorescence photoswitching in DNA.* J Phys Chem B; 116(34):10290-3

[161] **Ramsay N, Jemth AS, Brown A, Crampton N, Dear P, Holliger P.** 2010. *CyDNA: synthesis and replication of highly Cy-dye substituted DNA by an evolved polymerase.* J Am Chem Soc; 132(14):5096-104

[162] *http://encyklopedia.pwm.pl/haslo/3962661/promieniowanie-nadfioletowe.html*
Access: 26.08.2014

[163] *http://www.spacewx.com/pdf/SET_21348_2004.pdf*
Access: 26.08.2014

[164] **Sinha RP, Kumar HD, Kumar A, Hader DP.** 1995. *Effects of UV-B Irradiation on Growth, Survival, Pigmentation and Nitrogen Metabolism Enzymes in Cyanobacteria.* Acta Protozoologica; 34:187-192

[165] **Hader DP, Kumar HD, Smith RC, Worrest RC.** 2008. *Effects of solar UV radiation on aquatic ecosystems and interactions with climate change.* Photochem Photobiol Sci; 6(3):267-85

[166] **Norval M, Cullen AP, de Gruijl FR, Longstreth J, Takizawa Y, Lucas RM, Noonan FP, van der Leun JC.** 2007. *The effects on human health from stratospheric ozone depletion and its interactions with climate change.* Photochem Photobiol Sci; 6(3):232-51

[167] **Solomon KR.** 2010. *Effects of ozone depletion and UV-B radiation on humans and the environment.* Atmosphere-Ocean, 46:1, 185-202

[168] **Zeeshan M and Prasad SM.** 2009. *Differential response of growth, photosynthesis, antioxidant enzymes and lipid peroxidation to UV-B radiation in three cyanobacteria.* South African Journal of Botany; 75:466–474

[169] **Llabres M, Agusti S, Alonso-Laita P, Herndl GJ.** 2010. *Synechococcus and Prochlorococcus cell death induced by UV radiation and the penetration of lethal UVR in the Mediterranean Sea.* Mar Ecol Prog Ser; 399: 27–37

[170] **Gould TJ, Verkhusha VV, Hess ST.** 2009. *Imaging biological structures with fluorescence photoactivation localization microscopy.* Nat Protoc; 4(3):291-308

[171] **Pletnev S, Subach FV, Dauter Z, Wlodawer A, Verkhusha VV.** 2012. *A structural basis for reversible photoswitching of absorbance spectra in red fluorescent protein rsTagRFP.* J Mol Biol; 417(3):144-51

[172] **Schafer LV, Groenhof G, Boggio-Pasqua M, Robb MA, Grubmuller H.** 2008. *Chromophore protonation state controls photoswitching of the fluoroprotein asFP595.* PLoS Comput Biol; 4(3):e1000034

[173] **Violot S, Carpentier P, Blanchoin L, Bourgeois D.** 2009. *Violot S, Carpentier P, Blanchoin L, Bourgeois D. 2009. Reverse pH-dependence of chromophore protonation explains the large Stokes shift of the red fluorescent protein mKeima.* J Am Chem Soc; 131(30):10356-7

[174] **Faro AR, Adam V, Carpentier P, Darnault C, Bourgeois D, de Rosny E.** 2010. *Low-temperature switching by photoinduced protonation in photochromic fluorescent proteins.* Photochem Photobiol Sci; 9(2):254-62

[175] **Voliani V, Bizzarri R, Nifosi R, Abbruzzetti S, Grandi E, Viappiani C, Beltram F.** 2008. *Cis-trans photoisomerization of fluorescent-protein chromophores.* J Phys Chem B; 112(34):10714-22

[176] **Mudalige K, Habuchi S, Goodwin PM, Pai RK, De Schryver F, Cotlet M.** 2010. *Photophysics of the red chromophore of HcRed: evidence for cis-trans isomerization and protonation-state changes.* J Phys Chem B; 114(13):4678-85

[177] **Dickson RM, Cubitt AB, Tsien RY, Moerner WE.** 1997. *On/off blinking and switching behaviour of single molecules of green fluorescent protein.* Nature; 388(6640):355-8

[178] **Verkhusha VV, Sorkin A.** 2005. *Conversion of the monomeric red fluorescent protein into a photoactivatable probe.* Chem Biol; 12(3):279-85

[179] **Chattoraj M, King BA, Bublitz GU, Boxer SG.** 1996. *Ultra-fast excited state dynamics in green fluorescent protein: multiple states and proton transfer.* Proc Natl Acad Sci U S A; 93(16): 8362–8367

[180] **Niwa H, Inouye S, Hirano T, Matsuno T, Kojima S, Kubota M, Ohashi M, Tsuji FI.** 1996. *Chemical nature of the light emitter of the Aequorea green fluorescent protein.* Proc Natl Acad Sci U S A; 93(24):13617-22

[181] **Brejc K, Sixma TK, Kitts PA, Kain SR, Tsien RY, Ormo M, Remington SJ.** 1997. *Structural basis for dual excitation and photoisomerization of the Aequorea victoria green fluorescent protein.* Proc Natl Acad Sci U S A; 94(6):2306-11

[182] **Yokoe H and Meyer T.** 1996. *Spatial dynamics of GFP-tagged proteins investigated by local fluorescence enhancement.* Nat Biotechnol; 14(10):1252-6

[183] **van Thor JJ, Gensch T, Hellingwerf KJ, Johnson LN.** 2002. *Phototransformation of green fluorescent protein with UV and visible light leads to decarboxylation of glutamate 222.* Nat Struct Biol; 9(1):37-41

[184] **Bell AF, Stoner-Ma D, Wachter RM, Tonge PJ.** 2003. *Light-driven decarboxylation of wild-type green fluorescent protein.* J Am Chem Soc; 125(23):6919-26.

[185] **Dittrich PS, Schäfer SP, Schwille P.** 2005. *Characterization of the photoconversion on reaction of the fluorescent protein Kaede on the single-molecule level.* Biophys J; 89(5):3446-55

[186] **Chudakov DM, Feofanov AV, Mudrik NN, Lukyanov S, Lukyanov KA.** 2003a. *Chromophore environment provides clue to kindling fluorescent protein riddle.* J Biol Chem; 278(9):7215-9

[187] **Ando R, Mizuno H, Miyawaki A.** 2004. *Regulated fast nucleocytoplasmic shuttling observed by reversible protein highlighting.* Science; 306(5700):1370-3

[188] **Lukyanov KA, Fradkov AF, Gurskaya NG, Matz MV, Labas YA, Savitsky AP, Markelov ML, Zaraisky AG, Zhao X, Fang Y, Tan W, Lukyanov SA.** 2000. *Natural animal coloration can Be determined by a nonfluorescent green fluorescent protein homolog.* J Biol Chem; 275(34):25879-82

[189] **Quillin ML, Anstrom DM, Shu X, O'Leary S, Kallio K, Chudakov DM, Remington SJ.** 2005. *Kindling fluorescent protein from Anemonia sulcata: dark-state structure at 1.38 A resolution.* Biochemistry; 44(15):5774-87

[190] **Wilmann PG, Petersen J, Devenish RJ, Prescott M, Rossjohn J.** 2005. *Variations on the GFP chromophore: A polypeptide fragmentation within the chromophore revealed in the 2.1-A crystal structure of a nonfluorescent chromoprotein from Anemonia sulcata.* J Biol Chem; 280(4):2401-4

[191] **Andresen M, Wahl MC, Stiel AC, Grater F, Schafer LV, Trowitzsch S, Weber G, Eggeling C, Grubmuller H, Hell SW, Jakobs S.** 2005. *Structure and mechanism of the reversible photoswitch of a fluorescent protein.* Proc Natl Acad Sci U S A; 102(37):13070-4

[192] **Brakemann T, Weber G, Andresen M, Groenhof G, Stiel AC, Trowitzsch S, Eggeling C, Grubmuller H, Hell SW, Wahl MC, Jakobs S.** 2010. *Molecular basis of the light-driven switching of the photochromic fluorescent protein Padron.* J Biol Chem; 285(19):14603-9

[193] **Faro AR, Carpentier P, Jonasson G, Pompidor G, Arcizet D, Demachy I, Bourgeois D.** 2011. *Low-temperature chromophore isomerization reveals the photoswitching mechanism of the fluorescent protein Padron.* J Am Chem Soc; 133(41):16362-5

[194] **Andresen M, Stiel AC, Trowitzsch S, Weber G, Eggeling C, Wahl MC, Hell SW, Jakobs S.** 2007. *Structural basis for reversible photoswitching in Dronpa.* Proc Natl Acad Sci U S A; 104(32):13005-9

[195] **Mizuno H, Mal TK, Walchli M, Kikuchi A, Fukano T, Ando R, Jeyakanthan J, Taka J, Shiro Y, Ikura M, Miyawaki A.** 2008. *Light-dependent regulation of structural flexibility in a photochromic fluorescent protein.* Proc Natl Acad Sci U S A; 105(27):9227-32

[196] **Fron E, Flors C, Schweitzer G, Habuchi S, Mizuno H, Ando R, Schryver FC, Miyawaki A, Hofkens J.** 2007. *Ultrafast excited-state dynamics of the photoswitchable protein Dronpa.* J Am Chem Soc; 129(16):4870-1

[197] **Li X, Chung LW, Mizuno H, Miyawaki A, Morokuma K.** 2010. *A theoretical study on the nature of on- and off-states of reversibly photoswitching fluorescent protein Dronpa: absorption, emission, protonation, and Raman.* J Phys Chem B; 114(2):1114-26

[198] **Steinhauer C, Forthmann C, Vogelsang J, Tinnefeld P.** 2008. *Superresolution microscopy on the basis of engineered dark states.* J Am Chem Soc; 130(50):16840-1

[199] **Vogelsang J, Kasper R, Steinhauer C, Person B, Heilemann M, Sauer M, Tinnefeld P.** 2008. *A reducing and oxidizing system minimizes photobleaching and blinking of fluorescent dyes.* Angew Chem Int Ed Engl; 47(29):5465-9

[200] **Folling J, Bossi M, Bock H, Medda R, Wurm CA, Hein B, Jakobs S, Eggeling C, Hell SW.** 2008. *Fluorescence nanoscopy by ground-state depletion and single-molecule return.* Nat Methods; 5(11):943-5

[201] **Dempsey GT, Bates M, Kowtoniuk WE, Liu DR, Tsien RY, Zhuang X.** 2009. *Photoswitching mechanism of cyanine dyes.* J Am Chem Soc; 131(51):18192-3

[202] **van de Linde S, Sauer M, Heilemann M.** 2008. *Subdiffraction-resolution fluorescence imaging of proteins in the mitochondrial inner membrane with photoswitchable fluorophores.* J Struct Biol; 164(3):250-4

[203] **Grab AL, Hagmann M, Dahint R, Cremer C.** 2014. *Localization microscopy (SPDM) facilitates high precision control of lithographically produced nanostructures.* Micron; 68:1-7

[204] **Hess ST, Gould TJ, Gudheti MV, Maas SA, Mills KD, Zimmerberg J.** 2007. *Dynamic clustered distribution of hemagglutinin resolved at 40 nm in living cell membranes discriminates between raft theories.* Proc Natl Acad Sci U S A; 104(44):17370-5

[205] **Manley S, Gillette JM, Patterson GH, Shroff H, Hess HF, Betzig E, Lippincott-Schwartz J.** 2008. *High-density mapping of single-molecule trajectories with photoactivated localization microscopy.* Nat Methods; 5(2):155-7

[206] **Shroff H, Galbraith CG, Galbraith JA, Betzig E.** 2008. *Live-cell photoactivated localization microscopy of nanoscale adhesion dynamics.* Nat Methods; 5(5):417-23

[207] **Kedziora KM, Prehn JH, Dobrucki J, Bernas T.** 2011. *Method of calibration of a fluorescence microscope for quantitative studies.* J Microsc; 244(1):101-11

[208] **De Castro LF, Zacharias M.** 2002. *DAPI binding to the DNA minor groove: a continuum solvent analysis.* J Mol Recognit; 15(4):209-20

[209] **Stokke T, Steen HB.** 1986b. *Fluorescence spectra of Hoechst 33258 bound to chromatin.* Biochim Biophys Acta; 868(1):17-23

[210] **Weisblum B, Haenssler E.** 1974. *Fluorometric properties of the bibenzimidazole derivative Hoechst 33258, a fluorescent probe specific for AT concentration in chromosomal DNA.* Chromosoma; 46(3):255-60

[211] **Lakowicz JR, Gryczynski I, Malak H, Schrader M, Engelhardt P, Kano H, Hell SW.** 1997. *Time-resolved fluorescence spectroscopy and imaging of DNA labeled with DAPI and Hoechst 33342 using three-photon excitation.* Biophys J; 72(2 Pt 1):567-78

[212] **Cosa G, Focsaneanu KS, McLean JR, McNamee JP, Scaiano JC.** 2001. *Photophysical properties of fluorescent DNA-dyes bound to single- and double-stranded DNA in aqueous buffered solution.* Photochem Photobiol; 73(6):585-99

[213] *http://www.lifetechnologies.com/order/catalog/product/V35003*
Access: 20.02.2015

[214] *http://www.mobitec.com/probes/docs/sections/0203.pdf*
Access: 20.02.2015

[215] *http://pubchem.ncbi.nlm.nih.gov/summary/summary.cgi?cid=121834*
Access: 20.02.2015

[216] **Plasek J, Jarolim P.** 1987. *nteraction of the fluorescent probe 1,6-diphenyl-1,3,5-hexatriene with biomembranes.* Gen Physiol Biophys; 6(5):425-37

[217] **Bouchy M, Donner M, Andre JC.** 1981. *Evolution of fluorescence polarization of 1,6-diphenyl-1,3,5-hexatriene (DPH) during the labelling of living cells.* Experimental Cell Research; 133(1):39-46

[218] *http://www.lifetechnologies.com/order/catalog/product/A30000*
Access: 20.02.2015

[219] **Gruell F, Kirchgessner M, Kaufmann R, Hausmann M, Kebschull U.** 2011. *Accelerating Image Analysis for Localization Microscopy with FPGAs. 21st International Conference on Field Programmable Logic and Applications.* IEEE; 2011. page 1–5

[220] **Baddeley D, Cannell MB, Soeller C.** 2010. *Visualization of localization microscopy data.* Microsc Microanal; 16(1):64-72

[221] **Loontiens FG, McLaughlin LW, Diekmann S, Clegg RM.** 1991. *Binding of Hoechst 33258 and 4',6'-diamidino-2-phenylindole to self-complementary decadeoxynucleotides with modified exocyclic base substituents.* Biochemistry; 30(1):182-9

[222] **Loontiens FG, Regenfuss P, Zechel A, Dumortier L, Clegg RM.** 1990. *Binding characteristics of Hoechst 33258 with calf thymus DNA, poly[d(A-T)], and d(CCGGAATTCCGG): multiple stoichiometries and determination of tight binding with a wide spectrum of site affinities.* Biochemistry; 29(38):9029-39

[223] **Huang B, Wang W, Bates M, Zhuang X.** 2008. *Three-dimensional super-resolution imaging by stochastic optical reconstruction microscopy.* Science; 319(5864):810-3

[224] **Juette MF, Gould TJ, Lessard MD, Mlodzianoski MJ, Nagpure BS, Bennett BT, Hess ST, Bewersdorf J.** 2008. *Three-dimensional sub-100 nm resolution fluorescence microscopy of thick samples.* Nat Methods; 5(6):527-9